

# Arrival and Passage Times From a Spin-Boson Detector Model

Dissertation

zur Erlangung des Doktorgrades  
der Mathematisch-Naturwissenschaftlichen Fakultäten  
der Georg-August-Universität zu Göttingen

Vorgelegt von

Jens Timo Neumann  
aus Hildesheim

Göttingen 2007



D7

Referent: Prof. Dr. Gerhard C. Hegerfeldt

Korreferent: Prof. Dr. Kurt Schönhammer

Tag der mündlichen Prüfung: 13. 2. 2007



# Contents

<b>1</b>	<b>Introduction</b>	<b>5</b>
<b>I</b>	<b>A spin-boson detector model for arrival times</b>	<b>9</b>
<b>2</b>	<b>Arrival times: Introduction</b>	<b>11</b>
2.1	Quantum arrival times . . . . .	11
2.2	Allcock's proposal: Absorbing potentials . . . . .	11
2.3	Kijowski's axiomatic arrival-time density . . . . .	13
2.3.1	Intuitive derivation . . . . .	13
2.3.2	Kijowski's axiomatic derivation . . . . .	15
2.4	The time-of-arrival operator . . . . .	18
2.5	The fluorescence model . . . . .	19
2.5.1	The model. Basic properties . . . . .	19
2.5.2	The quantum mechanical flux . . . . .	21
2.5.3	Kijowski's density . . . . .	22
2.5.4	One-channel limit: Absorbing potential . . . . .	23
2.5.5	Possible objections against the fluorescence model . . . . .	24
2.6	Plan of Part I . . . . .	25
<b>3</b>	<b>The spin-boson detector model</b>	<b>27</b>
3.1	The spin-boson detector model . . . . .	27
3.1.1	Physical idea . . . . .	27
3.1.2	Hamiltonian . . . . .	29
3.1.3	The detection process . . . . .	30
3.2	Investigation by unitary QM . . . . .	30
3.2.1	A simplified model . . . . .	30
3.2.2	Energy eigenstates . . . . .	31
3.2.3	Jaynes-Cummings approach . . . . .	36
3.2.4	Detection of a wave packet . . . . .	40
3.2.5	Examples with constant density of states . . . . .	41
3.2.6	Example with non-constant density of states . . . . .	43
<b>4</b>	<b>The continuum limit and the quantum jump approach</b>	<b>45</b>
4.1	The quantum jump approach: Conditional time development . . . . .	45
4.2	Conditional Hamiltonian and probability density for detection . . . . .	47



4.2.1	A simplified model . . . . .	47
4.2.2	Example with constant density of states . . . . .	50
4.2.3	Example with non-constant density of states . . . . .	51
4.2.4	The three-dimensional model with several spins . . . . .	52
4.3	Example: Detector with smooth sensitivity function . . . . .	55
4.3.1	General setup . . . . .	55
4.3.2	Eigenfunctions . . . . .	56
4.3.3	Numerical example . . . . .	59
4.4	Detector dynamics: false positives, detection, and domino effect . . . . .	61
<b>5</b>	<b>Application to arrival times: Discussion and extensions</b>	<b>65</b>
5.1	Relation of the detector model to the fluorescence model . . . . .	65
5.2	Attempts to reduce the back-reaction . . . . .	66
5.2.1	General remarks . . . . .	66
5.2.2	Large number of spins, weak coupling . . . . .	67
5.2.3	Optimized detectors . . . . .	68
5.3	Outlook: Application to passage times . . . . .	70
<b>II</b>	<b>Application to passage times</b>	<b>73</b>
<b>6</b>	<b>Passage times: Introduction</b>	<b>75</b>
6.1	Quantum passage times . . . . .	75
6.2	The dwell-time operator by Ekstein and Siegert . . . . .	76
6.3	The passage time as difference of arrival times . . . . .	78
6.4	Clock models . . . . .	79
6.4.1	The quantum clock of Wigner and Salecker . . . . .	79
6.4.2	Applications to dwell times . . . . .	80
6.5	Plan of Part II . . . . .	82
<b>7</b>	<b>Application of the spin-boson detector model</b>	<b>83</b>
7.1	Measurement scheme . . . . .	83
7.2	Quantum jump approach: The reset operation . . . . .	84
7.3	Evaluation of the reset state . . . . .	85
7.3.1	The general result . . . . .	85
7.3.2	Examples with constant and non-constant density of states . . . . .	86
7.3.3	The continuum limit . . . . .	90
7.3.4	Continuum limit: Examples . . . . .	91
7.4	Short discussion of the reset state . . . . .	92
7.5	Subsequent time development . . . . .	93
7.6	Passage-time density . . . . .	94
<b>8</b>	<b>Discussion of the passage-time density</b>	<b>97</b>
8.1	Numerical investigation . . . . .	97
8.1.1	Three examples . . . . .	97
8.1.2	Broadening mechanisms . . . . .	98
8.2	Width of the passage-time density . . . . .	102



---

8.2.1	Estimating the precision . . . . .	102
8.2.2	Optimal parameters . . . . .	103
8.2.3	A detector-independent lower bound for the width . . . .	105
<b>III</b>	<b>Summary and Conclusion</b>	<b>107</b>
<b>9</b>	<b>Time observables from a spin-boson detector model</b>	<b>109</b>
9.1	Summary . . . . .	109
9.2	Outlook . . . . .	111
<b>IV</b>	<b>Appendix</b>	<b>113</b>
<b>A</b>	<b>Pauli's 'No-Go footnote'</b>	<b>115</b>







# Chapter 1

## Introduction

The aim of the present thesis is twofold: On one hand it considers the treatment of time observables in quantum mechanics. In particular, it is concerned with the application of a particular spin-boson detector model to arrival and passage times. On the other hand it explores the possibility of extending the quantum jump approach to a model beyond its original, quantum optical framework. It also examines by means of numerical examples whether the quantum jump approach, which employs a continuum of bath modes, promises to provide a good approximation to situations where one actually has to deal with a number of discrete bath modes.

Quantum theory has been one of the most successful and most important scientific theories of the past century, and its success and importance still continue. After the introduction of the *Wirkungsquantum* by Planck in 1900 and the attempts to apply this new concept to atomic spectra by Bohr in 1913, a consistent mathematical formalism was developed in the mid-twenties, the main contributions being the matrix-mechanics by Heisenberg [Hei25] and the wave-mechanics by Schrödinger [Sch26]. Complemented with contributions of other authors as, e.g., Born and Jordan [BJ26, BHJ26] or Dirac [Dir26], the formalism was brought into that form which is still the standard in textbooks on quantum mechanics<sup>1</sup>. Since then, the importance of quantum mechanics has continuously been increasing as new branches arose. Examples for these new branches are quantum optics (including the important commercial application of the laser), the theory of semi-conductors (including the application in modern computers), and the rather new and rapidly developing field of quantum computing and quantum information.

Surprising as it might be in face of all this success, there are still open questions at the very foundations of quantum mechanics. One such a field of open questions is the treatment of time observables. This indeed may appear surprising since it is very natural for a physicist to ask questions concerning time as an observable, like, e.g., ‘When does this particle arrive at a specific position in space?’, or, ‘How much time does this particle spend in a particular region of space?’ In the framework of classical physics questions of this kind

---

<sup>1</sup>A beautiful systematic account can be found in Reference [vN32]; for details of the historical development see, e.g., [Jam74].



have a rather obvious meaning and are easily answered (at least in principle — technically, it may be pretty much complicated to conduct an appropriate experiment, but these complications are not due to conceptual difficulties concerning the meaning of ‘to arrive somewhere at a given instant of time’ or ‘to spend time in a region’). Indeed, time-of-flight experiments are a standard tool for many experimentalists. In typical time-of-flight experiments a classical treatment is justified since the particles of interest are very fast, and hence the quantum nature of their wave function plays no role. However, the advance of cooling techniques has made it possible to create ultracold gases in a trap and to produce very slow atoms, e.g., by opening the trap. For these low velocities the quantum nature of the center-of-mass wave function of an atom can have noticeable quantum effects. Such quantum effects of the center-of-mass wave function have been seen, e.g., in the diffraction and interference experiments by Szriftgiser et al. using temporal instead of spatial slits [SGOAD96].

But when a quantum mechanical treatment becomes necessary, the notion of time-related observables suddenly is far from clear. Questions concerning, e.g., position, momentum, and energy, can be treated by means of the well known position operator  $\hat{x}$ , the momentum operator  $\hat{p}$ , and the Hamiltonian  $H$ . The existence of a self-adjoint time operator conjugate to the Hamiltonian, however, is widely regarded as precluded for most systems of physical interest by an argument Pauli put forward in a famous footnote [Pau33], see Appendix A. Pauli’s argument has loopholes allowing for the definition of *bounded* time operators conjugate to a Hamiltonian [Gal02]. The main progress regarding time in quantum mechanics, though, has not been made by searching for *the* general time operator but by considering specific time-related questions.

Two of such specific time-related questions are investigated in the present thesis: In Part I we investigate some aspects of ‘arrival times’, and in Part II we consider aspects of ‘passage times’. The approach taken in this thesis may be called ‘operational’: We do *not* aim at ‘ideal’ quantities depending on the system of interest alone, which then may be linked by more or less sound arguments to some physical quantities. Instead, we will consider *Gedanken* experiments in which the system of interest is coupled to a particular measurement device, and calculate the outcome of these experiments.

In Part I a spin-boson detector model is presented and its application to the measurement of quantum arrival times is investigated. It turns out that in a continuum limit the arrival-time measurement is effectively described by means of a complex (‘absorbing’) potential model. A similar result had been obtained earlier for a particular limit of another operational approach to quantum arrival times, the so called ‘fluorescence model’. This agreement between the effective description of two physically different models helps to illuminate the physical background of complex potentials, which originally had been proposed rather heuristically. Transmission and reflection without detection as well as a detection delay are found in the present spin-boson detector model as well as in the fluorescence model, and are typical for the complex potential approach. They may thus be viewed as typical properties of arrival-time measurements, their occurrence being to some extent independent of the particular kind of model



under consideration.

In Part II the spin-boson detector model then is applied to a specific measurement scheme for quantum passage times. It turns out that detectors responding too slowly to the presence of the particle yield rather broad passage-time densities, as do detectors responding very quickly. The broadening mechanism in the latter case is seen to be a quantum effect due to the distortion of the wave function by the measurement. In intermediate cases, however, narrow densities can be obtained. For an optimal setup the precision is estimated to behave as  $E^{-3/4}$ , where  $E$  is the kinetic energy of the particle. One thus sees that an  $E^{-1}$  behavior obtained earlier with quantum clock models is not a fundamental quantum limit.

The calculational method for most of the investigation presented in the present thesis is the so called quantum jump approach. This approach was originally formulated in the framework of quantum optics and is extended in the present thesis to the spin-boson model at hand. In particular, employing the quantum jump approach means that we treat the spin-boson detector model, which originally uses discrete boson modes, by the limit of continuous boson modes and under the assumption that the Markov property holds. For a number of examples, however, results from the quantum jump approach are compared to those obtained from straightforward calculations in the discrete model with only a modest number of boson modes,  $N \approx 15 \dots 40$ . Such comparisons have been presented for the first time, to our knowledge, in References [HNS06, HNS07] on which the present thesis is based in part. There, only examples with constant density of states were considered while in the present thesis also examples with non-constant density of states are investigated. In spite of the modest number of boson modes the results are in very good agreement. This is interesting since it does not only illustrate the validity of the quantum jump approach. It further suggests that under certain conditions the continuum limit of the quantum jump approach may provide a good approximation to cases where one actually has to deal with a discrete model as, e.g., in cavity quantum optics. Such an approximation is interesting since the explicit treatment of a number of discrete bath modes typically is rather cumbersome. The quantum jump approach provides a continuum model with reduced dimensions which is much easier to work with.

Part I and Part II of the present thesis are each opened by a separate introduction. The introductions review some relevant literature, but are *not* meant to be a complete review of the extensive literature on time in quantum mechanics. A collection of contributions addressing several aspects of time in quantum mechanics, accompanied by broad references, can be found, e.g., in Reference [MSE02]. Each introduction ends with a plan of the respective part.







## Part I

# A spin-boson detector model for arrival times







## Chapter 2

# Arrival times: Introduction

Some approaches to quantum arrival times are briefly sketched. This is *not* meant to be a complete review of the extensive literature on quantum arrival times; we just gather for the reader's convenience some approaches relevant for the present thesis. For a more exhaustive and detailed review see, e.g., Reference [ML00]. Further, an outline of Part I is given.

### 2.1 Quantum arrival times

The probably simplest approach to a quantum mechanical formulation of a time-of-flight experiment is considering ‘arrival times’. One would prepare a particle at  $t = 0$  with localized but extended wave function and then ask for the arrival time of the particle at some given point of space. Repeating this experiment, one would get an ‘arrival-time density’ depending on the particle's wave function. But it is not clear from the start how one should measure the arrival time of the particle at some point of space, and what the resulting density should look like. In particular, it is not clear how this density is influenced by the spatial extent and by the spreading of the wave packet describing the particle, and to what extent it depends not only on the wave function but also on the particular measurement process.

### 2.2 Allcock's proposal: Absorbing potentials

In the late sixties Allcock investigated the problem of arrival times in quantum mechanics in a series of papers [All69a, All69b, All69c]. He suggested to include a ‘detector’ in the Hamiltonian, modeled by an imaginary step potential. This approach may appear rather heuristic since *a priori* the physical background of the imaginary potential is not clear. In main results, however, it agrees nicely with other approaches, as will be noted in the course of this introduction. Moreover, complex potentials have recently been related to particular physical models for the detection process, see Section 2.5.4. Such a relation is also seen (among other results) in the present thesis.

In case of a detector extending over the  $\mathbb{R}_+$  axis the Hamiltonian proposed



by Allcock reads

$$H = \frac{\hat{p}^2}{2m} - iV\Theta(\hat{x}),$$

where  $V > 0$  and  $\Theta$  is Heaviside's step function. This Hamiltonian is not self-adjoint, and hence the time development is not unitary. In fact, the norm of the wave function decreases, the particle being 'absorbed' into the imaginary potential. Allcock then identified the absorption rate with the measured arrival-time density at  $x = 0$ ,

$$\Pi_{\text{Allcock}}(t) = -\frac{d}{dt} \langle \psi_t | \psi_t \rangle = \frac{i}{\hbar} \langle \psi_t | H - H^\dagger | \psi_t \rangle = \frac{2V}{\hbar} \int_0^\infty dx |\langle x | \psi_t \rangle|^2. \quad (2.1)$$

To obtain the second equality the Schrödinger equation has been used.

In general, this density will not be normalized to one since part of the wave packet will be reflected from the step potential rather than being absorbed. To be specific, the eigenstate of  $H$  for energy eigenvalue  $E_k$ , corresponding to a plane wave incident from the left, is given by

$$\langle x | \Phi_k \rangle = \sqrt{\frac{1}{2\pi}} \begin{cases} e^{ikx} + R(k)e^{-ikx}, & x < 0 \\ T(k)e^{iq(k)x}, & x > 0 \end{cases},$$

where  $k = \sqrt{2mE_k}/\hbar$  and

$$q(k) = \sqrt{k^2 + i\frac{2m}{\hbar^2}V}, \quad \text{Im } q > 0. \quad (2.2)$$

The coefficients  $R$ ,  $T$  are determined by the usual matching condition that both  $\langle x | \Phi_k \rangle$  and its derivative with respect to  $x$  must be continuous at  $x = 0$ , yielding

$$R(k) = \frac{k - q}{k + q}, \quad T(k) = \frac{2k}{k + q}. \quad (2.3)$$

As can be seen from Equations (2.2) and (2.3), the coefficient  $R(k)$  for to the reflection is in general non-zero. Additionally, it depends on the wave number  $k$ . Consequently, the momentum density of the actually absorbed part of the wave packet must be expected to differ from that of the original wave packet. This leads to deviations of the absorption rate as compared to 'ideal' quantities related to the original wave packet alone. Also, since  $\text{Im } q(k) < \infty$ , the penetration depth  $[\text{Im } q(k)]^{-1}$  is non-zero. In other words, that part of the wave packet which is not reflected may penetrate to some depth into the potential before being absorbed, thus causing a 'detection delay'. In case of finite extension of the vector potential, part of the wave packet will possibly even be transmitted through the potential rather than being absorbed. This leads to a second source of non-normalization of  $\Pi_{\text{Allcock}}$ . As the reflection also the penetration depth and thus delay and transmission depend on  $k$ . It was noted already by Allcock and can also be seen from Equations (2.2) and (2.3) that decreasing  $V$  reduces reflection but enlarges delay (and transmission), and, vice versa, increasing  $V$  reduces delay (and transmission) but enlarges reflection.



Allcock though managed to obtain an ‘approximate density’ from a semi-infinite step potential as above. He investigated the limit of very small  $V$  to avoid reflection and dealt with the delay by means of a deconvolution (similar to the deconvolution technique sketched in Section 2.5). This ‘approximate density’ turns out to agree with the density derived axiomatically by Kijowski, which will be discussed in the next subsection.

The delay/transmission-versus-reflection problem was at least in part due to the fact that Allcock restricted himself to rectangular potentials. Much more recently, it has been shown in References [MBM95, PMS98] that it is possible to absorb nearly the complete wave packet in a very short spatial interval; given a wave packet of specific energy range, an appropriate imaginary potential can be constructed by means of inverse scattering techniques. A rather simple example for an optimization scheme is given in Section 5.2.3.

### 2.3 Kijowski’s axiomatic arrival-time density

Allcock’s proposal is based on the introduction of a measurement device, viz. the absorbing potential, and thus may be called ‘operational’ (although originally the physical background of the absorbing potential has not been clear). In contrast to this, Kijowski [Kij74] aimed at an ‘ideal’ arrival-time density depending on the particle’s wave function alone. We first give a rather intuitive derivation of his arrival-time density. This derivation has been suggested by Hegerfeldt. Kijowski’s original, axiomatic derivation is sketched in Section 2.3.2.

#### 2.3.1 Intuitive derivation

We first consider in one spatial dimension an ensemble of free classical particles with a normalized time-dependent phase-space density  $\varrho_t(x, p)$ . For simplicity, we stick to the case of particles with only positive momenta,  $\varrho_t(x, p) \equiv 0$  if  $p < 0$ . It is easy to see that the fraction of particles which pass the position  $x = a$  in the infinitesimal time interval  $[t, t + dt]$  is given by

$$\Pi_{\text{classical}}^{(a)}(t) dt = \int_0^\infty dp \varrho_t(a, p) \frac{p}{m} dt.$$

Thus,

$$\Pi_{\text{classical}}^{(a)}(t) = \int_0^\infty dp \varrho_t(a, p) \frac{p}{m} = \int dx \int_0^\infty dp \varrho_t(x, p) \delta(x - a) \frac{p}{m}, \quad (2.4)$$

where  $\delta$  is Dirac’s  $\delta$  function, is the classical probability density for arrival, at the time  $t$ , at the position  $x = a$ . When trying to transfer this expression to quantum mechanics, one identifies  $\varrho_t \equiv \langle \psi_t | \psi_t \rangle$  where  $|\psi_t\rangle$  is the quantum mechanical wave function, and replaces position  $x$  and momentum  $p$  with the corresponding operators  $\hat{x}$  and  $\hat{p}$ . But one also has to choose a symmetrization in  $x$  and  $p$ , which is not unique. A simple example for a symmetrization would be

$$\delta(x - a)p = \frac{1}{2} [\delta(x - a)p + p\delta(x - a)],$$



which yields the quantum mechanical flux at the time  $t$  and at the position  $x = a$ ,

$$\begin{aligned}
 J(a, t) &= -i \frac{\hbar}{2m} \left[ \overline{\psi(a, t)} \psi'(a, t) - \overline{\psi'(a, t)} \psi(a, t) \right] \\
 &= \frac{1}{2m} \int dx \left\{ \overline{\psi(x, t)} \delta(x - a) \left[ \left( -i \hbar \frac{\partial}{\partial x} \right) \psi(x, t) \right] \right. \\
 &\quad \left. + \left[ \left( i \hbar \frac{\partial}{\partial x} \right) \overline{\psi(x, t)} \right] \delta(x - a) \psi(x, t) \right\} \\
 &= \left\langle \psi_t \left| \frac{1}{2m} [\delta(\hat{x} - a) \hat{p} + \hat{p} \delta(\hat{x} - a)] \right| \psi_t \right\rangle.
 \end{aligned}$$

At first glance the quantum mechanical flux indeed appears to be a natural candidate for a quantum arrival-time density. But even for wave functions with only positive momenta,  $\tilde{\psi}(p) = 0$  if  $p < 0$ , the flux can become negative and thus cannot be regarded as a probability density. An example for this ‘backflow effect’ can be found, e.g., in Reference [HSM03].

Another possible symmetrization is

$$\delta(x - a)p = \sqrt{p} \delta(x - a) \sqrt{p},$$

which yields the positive density

$$\Pi_K^{(a)}(t) = \left\langle \psi_t \left| \frac{1}{m} \sqrt{\hat{p}} \delta(\hat{x} - a) \sqrt{\hat{p}} \right| \psi_t \right\rangle. \quad (2.5)$$

This expression can be evaluated by inserting  $\mathbb{1} = \int_{-\infty}^{\infty} dp |p\rangle \langle p|$  and  $\mathbb{1} = \int_{-\infty}^{\infty} dx |x\rangle \langle x|$ , with momentum eigenstates  $|p\rangle$  and position eigenstates  $|x\rangle$  with  $\langle x|p\rangle = \sqrt{1/2\pi\hbar} e^{ipx/\hbar}$ . One finds

$$\begin{aligned}
 \Pi_K^{(a)}(t) &= \int_0^{\infty} dp dp' \int_{-\infty}^{\infty} dx dx' \frac{1}{m} \left\langle \psi_t \left| \sqrt{\hat{p}} |p\rangle \right\rangle \langle p|x\rangle \langle x|\delta(\hat{x} - a)|x'\rangle \right. \\
 &\quad \left. \times \langle x'|p'\rangle \left\langle p' \left| \sqrt{\hat{p}} \right| \psi_t \right\rangle \right. \\
 &= \frac{1}{2\pi\hbar m} \left| \int_0^{\infty} dp \sqrt{p} e^{iap/\hbar} \tilde{\psi}_t(p) \right|^2, \quad (2.6)
 \end{aligned}$$

where  $\tilde{\psi}_t(p)$  is the wave packet in momentum space at time  $t$ . This agrees with Kijowski’s arrival-time density derived axiomatically in Section 2.3.2 [see Equation (2.6’)]. The advantage of the derivation sketched in the present subsection, however, is that the density  $\Pi_K^{(a)}$  is easily seen to emerge by an appropriate symmetrization rule from the classical arrival-time density given in Equation (2.4).



### 2.3.2 Kijowski's axiomatic derivation

Kijowski's original derivation of an ideal arrival-time density for free particles with only positive momenta is based on an axiomatic characterization of arrival-time densities. The starting point is the observation that the arrival-time density for an ensemble of *classical* point particles which at  $t = 0$  have a given position and momentum density can be uniquely characterized by a bunch of surprisingly few properties. Kijowski then showed that an analogous reasoning in quantum mechanical context also uniquely characterizes a particular density which he consequently regarded as quantum arrival-time density. In one spatial dimension his reasoning reads as follows.

First, the arrival-time problem of classical physics is considered. Let  $\varrho_0(x, p)$  be the position and momentum density which the ensemble is prepared with at  $t = 0$ ; since the particles are assumed to be free the density at a time  $t$  reads

$$\varrho_t(x, p) = \varrho_0\left(x - \frac{p}{m}t, p\right).$$

The candidates for the density of time-of-arrival at a position  $x = a$  are given by means of distributions  $F^{(a)}$ ,

$$\Pi_F^{(a)}(t) = F^{(a)}[\varrho_t] = \int dx dp F^{(a)}(x, p) \varrho_t(x, p).$$

The true arrival-time density for an ensemble of free particles,

$$\Pi_{\text{classical}}^{(a)}(t) = \int_0^\infty dp \frac{p}{m} \varrho_0\left(a - \frac{p}{m}t, p\right), \quad (2.4')$$

corresponds to the distribution

$$F_{0,\text{cl}}^{(a)}(x, p) = \frac{p}{m} \delta(x - a); \quad (2.7)$$

this is just the expression that was symmetrized in a twofold way in the preceding subsection. These distributions  $F^{(a)}$  are supposed to be positive,

$$\varrho \geq 0 \implies F^{(a)}[\varrho] \geq 0, \quad (2.8)$$

and normalized,

$$\int dx dp \varrho_0(x, p) = 1 \implies \int_{-\infty}^\infty dt F^{(a)}[\varrho_t] = 1. \quad (2.9)$$

While these are just properties of general probability densities, the specific position  $x = a$  is characterized by means of PT symmetry,

$$\varrho'(x, p) = \varrho(2a - x, p) \implies F^{(a)}[\varrho'] = F^{(a)}[\varrho]. \quad (2.10)$$

Kijowski then proves the following theorem [Kij74]:



**Theorem 2.3.1**

Let  $F^{(a)}$  fulfill Equations (2.8), (2.9), and (2.10), and let further

$$\int_{-\infty}^{\infty} dt t^2 F^{(a)}(\varrho_t) < \infty.$$

Then

$$\int_{-\infty}^{\infty} dt t F^{(a)}[\varrho_t] = \int_{-\infty}^{\infty} dt t F_{0,\text{cl}}^{(a)}[\varrho_t] =: \langle t^{(a)}[\varrho_0] \rangle \quad (2.11)$$

for all densities  $\varrho_0(x, p)$ , where  $F_{0,\text{cl}}^{(a)}$  has been defined in Equation (2.7). Further,

$$\int_{-\infty}^{\infty} dt \left( t - \langle t^{(a)}[\varrho_0] \rangle \right)^2 F^{(a)}[\varrho_t] \geq \int_{-\infty}^{\infty} dt \left( t - \langle t^{(a)}[\varrho_0] \rangle \right)^2 F_{0,\text{cl}}^{(a)}[\varrho_t],$$

and the equality sign holds for all densities  $\varrho_0(x, p)$  if and only if  $F^{(a)} = F_{0,\text{cl}}^{(a)}$ .

Theorem 2.3.1 states two interesting facts. First, Equation (2.11) means that the average arrival time is independent of the choice of  $F^{(a)}$ . Second, the true arrival-time density is uniquely characterized by the property of minimal width for all densities  $\varrho_0(x, p)$ . This characterization appears rather technical at first glance. It may become more plausible, however, by the view that for *any* given density  $\varrho_0(x, p)$  the width of the true arrival-time density is an optimum defined by the properties of  $\varrho_0$  alone; all other arrival-time densities  $\Pi_F^{(a)}$  are additionally broadened, i.e., made more uncertain by the properties of the respective  $F^{(a)}$ .

In the quantum mechanical case the particle is prepared at  $t = 0$  in a state  $|\psi_0\rangle$ . Again, Kijowski assumes that the particle is free, i.e., the Hamiltonian is given by  $H = \hat{p}^2/2m$ , and that there are only positive momenta in the momentum density,  $\langle p|\psi_0\rangle = 0$  for  $p < 0$ . We denote the space of the states under consideration<sup>1</sup> by  $\mathcal{D}_+$ . Since the particle is free the state at time  $t$  is given in momentum representation by

$$\tilde{\psi}_t(p) = e^{-ip^2 t/2m\hbar} \langle p|\psi_0\rangle.$$

The candidates for the density of time-of-arrival at a position  $x = a$  are given by bilinear forms of the wave function,

$$\Pi_F^{(a)}(t) = F^{(a)}[|\psi_t\rangle] = \int dp dp' F^{(a)}(p, p') \overline{\tilde{\psi}_t(p)} \tilde{\psi}_t(p').$$

Again, these forms are to be positive,

$$|\psi\rangle \in \mathcal{D}_+ \implies F^{(a)}[|\psi\rangle] \geq 0, \quad (2.12)$$

and normalized,

$$\| |\psi_0\rangle \|^2 = 1 \implies \int_{-\infty}^{\infty} dt F^{(a)}[|\psi_t\rangle] = 1. \quad (2.13)$$

---

<sup>1</sup>To be specific, 'states under consideration' are those space which in momentum representation  $\tilde{\psi}(p) = \langle p|\psi\rangle$  are represented by test functions with support in  $\mathbb{R}_+$ .



In order to characterize analogously to Equation (2.10) the position  $x = a$  where the arrival time is to be measured, note that a translation in position space by  $y$  amounts to a phase shift  $\tilde{\psi}(p) \mapsto e^{iyp/\hbar} \tilde{\psi}(p)$  in momentum space, and that a parity transformation  $x \mapsto -x$  amounts to a complex conjugation,  $\tilde{\psi}(p) \mapsto \overline{\tilde{\psi}(p)}$ . Thus, the analogue to Equation (2.10) reads

$$\tilde{\psi}'(p) = e^{2iap/\hbar} \overline{\tilde{\psi}(p)} \implies F^{(a)}[|\psi'\rangle] = F^{(a)}[|\psi\rangle]. \quad (2.14)$$

Kijowski then defines the density

$$\Pi_K^{(a)}(t) := \frac{1}{2\pi\hbar m} \left| \int_{-\infty}^{\infty} dp \sqrt{p} e^{iap/\hbar} \tilde{\psi}_0(p) e^{-ip^2 t/2m\hbar} \right|^2, \quad (2.6')$$

corresponding to

$$F_0^{(a)}(p, p') = \frac{1}{2\pi\hbar m} \sqrt{pp'} e^{ia(p'-p)/\hbar}. \quad (2.15)$$

In Reference [Kij74] this definition is rather *ad hoc*. We note, however, that  $\Pi_K^{(a)}$  is just the density of Equation (2.5), as evaluated in Equation (2.6); in the preceding subsection, this density was seen to emerge from the classical arrival-time density by means of an appropriate symmetrization rule. Finally, Kijowski proves the following theorem:

**Theorem 2.3.2**

Let  $F^{(a)}$  fulfill Equations (2.12), (2.13), and (2.14), and let further

$$\int_{-\infty}^{\infty} dt t^2 F^{(a)}[|\psi_t\rangle] < \infty.$$

Then

$$\int_{-\infty}^{\infty} dt t F^{(a)}[|\psi_t\rangle] = \int_{-\infty}^{\infty} dt t F_0^{(a)}[|\psi_t\rangle] =: \langle t^{(a)}(|\psi_0\rangle) \rangle$$

for all initial states  $|\psi_0\rangle \in \mathcal{D}_+$ , where  $F_0^{(a)}$  has been defined in Equation (2.15). Further,

$$\begin{aligned} \int_{-\infty}^{\infty} dt \left( t - \langle t^{(a)}(|\psi_0\rangle) \rangle \right)^2 F^{(a)}[|\psi_t\rangle] \\ \geq \int_{-\infty}^{\infty} dt \left( t - \langle t^{(a)}(|\psi_0\rangle) \rangle \right)^2 F_0^{(a)}[|\psi_t\rangle], \end{aligned}$$

and the equality sign holds for all initial states  $|\psi_0\rangle \in \mathcal{D}_+$  if and only if  $F^{(a)} = F_0^{(a)}$ .

Thus, the average arrival time is independent of the choice of  $F^{(a)}$ , and the arrival-time density  $\Pi_K^{(a)}$  given in Equation (2.6') is uniquely characterized as the narrowest one of all admissible candidates. In analogy to the classical case Kijowski therefore regarded  $\Pi_K^{(a)}$  as an ideal *quantum arrival-time density*. Further significance is lend to  $\Pi_K^{(a)}$  by the observation that it agrees with Allcock's 'approximate density' mentioned in Section 2.2, and that it can also be obtained by means of a positive operator valued measure, see Section 2.4. The relation of  $\Pi_K^{(a)}$  to a measurement based approach will be discussed in Section 2.5.



## 2.4 The time-of-arrival operator

In 1969, Aharonov and Bohm introduced in Reference [AB61] (among other things) a ‘clock’ to measure time by means of position and momentum of a freely moving test particle. In the same spirit, Muga, Sala, Palao, and Leavens, asserted in References [MSP98, MLP98] that a freely moving *classical* particle of mass  $m$  which is located at position  $x$  and has momentum  $p$  arrives at position  $a$  after a time  $t_a = m(a - x)/p$ . They concluded that, by proper symmetrization, a quantum mechanical ‘time-of-arrival operator’ related to the arrival time of a free particle at the spatial position  $x = a$  is given by

$$\hat{t}_a = \frac{m}{2} ([a - \hat{x}] \hat{p}^{-1} + \hat{p}^{-1} [a - \hat{x}]) . \quad (2.16)$$

Several mathematical properties of this operator are discussed in Reference [EM00b] (for more on  $\hat{t}_a$  see also Reference [ORU99] and references therein). We mention here that it is not self-adjoint but maximally symmetric with deficiency indices  $(2, 0)$ <sup>2</sup>. Its domain is given by those square integrable functions  $\phi$  which in momentum representation vanish at  $p = 0$  according to  $\lim_{p \rightarrow 0} \phi(p) p^{-3/2} = 0$ . For each value  $t \in \mathbb{R}$  there are two degenerate weak eigenfunctions which in momentum representation read

$$\langle k | t, \pm; a \rangle = \sqrt{\frac{\hbar |k|}{2\pi m}} e^{i\hbar k^2 t / 2m} e^{-ika} \Theta(\pm k),$$

where  $|k\rangle$  with  $\langle x | k \rangle = \sqrt{1/2\pi} e^{ikx}$  is a momentum eigenstate,  $\hat{p} |k\rangle = \hbar k |k\rangle$ , i.e.,  $k = p/\hbar$ . The eigenstates  $|t, \pm; a\rangle$  are not orthogonal but fulfill

$$\langle t', \sigma'; a | t, \sigma; a \rangle = \frac{\delta_{\sigma, \sigma'}}{2} \left( \delta(t' - t) + \frac{i}{\pi} \mathcal{P} \frac{1}{t - t'} \right), \quad \sigma, \sigma' = \pm,$$

where  $\mathcal{P}$  denotes the principal value. Still, the eigenstates  $|t, \pm; a\rangle$  provide a resolution of the identity,

$$\mathbf{1} = \sum_{\pm} \int_{-\infty}^{\infty} dT |T, \pm, a\rangle \langle T, \pm, a|.$$

This allows to define an arrival-time density in terms of a positive operator valued measure (POVM)<sup>3</sup>. The arrival-time density obtained from the Aharonov-Bohm operator  $\hat{t}_a$  given in Equation (2.16) reads

$$\begin{aligned} \Pi_{\text{AB}}^{(a)}(t) &= \left\langle \psi_0 \left| \sum_{\pm} |t, \pm, a\rangle \langle t, \pm, a| \right| \psi_0 \right\rangle \\ &= \frac{\hbar}{2\pi m} \sum_{\pm} \left| \int_0^{\infty} dk \tilde{\psi}(\pm k) \sqrt{k} e^{-i\hbar k^2 t / 2m} e^{\pm ika} \right|^2; \end{aligned}$$

<sup>2</sup>That means that the adjoint operator has two eigenstates with eigenvalue  $i$  and none with eigenvalue  $-i$ .

<sup>3</sup>POVMs generalize standard quantum mechanics: While in standard quantum mechanics observables correspond to self-adjoint operators, and probabilities are evaluated as expectation values of the projection operators onto the corresponding eigenspaces, the theory of POVMs shows that measurement probabilities can also be derived from eigenstates of maximally symmetric operators, see, e.g., Reference [BGL95].



this density is evidently positive, and for only positive momenta,  $\tilde{\psi}(k) \equiv 0$  if  $k < 0$ , it agrees with Kijowski's density  $\Pi_K^{(a)}$  given in Equation (2.6').

## 2.5 The fluorescence model

### 2.5.1 The model. Basic properties

The approaches to the arrival-time problem sketched in the preceding sections were of more mathematical nature. In particular, no measurement procedure for the density  $\Pi_K^{(a)}$  was proposed, and its status, properties, and generalizations, are still being critically discussed, see, e.g., the discussion in References [Lea02, EMNRh03, Lea05]. Complementing these approaches, an operational and realistic laser-based approach to the arrival-time problem has been investigated only recently by Hegerfeldt, Muga, and collaborators [DEHM02, HSM03, NEMH03a, DEHM03, HSMN04, RDN<sup>+</sup>04, HHM05]. This 'fluorescence model' proposes to measure the arrival time by means of laser induced fluorescence: One considers a two-level atom with center-of-mass motion, illuminates some region of space with a laser resonant on the atom's transition frequency or slightly detuned, and takes the detection time of the first fluorescence photon as measured arrival-time in the illuminated region, see Figure 2.1. The probability density for the first fluorescence photon to be detected at time

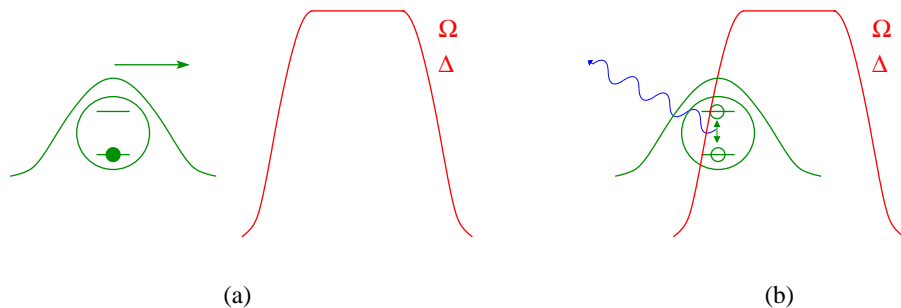


**Figure 2.1:** Basic idea of the fluorescence model for the measurement of quantum arrival times: A moving atom is described as a two level system with an extended spatial wave function. Some region of space is illuminated by a laser with Rabi frequency  $\Omega(x)$  and possibly with a detuning  $\Delta(x)$  with respect to the transition frequency of the atom. The atom is prepared in its ground state far away from the laser-illuminated region (a). When the wave function significantly overlaps the laser-illuminated region the transition between the two atomic levels is pumped by the laser, and the atom starts to emit fluorescence photons (b). The first fluorescence photon indicates the 'measured' arrival in the laser-illuminated region.

$t$  can be calculated by means of the quantum jump approach, sketched in different context in Section 4.1. It turns out [Heg03] that the state of the two-level



system, as long as no photon is detected, obeys a Schrödinger equation<sup>4</sup>

$$\begin{aligned} i\hbar \frac{\partial}{\partial t} |\Psi_{\text{cond}}^t\rangle &= \left[ \frac{\hat{p}^2}{2m} + \frac{\hbar}{2} \{ \Omega(\hat{x}) [|2\rangle\langle 1| + |1\rangle\langle 2|] \right. \\ &\quad \left. - [i\gamma + 2\Delta(\hat{x})] |2\rangle\langle 2| \} \right] |\Psi_{\text{cond}}^t\rangle \\ &=: H_{\text{cond}}^{\text{fl}} |\Psi_{\text{cond}}^t\rangle, \end{aligned} \quad (2.17)$$

where  $|1\rangle$ ,  $|2\rangle$  are the ground state and the excited state of the two-level system, resp., and  $|\Psi_{\text{cond}}^t\rangle = |\psi_1^t\rangle|1\rangle + |\psi_2^t\rangle|2\rangle$  with the spatial wave functions  $|\psi_i^t\rangle$  is the state of the two-level atom under consideration.  $\Omega(x)$  and  $\Delta(x)$  are space dependent Rabi frequency and detuning of the laser, which is treated as a classical electromagnetic field, and  $\gamma$  is the Einstein coefficient ('decay rate') of the two-level system. The subscript 'cond' stands for 'conditional', reminding the reader that this time development holds only under the condition that no fluorescence photon has been detected until time  $t$ ; the superscript 'fl' indicates the fluorescence model.

The Hamiltonian  $H_{\text{cond}}^{\text{fl}}$  defined in Equation (2.17) is not self-adjoint due to the contribution  $-i\hbar\gamma/2|2\rangle\langle 2|$ , and hence the norm of the state is not conserved. Indeed (compare Section 4.1),

$$P_0^{\text{fl}}(t) = \langle \Psi_{\text{cond}}^t | \Psi_{\text{cond}}^t \rangle$$

is the probability that no fluorescence photon is detected until  $t$ , and consequently the probability density for detecting the first fluorescence photon at time  $t$  is given by [compare Section 2.2 and in particular Equation (2.1)]

$$w_1^{\text{fl}}(t) = -\frac{d}{dt} P_0^{\text{fl}}(t) = \frac{i}{\hbar} \left\langle \Psi_{\text{cond}}^t \left| H_{\text{cond}}^{\text{fl}} - \left( H_{\text{cond}}^{\text{fl}} \right)^\dagger \right| \Psi_{\text{cond}}^t \right\rangle = \gamma \langle \psi_2^t | \psi_2^t \rangle.$$

We consider the simple case of a resonant laser illuminating the right half space,  $\Delta(x) \equiv 0$  and  $\Omega(x) = \Omega\Theta(x)$ . The eigenstate of  $H_{\text{cond}}^{\text{fl}}$  for energy eigenvalue  $E_k$ , and corresponding to a plane wave incident from the left while the atom initially is in its ground state, is given by [DEHM02]

$$\langle x | \Phi_k \rangle = \sqrt{\frac{1}{2\pi}} \begin{cases} \begin{pmatrix} e^{ikx} + R_1 e^{-ikx} \\ R_2 e^{-iqx} \end{pmatrix}, & x < 0 \\ C_+ \begin{pmatrix} 1 \\ 2\lambda_+/\Omega \end{pmatrix} e^{ik_+x} + C_- \begin{pmatrix} 1 \\ 2\lambda_-/\Omega \end{pmatrix} e^{ik_-x}, & 0 < x \end{cases}, \quad (2.18)$$

where we have set  $|1\rangle = \begin{pmatrix} 1 \\ 0 \end{pmatrix}$ ,  $|2\rangle = \begin{pmatrix} 0 \\ 1 \end{pmatrix}$ , and

$$\begin{aligned} k &= \frac{\sqrt{2mE_k}}{\hbar}, & q &= \sqrt{k^2 + i\frac{m\gamma}{\hbar}}, \quad \text{Im } q > 0, \\ \lambda_{\pm} &= -\frac{i}{4} \left( \gamma \mp \sqrt{\gamma^2 - 4\Omega^4} \right), & k_{\pm} &= \sqrt{k^2 - \frac{2m\lambda_{\pm}}{\hbar}}, \quad \text{Im } k_{\pm} \geq 0. \end{aligned} \quad (2.19)$$

---

<sup>4</sup>In the derivation of this equation the electric-dipole and rotating-wave approximations familiar from quantum optics have been used.



From the matching condition that both  $\langle x | \Phi_k \rangle$  and its derivative with respect to  $x$  have to be continuous at  $x = 0$  one finds

$$\begin{aligned} R_1 &= \frac{\lambda_+ (q + k_+) (k - k_-) - \lambda_- (q + k_-) (k - k_+)}{D}, & C_+ &= -2 \frac{k (q + k_-) \lambda_-}{D}, \\ R_2 &= \frac{k (k_- - k_+) \Omega}{D}, & C_- &= 2 \frac{k (q + k_+) \lambda_+}{D}, \end{aligned} \quad (2.20)$$

with the common denominator

$$D = (k + k_-) (q + k_+) \lambda_+ - (k + k_+) (q + k_-) \lambda_-.$$

The contribution  $R_1 e^{-ikx} |1\rangle$  corresponds to the event that the atom is reflected from the laser in ground state and will therefore never emit a fluorescence photon, leading to a non-normalized first-photon density  $w_1^{\text{fl}}(t)$ . (Remember that only the time development up to the first fluorescence photon is considered, and thus  $R_1$  is indeed the amplitude for reflection in ground state without ever having emitted a fluorescence photon.)<sup>5</sup> In addition, the pumping of occupation number from ground state  $|1\rangle$  to excited state  $|2\rangle$  and the decay  $|2\rangle \rightarrow |1\rangle$  take some time, leading to a delay in the first-photon density  $w_1^{\text{fl}}(t)$  as compared to ideal arrival-time densities. Similar to Allcock's absorbing potential approach (Section 2.2), decreasing the delay (by tuning  $\Omega$  and  $\gamma$ ) will enlarge the reflection without detection, and vice versa. Still, some interesting results could be derived from the fluorescence model; we will sketch three of these in the sequel.

### 2.5.2 The quantum mechanical flux

As can be found from Equations (2.19) and (2.20), reflection without detection becomes negligible,  $|R_1|^2 \ll 1$ , in a 'weak measurement regime'  $\Omega/\gamma \ll 1$ . Increasing  $\gamma$  with all other parameters kept fixed, however, leads to a strong delay of the first fluorescence photon. In the limit  $\gamma \rightarrow \infty$  the wave packet even remains unaffected, without reflection but also without any excitation [DEHM02]. This is consistent with the observation that a two-level system *at rest* driven for  $t > 0$  by a resonant laser has a probability density for the first fluorescence photon which reads [KKW87]

$$W(t) = \frac{\gamma \Omega^2}{4|S|^2} e^{-\gamma t/2} \left| e^{St/2} - e^{-St/2} \right|^2 \Theta(t), \quad S := \frac{1}{2} \sqrt{\gamma^2 - 4\Omega^2}. \quad (2.21)$$

This yields an average waiting time

$$\langle t_{\text{rest}} \rangle = \int_0^\infty dt t W(t) = \frac{\gamma^2 + 2\Omega^2}{\gamma \Omega^2} \sim \frac{\gamma}{\Omega^2} \rightarrow \infty, \quad \gamma \rightarrow \infty, \quad \Omega \text{ fix.} \quad (2.22)$$

<sup>5</sup>Since there are no fluorescence photons considered in the present time development, this reflection clearly cannot be due to a recoil by an emission of such a photon. Instead, it is due to the interaction of the atom with the laser field: The laser pumps occupation number from  $|1\rangle$  to  $|2\rangle$ , changing the dipole moment of the atom; this in turn changes the laser field and hence its momentum density. Because of momentum conservation, the momentum of the atom is changed. A similar effect can be seen in classical mechanics, considering an electric dipole impinging on a homogeneous magnetic field in a half space.



Aiming at arrival times, one may deal with this delay by means of a deconvolution technique similar to a proposal by Allcock [All69a, All69b, All69c]. Assuming that the first-photon density  $w_1^{\text{fl}}$  is the convolution of some ‘ideal’ arrival-time density  $\Pi_{\text{id}}$  with the probability density  $W$  given in Equation (2.21), one has

$$w_1^{\text{fl}} = \Pi_{\text{id}} * W \implies \tilde{\Pi}_{\text{id}} = \frac{\tilde{w}_1^{\text{fl}}}{\tilde{W}},$$

where the asterisk,  $*$ , denotes the convolution and the tilde,  $\sim$ , denotes the Fourier transform. By means of the inverse Fourier transform one finally obtains [DEHM02]

$$\Pi_{\text{id}}(t) \rightarrow J(t, x=0), \quad \gamma \rightarrow \infty, \quad \Omega \text{ fix},$$

where  $J$  denotes the quantum mechanical flux. Thus, the fluorescence model in the weak coupling regime and by means of a deconvolution to handle the delay provides a way to measure the quantum mechanical flux. As noted in Section 2.3.1, however, even for wave packets with only positive momenta the flux can become negative for some  $t$  (‘backflow effect’) and thus cannot be regarded as a probability density for arrival times.

### 2.5.3 Kijowski’s density

As can be seen from Equation (2.21), one can also expect to eliminate the delay by means of a limit  $\Omega \rightarrow \infty$ ,  $\Omega/\gamma = \text{const}$ ,

$$\langle t_{\text{rest}} \rangle \sim \frac{1}{\gamma} \rightarrow 0, \quad \Omega \rightarrow \infty, \quad \frac{\Omega}{\gamma} = \text{const}.$$

As can be found from Equation (2.20), however, in this limit one has  $R_1 \rightarrow -1$ , i.e., the wave packet is completely reflected. Even for large but finite  $\Omega$  and  $\gamma$  much of the wave packet is reflected in ground state, and hence the first-photon density will be far from being normalized to one. Dividing by the time-integral,  $w_1^{\text{fl}}(t) / \int_{-\infty}^{\infty} dt w_1^{\text{fl}}(t)$ , would yield a normalized probability density; but in contrast to  $w_1^{\text{fl}}$  this density is not bilinear in the wave function. Brunetti and Fredenhagen recently developed a normalization procedure which preserves the bilinear structure of the probability density [BF02]. This normalization procedure does not deal with expectation values or probability densities but directly with the quantum mechanical operators, and hence is called ‘operator normalization’; its application to the fluorescence model has been investigated in Reference [HSM03].

For the present example,  $\Delta \equiv 0$  and  $\Omega(x) = \Omega\Theta(x)$ , wave packet incident from the left with only positive momenta, operator normalization yields a normalized first-photon density [HSM03]

$$\Pi_{\text{ON}}(t) = \gamma \int_{-\infty}^{\infty} dx \int_0^{\infty} dk dk' \frac{\overline{\tilde{\psi}(k)} \tilde{\psi}(k') \overline{\Phi_k^{(2)}(x)} \Phi_{k'}^{(2)}(x) e^{i\hbar(k^2 - k'^2)t/2m}}{\sqrt{(1 - |R_1(k)|^2) (1 - |R_1(k')|^2)}} \quad (2.23)$$



where  $\tilde{\psi}$  is the momentum density of the originally prepared wave packet,  $\Phi_k^{(2)}$  is the excited state component of the eigenstate of energy  $E_k = \hbar^2 k^2 / 2m$ , and  $R_1$  is given in Equation (2.20). This normalization can be seen as changing the momentum density of the incident wave packet by a factor  $(1 - |R_1(k)|^2)^{-1/2}$ ,

$$\tilde{\psi}(k) \mapsto (1 - |R_1(k)|^2)^{-1/2} \tilde{\psi}(k).$$

This change favors those momenta which are reflected the most (i.e., typically low momenta), and in this way compensates for the reflection losses. The limit  $\Omega \rightarrow \infty$ ,  $\Omega/\gamma = \text{const}$  of Equation (2.23) has been calculated in Reference [HSM03]. It turns out that in this limit, with negligible delay as indicated above and compensating for reflection losses by means of operator normalization, Kijowski's arrival-time density is recovered [see Section 2.3 and in particular Equation (2.6')],

$$\Pi_{\text{ON}}(t) \rightarrow \Pi_K^{(a)}(t), \quad \Omega \rightarrow \infty, \quad \frac{\Omega}{\gamma} = \text{const}.$$

This is an interesting result since the justifications for Kijowski's arrival-time density so far have been of more mathematical nature: It has been derived from the classical arrival-time density by an appropriate symmetrization rule (Section 2.3.1), or, by Kijowski himself, it has been derived axiomatically based on analogy to the classical arrival-time density (Section 2.3.2); it has also been derived from the absorbing potential approach by Allcock (Section 2.2), and from the time-of-arrival operator of Section 2.4. The fluorescence model in the present limit with operator normalization provides for the first time a derivation of this density from a realistic measurement procedure.

#### 2.5.4 One-channel limit: Absorbing potential

Interesting results can also be obtained from the fluorescence model in the limit

$$\frac{\hbar|2\Delta(x) + i\gamma|}{2} \gg \frac{\hbar}{2}\Omega(x), \quad E_k. \quad (2.24)$$

The conditional Schrödinger Equation (2.17) decouples in this limit. The amplitude of the excited state of the two-level system becomes approximately proportional to the ground-state amplitude,

$$|\psi_2^t\rangle \simeq \frac{\Omega(\hat{x})}{2\Delta(\hat{x}) + i\gamma} |\psi_1^t\rangle, \quad (2.25)$$

and the conditional time independent Schrödinger equation for the ground state reads

$$\left[ \frac{\hat{p}^2}{2m} - V(\hat{x}) \right] |\psi_1^t\rangle = E_k |\psi_1^t\rangle \quad (2.26)$$

with

$$V(x) = \frac{\hbar\Delta(x)\Omega(x)^2 - i\hbar\gamma\Omega(x)^2/2}{4\Delta(x)^2 + \gamma^2}. \quad (2.27)$$



The contribution of the excited state's occupation number to the no-photon probability  $P_0^{\text{fl}}(t) = \langle \psi_1^t | \psi_1^t \rangle + \langle \psi_2^t | \psi_2^t \rangle$  can be neglected due to Equations (2.24) and (2.25), and the first-photon density is calculated by means of the one-channel model with Equations (2.26) and (2.27) alone. We note that the complex potential  $V$  from Equation (2.27) becomes purely imaginary in case of a resonant laser,  $\Delta(x) \equiv 0$ . Thus, in this 'one-channel limit' the fluorescence model provides an operational justification for Allcock's heuristically introduced absorbing potential approach of Section 2.2.

Physically, the condition specified in Equation (2.24) means that the excited state decays very rapidly compared to the time-scales of the pumping and the center-of-mass motion. Thus, the first fluorescence photon is emitted, i.e., the particle is detected, at the instant of time and at the position in space when and where the excitation took place. The only possible source of detection delay (up to the time needed for detecting the fluorescence photon, which is not included in this model) is the time needed for pumping.

### 2.5.5 Possible objections against the fluorescence model

The three interesting results sketched in the preceding section show that the fluorescence model is indeed a very useful model. There are, however, two main objections which one may raise against this model. First, it is not a fully quantum mechanical model — the pumping laser is modeled as a classical electromagnetic field. Second, there is a strong back-reaction on the particle under consideration which includes the possibility of reflection without detection. In extreme cases this may render the measurement useless, in any case it requires some sophistication to obtain useful results. This strong back-reaction is not surprising since the measurement scheme is based on a strong interaction with the particle under consideration through its internal degrees of freedom.

Both objections do not apply to the spin-boson detector model investigated in the present thesis. This model is formulated in fully quantum mechanical terms (see Section 3.1), and the particle under consideration does not interact via its internal degrees of freedom with the measurement device. Indeed, internal degrees of freedom of the particle are not at all included in the model. The measurement procedure rather regards the particle only as a catalyst for a transition in the detector and its associated environment. As regards to these two points, the spin-boson model is fundamentally different from the fluorescence model. The investigation of such model is interesting whether or not the results will turn out to agree with the fluorescence model: If some results differ from those obtained from the fluorescence model, this will help to identify apparatus dependent artefacts; if other results of the two different models agree, it is more likely that these results indeed show intrinsic features of quantum arrival-times (or any other time observable where different measurement schemes yield the same results).



## 2.6 Plan of Part I

Part I is organized as follows. Chapter 3 is devoted to the introduction of the spin-boson detector model and to a first investigation of a simplified, single-spin model by means of standard unitary quantum mechanics. In particular, a Jaynes-Cummings like model with only one boson mode is investigated analytically in Section 3.2.3. The model with several, discrete boson modes is investigated numerically by considering a couple of examples in Sections 3.2.5 and 3.2.6. In Chapter 4 we treat the limit of continuous boson modes, under the assumption that the Markov property holds. The calculational method is the so called ‘quantum jump approach’ which in the present thesis is extended from quantum optics to the spin-boson model at hand. The main ideas of this approach, as far as they are relevant in the present context, are sketched in Section 4.1. For greater clarity we start the application of the quantum jump approach with the simplified, single-spin model. The continuum limit of the examples considered in Sections 3.2.5 and 3.2.6 is evaluated numerically in Sections 4.2.2 and 4.2.3, and the results are compared to those obtained in the case of discrete boson modes. The extension of the continuum limit to the full, three-dimensional model with several spins is presented in Section 4.2.4. In Chapter 5 we discuss the relation of the spin-boson model to the fluorescence model (Section 5.1) as well as possible optimization schemes (Section 5.2).







## Chapter 3

# The spin-boson detector model

A particular model for the measurement of arrival-time densities is presented. The detector consists of a collection of spins in a metastable state; in the presence of the particle the coupling of the spins to their environment is enhanced. The appearance of bosons from particular spins signals the presence of the particle at the spin location, the first boson indicates its arrival. Further, a simplified model is introduced, consisting of only one spin and considering only one spatial dimension. This simplified model allows for a discussion by means of standard, unitary quantum mechanics. An analytical treatment is given to some extent for the case of a single boson mode, comparable to the Jaynes-Cummings model of quantum optics. For the case of several, discrete boson modes examples are investigated numerically.

### 3.1 The spin-boson detector model

#### 3.1.1 Physical idea

An interesting quantum mechanical model for particle detection has been suggested some years ago by Schulman. The internal dynamics of the detector, in particular the probability of erroneous detections and the details of the amplification process, have been investigated (partly in collaboration with Gaveau) in References [GS90, Sch91, Sch97]. Thus, we will remark only rather briefly on these issues. The internal dynamics of the detector have been discussed by means of quantum mechanics in these references, while the motion of the particle was assumed to be classical. In the present context of quantum arrival times, though, we are particularly interested in the effects of the quantum nature of the center-of-mass motion. These effects will be investigated in the subsequent chapters.

The physical idea of the model is as follows: The detector consists of a three-dimensional array of spins with ferromagnetic interaction. In the presence of a homogeneous magnetic field, and for sufficiently low temperature, all spins are aligned with the field. Reversing the field very fast, such that the spins



cannot follow the reversal, one can produce a metastable state of this compound spin system, see Figure 3.1 (a). If the strength of the field is just above the threshold for a single spin flip to be energetically favorable, and if the coupling of the spins to their environment (the ‘bath’) is only weak, this state can be very long-living. But when the particle’s wave function overlaps with that of a spin, the coupling of this spin to the bath is strongly enhanced. Thus when the particle is close to a spin, this spin flips much faster due to the enhanced spin-bath coupling, and a boson of the according energy is created, see Figure 3.1 (b). By means of the ferromagnetic interaction, the flipped spin in turn triggers the subsequent spontaneous flipping of the neighboring spins, and finally by a kind of domino effect of all spins, even in the absence of the particle. Each spin flip is accompanied by a boson creation. In this way, the single spin flip induced by the presence of the particle is amplified to a macroscopic event, see Figure 3.1 (c). Either the change in the detector state or in the bath state can be measured.

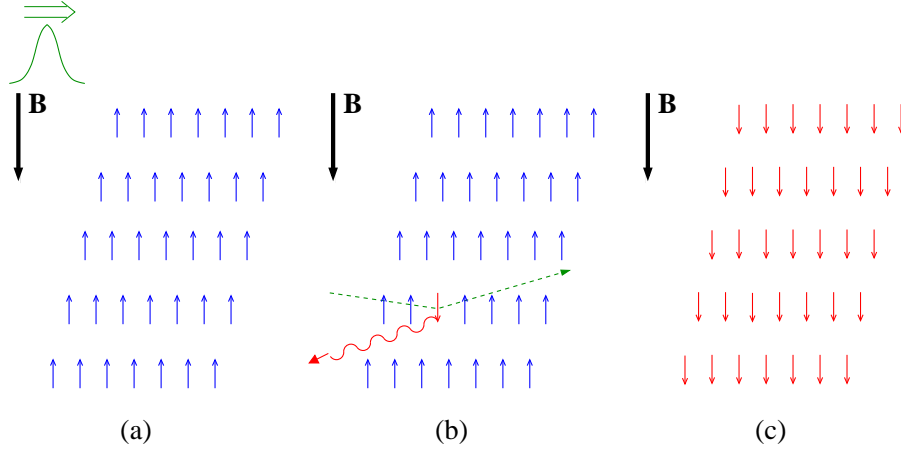


**Figure 3.1:** Initially, the detector is in a metastable state (a). When the particle is close to a spin, the spin-bath coupling is strongly enhanced; this spin flips and a boson of the according energy is created (b). Due to the reduced ferromagnetic forces, all spins flip by a kind of domino effect even in the absence of the particle (c).

**Remark 3.1.1** Apart from the particular realization, the spin-boson detector model is essentially based on the idea of using a detection device which is initially in a metastable state; the microscopic interaction with the particle under consideration then triggers the macroscopic transition to an energetically favorable state. This is indeed a realistic and important concept. It is realized, e.g., in the familiar cloud chamber: The chamber is filled with a gas in a metastable state, and a passing particle ionizes a gas molecule. This ionized molecule then serves as a germ for condensation, which is a macroscopic event. Thus, the spin-boson detector model is more than a mere toy-model for a *Gedanken* experiment. It is worthwhile to be investigated as a solvable model incorporating



a realistic concept of measurement and amplification.

### 3.1.2 Hamiltonian

The mathematical description for the spin-boson detector model sketched in the preceding subsection is based on the following Hamiltonian. Let the excited state of the  $j^{\text{th}}$  spin be denoted by  $|\uparrow\rangle_j$  and its ground state by  $|\downarrow\rangle_j$ , and define

$$\hat{\sigma}_z^{(j)} := |\uparrow\rangle_j \langle \uparrow| - |\downarrow\rangle_j \langle \downarrow|.$$

The Hamiltonian for the detector alone is given by

$$H_{\text{det}} = \frac{1}{2} \sum_j \hbar \omega_0^{(j)} \hat{\sigma}_z^{(j)} - \frac{1}{2} \sum_{j < k} \hbar \omega_j^{(jk)} \hat{\sigma}_z^{(j)} \otimes \hat{\sigma}_z^{(k)}, \quad (3.1)$$

where  $\hbar \omega_0^{(j)}$  is the energy difference between ground state and excited state of the  $j^{\text{th}}$  spin, and  $\hbar \omega_j^{(jk)} \geq 0$  is the coupling energy between the spins  $j$  and  $k$ . The environment is modeled as bath of bosons (phonons or photons) with wave vectors  $\boldsymbol{\ell}$  and energy  $\hbar \omega_{\boldsymbol{\ell}}$ ,  $\ell = \|\boldsymbol{\ell}\|$ . The free Hamiltonian of the environment is

$$H_{\text{bath}} = \sum_{\boldsymbol{\ell}} \hbar \omega_{\boldsymbol{\ell}} \hat{a}_{\boldsymbol{\ell}}^\dagger \hat{a}_{\boldsymbol{\ell}},$$

where  $\hat{a}_{\boldsymbol{\ell}}$  is the annihilation operator for a boson with wave vector  $\boldsymbol{\ell}$ . In Chapter 4 a continuum limit for the boson modes will be taken. In general, the spins will be coupled to the bath, and there is the possibility of spontaneous spin flips due to

$$H_{\text{spn}} = \sum_{j, \boldsymbol{\ell}} \hbar \left( \gamma_{\boldsymbol{\ell}}^{(j)} e^{i f_{\boldsymbol{\ell}}^{(j)}} \hat{a}_{\boldsymbol{\ell}}^\dagger \hat{\sigma}_-^{(j)} + \text{H.c.} \right).$$

There,  $\hat{\sigma}_-^{(j)}$  is the lowering operator for the  $j^{\text{th}}$  spin, its adjoint being the corresponding raising operator which is denoted by  $\hat{\sigma}_+^{(j)}$ ,

$$\hat{\sigma}_-^{(j)} := |\downarrow\rangle_j \langle \uparrow|, \quad \hat{\sigma}_+^{(j)} := \left( \hat{\sigma}_-^{(j)} \right)^\dagger = |\uparrow\rangle_j \langle \downarrow|.$$

The coupling constants  $\gamma_{\boldsymbol{\ell}}^{(j)}$  and the phases  $f_{\boldsymbol{\ell}}^{(j)}$  depend on the particular realization of the detector and the bath. The crucial ingredient, now, is the enhancement of the coupling between the  $j^{\text{th}}$  spin and the bath when the particle is close to this spin. Let the  $j^{\text{th}}$  spin be located in a spatial region  $\mathcal{G}^{(j)}$ . The enhancement is taken to be proportional to a sensitivity function  $\chi^{(j)}$  which vanishes outside  $\mathcal{G}^{(j)}$ . An example would be the characteristic function which is 1 on  $\mathcal{G}^{(j)}$  and zero outside, but other and in particular smooth sensitivity functions are also allowed. The additional coupling depending on the particle's position is thus

$$H_{\text{coup}} = \sum_j \chi^{(j)}(\hat{\mathbf{x}}) \sum_{\boldsymbol{\ell}} \hbar \left( g_{\boldsymbol{\ell}}^{(j)} e^{i f_{\boldsymbol{\ell}}^{(j)}} \hat{a}_{\boldsymbol{\ell}}^\dagger \hat{\sigma}_-^{(j)} + \text{H.c.} \right), \quad (3.2)$$



with

$$|g_{\ell}^{(j)}|^2 \gg |\gamma_{\ell}^{(j)}|^2. \quad (3.3)$$

The full Hamiltonian finally is

$$H = H_{\text{part}} + H_{\text{det}} + H_{\text{bath}} + H_{\text{spon}} + H_{\text{coup}}, \quad (3.4)$$

where  $H_{\text{part}}$  is the free Hamiltonian of the particle,

$$H_{\text{part}} = \frac{\hat{\mathbf{p}}^2}{2m}.$$

**Remark 3.1.2** We note that in the coupling Hamiltonians  $H_{\text{coup}}$  and  $H_{\text{spon}}$  a boson creation operator  $\hat{a}_{\ell}^{\dagger}$  is always accompanied by a spin lowering operator  $\hat{\sigma}_{-}^{(j)}$ , and, vice versa, a boson annihilation operator  $\hat{a}_{\ell}$  is always accompanied by a spin raising operator  $\hat{\sigma}_{+}^{(j)}$ . Thus, the ‘excitation number’, i.e., the sum of the number of bosons and the number of up-spins, is a conserved quantity in the present model.

### 3.1.3 The detection process

The detection process starts with the bath in its ground state  $|0\rangle$  (no bosons present) and all  $D$  spins in the excited state  $|\uparrow_1 \dots \uparrow_D\rangle$ . In view of Remark 3.1.2 it is sufficient to measure the vacuum state  $|0\rangle$  of the bath in order to check whether or not a spin has flipped. We stress that no direct observation of the particle or the detector is necessary, and that there is no explicit interaction of the particle with the detector or the bath. The particle is merely regarded as a catalyst for a change in the detector-bath state.

The general ideas of the detection and the subsequent amplification have been sketched in Section 3.1.1, see in particular Figure 3.1. Two issues are of particular importance for the usability of the spin-boson model as a detector for a moving particle: the likelihood of a ‘false positive’, i.e., a spontaneous first spin flip in the absence of the particle, and an understanding of the amplification process. Both have been investigated in detail in References [GS90, Sch91, Sch97] by means of standard, unitary quantum mechanics. The main results, however, can also be found from the results presented in Chapter 4, obtained by means of the quantum jump approach (see Section 4.1). We will comment on these issues in Section 4.4, when the relevant equations have been derived.

## 3.2 Investigation by unitary quantum mechanics

### 3.2.1 A simplified model

We first consider a simplified model consisting of a particle in one dimension and only one spin. This simplification is reasonable if the radius of the coupling region  $\mathcal{G}^{(j)}$  is smaller than the distance between the spins<sup>1</sup>. The vectors  $\mathbf{x}$  and

<sup>1</sup>In Section 3.2.2, however, for calculational convenience we will extend the region  $\mathcal{G}^{(j)}$  to a half-line,  $\chi(x) \rightarrow \Theta(x)$ .



$\ell$  are replaced by  $x$  and  $\ell$ . Also, we will neglect  $H_{\text{spn}}$  in view of Equation (3.3). Obviously, false positives and amplification play no role in this simplified model. We will therefore concentrate on the evaluation of the probability density for the spin to flip, indicating the particle's arrival.

The free Hamiltonian for the particle motion in one dimension is

$$H_{\text{part}}^{\text{1d}} = \frac{\hat{p}^2}{2m}, \quad (3.5)$$

and the free detector Hamiltonian with only one spin simplifies to

$$H_{\text{det}}^1 = \frac{\hbar\omega_0}{2}\hat{\sigma}_z.$$

The free bath Hamiltonian is given by

$$H_{\text{bath}}^{\text{1d}} = \sum_{\ell} \hbar\omega_{\ell} \hat{a}_{\ell}^{\dagger} \hat{a}_{\ell}. \quad (3.6)$$

Further, let the spin be located in the interval  $[0, d] \equiv \mathcal{I}_d$  so that

$$H_{\text{coup}}^{1,\text{1d}} = \chi_{\mathcal{I}_d}(\hat{x}) \sum_{\ell} \hbar \left( g_{\ell} e^{if_{\ell}} \hat{a}_{\ell}^{\dagger} \hat{\sigma}_- + \text{H.c.} \right),$$

where  $\chi_{\mathcal{I}_d}$  is the characteristic function of the interval  $\mathcal{I}_d$  or, more general, a smoothed out version of the characteristic function. The full Hamiltonian of the simplified model is then given by

$$H^{1,\text{1d}} = H_{\text{part}}^{\text{1d}} + H_{\text{det}}^1 + H_{\text{bath}}^{\text{1d}} + H_{\text{coup}}^{1,\text{1d}}.$$

This simplified model allows for a direct investigation by means of standard quantum mechanics.

### 3.2.2 Energy eigenstates

#### Evaluation of the relevant eigenstates

In order to get a first idea of how the spin-boson detector model works for an arrival-time measurement, we simplify the model a little further in the remainder of this chapter: We assume the detector to be semi-infinite, extended over the whole  $\mathbb{R}_+$  axis, and temporarily take

$$\chi_{\mathcal{I}_d}(x) = \Theta(x),$$

where  $\Theta$  is Heaviside's step function. In addition, we assume  $f_{\ell} \equiv 0$  for the phases in the coupling Hamiltonian. The stationary Schrödinger equation with energy eigenvalue  $E_k$ ,

$$H^{1,\text{1d}} |\Phi\rangle = E_k |\Phi\rangle,$$



can be solved piecewise in position space. For a plane wave coming from the left, initially no bosons present, and the spin in state  $|\uparrow\rangle$ , the solution for  $x < 0$  simply reads

$$\Phi_k^<(x) = \sqrt{\frac{1}{2\pi}} \left( \left[ e^{ikx} + R_0(k) e^{-ikx} \right] |\uparrow \ 0\rangle + \sum_{\ell} R_{\ell}(k) e^{-ik_{\ell}(k)x} |\downarrow \ 1_{\ell}\rangle \right), \quad k > 0, \quad (3.7)$$

where the wave numbers  $k$ ,  $k_{\ell}(k)$  are fixed by

$$\frac{\hbar^2 k^2}{2m} + \frac{\hbar\omega_0}{2} = E_k = \frac{\hbar^2 k_{\ell}(k)^2}{2m} - \frac{\hbar\omega_0}{2} + \hbar\omega_{\ell}, \quad (3.8)$$

and  $|\uparrow \ 0\rangle = |\uparrow\rangle |0\rangle$ ,  $|\downarrow \ 1_{\ell}\rangle$  accordingly. We note that

$$k_{\ell}(k) = \sqrt{k^2 + \frac{2m}{\hbar}(\omega_0 - \omega_{\ell})}$$

is imaginary if

$$\omega_{\ell} > \frac{\hbar k^2}{2m} + \omega_0. \quad (3.9)$$

In this case we choose the root with  $\text{Im } k_{\ell}(k) > 0$ , yielding an evanescent wave<sup>2</sup>. Otherwise,  $k_{\ell}(k) > 0$ .

We further note that there is the possibility that the particle is reflected from the detector. It may either be reflected with the detector spin flipped and a boson of mode  $\ell$  created, i.e., the particle has been detected. The coefficient for this event is  $R_{\ell}(k)$ . Or, it may be reflected without being detected, the coefficient being  $R_0(k)$ . The latter will lead to a non-normalized arrival-time density. As in the cases of Allcock's absorbing potentials (see Section 2.2) and of the fluorescence model (see Section 2.5), this no-detection probability is in general momentum dependent. Hence, the momentum density of the actually detected part of the wave packet must again be expected to differ from that of the originally prepared wave packet, leading to deviations of the 'measured' arrival-time density from corresponding 'ideal' quantities.

For  $x > 0$  the operator

$$H_{\Delta} := \left[ H^{1,\text{1d}} - \frac{\hat{p}^2}{2m} \right]_{x>0} = \frac{1}{2} \hbar\omega_0 \hat{\sigma}_z + \sum_{\ell} \hbar\omega_{\ell} \hat{a}_{\ell}^{\dagger} \hat{a}_{\ell} + \sum_{\ell} \hbar \left( g_{\ell} \hat{a}_{\ell}^{\dagger} \hat{\sigma}_{-} + \text{H.c.} \right)$$

is independent of  $x$ , due to the assumption  $\chi_{x_d}(x) = \Theta(x)$ , and it commutes with  $\hat{p}^2/2m$ . Since  $H_{\Delta}$  is a Hermitian operator its eigenvalues are real. They will be denoted by  $\hbar\Omega_{\mu}/2$ . The corresponding eigenvectors are superpositions of  $|\uparrow \ 0\rangle$  and  $|\downarrow \ 1_{\ell}\rangle$  and denoted by  $|\mu\rangle$  so that

$$H_{\Delta} |\mu\rangle = \frac{\hbar\Omega_{\mu}}{2} |\mu\rangle. \quad (3.10)$$

---

<sup>2</sup> Ascribing to the incident particle a kinetic energy  $\hbar^2 k^2/2m$ , and to the spin flip an energy gain  $\hbar\omega_0$ , one may wonder if the situation described by Equation (3.9) should not be forbidden by energy conservation. We note that this is not the case since states of the form  $|k\rangle |\uparrow\rangle |0\rangle$  or  $|-k_{\ell}\rangle |\downarrow\rangle |1_{\ell}\rangle$  are no eigenstates of the Hamiltonian and thus do not possess a definite energy.



The eigenvalues  $\hbar\Omega_\mu/2$  may be calculated numerically, using the matrix representation of  $H_\Delta$  in the basis of the states  $|\uparrow 0\rangle, |\downarrow 1_\ell\rangle$ <sup>3</sup>. Once they are known, the eigenvectors  $|\mu\rangle$  can be calculated in terms of the states  $|\uparrow 0\rangle, |\downarrow 1_\ell\rangle$  by a calculation outlined in Reference [GS95]: Multiplying Equation (3.10) from the left with  $\langle\uparrow 0|, \langle\downarrow 1_\ell|$ , resp., yields

$$\begin{aligned} \frac{\hbar\omega_0}{2} \langle\uparrow 0|\mu\rangle + \sum_\ell \hbar\overline{g_\ell} \langle\downarrow 1_\ell|\mu\rangle &= \frac{\hbar\Omega_\mu}{2} \langle\uparrow 0|\mu\rangle \\ \hbar(\omega_\ell - \omega_0/2) \langle\downarrow 1_\ell|\mu\rangle + \hbar g_\ell \langle\uparrow 0|\mu\rangle &= \frac{\hbar\Omega_\mu}{2} \langle\downarrow 1_\ell|\mu\rangle. \end{aligned}$$

From the second equation one has

$$\langle\downarrow 1_\ell|\mu\rangle = \frac{g_\ell \langle\uparrow 0|\mu\rangle}{\frac{1}{2}(\Omega_\mu + \omega_0) - \omega_\ell}. \quad (3.11)$$

Substituting this into the normalization condition

$$|\langle\uparrow 0|\mu\rangle|^2 + \sum_\ell |\langle\downarrow 1_\ell|\mu\rangle|^2 = 1$$

finally yields<sup>4</sup>

$$\langle\uparrow 0|\mu\rangle = \frac{1}{\sqrt{1 + \sum_\ell \frac{|g_\ell|^2}{[(\Omega_\mu + \omega_0)/2 - \omega_\ell]^2}}}. \quad (3.12)$$

Calculating  $\langle\uparrow 0|\mu\rangle$  from Equation (3.12) and substituting the result in Equation (3.11) gives the eigenvectors  $|\mu\rangle$  in terms of the  $|\uparrow 0\rangle, |\downarrow 1_\ell\rangle$ . In a numerical calculation, obtaining the  $|\mu\rangle$  this way will be much faster than using some standard algorithm for the evaluation of the eigenvectors of a general matrix, especially for large  $N$ .

To obtain now an eigenvector of  $H^{1,1d}$  on  $x > 0$  for the eigenvalue  $E_k$ , one has to choose an eigenfunction  $e^{iq_\mu(k)x}$  of  $\hat{p}^2/2m$  such that

$$E_k = \frac{[\hbar q_\mu(k)]^2}{2m} + \frac{\hbar\Omega_\mu}{2}.$$

From Equation (3.8) one has

$$q_\mu(k) = \sqrt{k^2 + \frac{m}{\hbar}(\omega_0 - \Omega_\mu)}. \quad (3.13)$$

Note that  $q_\mu(k)$  is imaginary if  $\Omega_\mu > \omega_0$  and

$$k^2 < \frac{m}{\hbar}(\Omega_\mu - \omega_0),$$

---

<sup>3</sup>This subspace of spin-bath states with excitation number 1 is sufficient since the detection process will start with detector and bath in state  $|\uparrow 0\rangle$ , see Section 3.1.3. The time development is then bound to the subspace of states with excitation number 1, due to excitation number conservation, see Remark 3.1.2.

<sup>4</sup>Actually, only the modulus of  $\langle\uparrow 0|\mu\rangle$  is fixed by Equation (3.11) and the normalization condition. The phase, however, turns out to be a meaningless overall-phase and is chosen according to convenience.



leading to exponential decay. Otherwise  $q_\mu(k)$  is real. The solution of the stationary Schrödinger equation for  $x > 0$  belonging to the eigenvalue  $E_k$  can then be written as

$$\Phi_k^>(x) = \sqrt{\frac{1}{2\pi}} \sum_{\mu} \alpha_{\mu}(k) e^{iq_{\mu}(k)x} |\boldsymbol{\mu}\rangle. \quad (3.14)$$

The coefficients  $\alpha_{\mu}(k)$ ,  $R_0(k)$ ,  $R_{\ell}(k)$  are obtained from the usual matching condition, i.e., both

$$\langle x | \Phi_k \rangle := \begin{cases} \Phi_k^<(x) & \text{if } x < 0 \\ \Phi_k^>(x) & \text{if } x \geq 0 \end{cases} \quad (3.15)$$

and its first derivative with respect to  $x$  have to be continuous at  $x = 0$ . To be specific, after multiplication from the left with  $\langle \uparrow 0 |$ ,  $\langle \downarrow 1_{\ell} |$ , resp., the matching conditions read

$$\begin{aligned} 1 + R_0(k) &= \sum_{\mu} \alpha_{\mu}(k) \langle \uparrow 0 | \boldsymbol{\mu} \rangle \\ ik - ikR_0(k) &= \sum_{\mu} iq_{\mu}(k) \alpha_{\mu}(k) \langle \uparrow 0 | \boldsymbol{\mu} \rangle \\ R_{\ell}(k) &= \sum_{\mu} \alpha_{\mu}(k) \langle \downarrow 1_{\ell} | \boldsymbol{\mu} \rangle \\ -ik_{\ell}(k)R_{\ell}(k) &= \sum_{\mu} iq_{\mu}(k) \alpha_{\mu}(k) \langle \downarrow 1_{\ell} | \boldsymbol{\mu} \rangle. \end{aligned} \quad (3.16)$$

For  $N$  boson modes, this is a system of  $2(N+1)$  coupled equations. We note that these equations depend on  $k$  and thus when investigating a wave packet, and integrating over  $k$ , they have to be solved for every  $k$  individually. The numerical effort can be reduced a little by eliminating  $R_0$ ,  $R_{\ell}$  from the equation system, and then solving the resulting system for the  $\alpha_{\mu}$ ,

$$\begin{aligned} 2k &= \sum_{\mu} [k + q_{\mu}(k)] \alpha_{\mu}(k) \langle \uparrow 0 | \boldsymbol{\mu} \rangle \\ 0 &= \sum_{\mu} [k + q_{\mu}(k)] \alpha_{\mu}(k) \langle \downarrow 1_{\ell} | \boldsymbol{\mu} \rangle. \end{aligned} \quad (3.17)$$

Then, one evaluates  $R_0$ ,  $R_{\ell}$  by substituting  $\alpha_{\mu}$  into Equations (3.16). However, Equations (3.17) still form a system of  $N+1$  coupled equations, dependent on  $k$ . Thus the numerical investigation of the time development of a wave packet still is rather time consuming.

### Subspace of states, orthogonality and normalization

The remainder of this subsection is devoted to some technical remarks.

We first note that the energy eigenstate  $|\Phi_k\rangle$  of Equation (3.15) is not the only state with energy eigenvalue  $E_k$ , even if one considers only states with



excitation number 1. A full basis of the space of states with excitation number 1 would be obtained by taking into account a number of further states. First, there are states corresponding to plane waves incident from the left but with the detector spin in its ground state and one boson present, described for  $x < 0$  by

$$\begin{aligned} \Phi_{k; \downarrow, \ell}^<(x) = & \sqrt{\frac{1}{2\pi}} \left( \left[ e^{ik_\ell x} + R_\ell^{(\downarrow, 1_\ell)}(k_\ell) e^{-ik_\ell x} \right] |\downarrow, 1_\ell\rangle \right. \\ & \left. + \sum_{\ell' \neq \ell} R_{\ell'}^{(\downarrow, 1_\ell)}(k_\ell) e^{-ik_{\ell'}(k_\ell)x} |\downarrow, 1_{\ell'}\rangle + R_0^{(\downarrow, 1_\ell)}(k_\ell) e^{-ik(k_\ell)x} |\uparrow, 0\rangle \right) \end{aligned}$$

where  $k_\ell$ ,  $k_{\ell'}$  and  $k$  are related to  $E_k$  as in Equation (3.8). Further, there are states corresponding to left going waves, described for  $x < 0$  by

$$\begin{aligned} \Phi_{-k; \uparrow, 0}^< &= \sqrt{\frac{1}{2\pi}} T_{\uparrow, 0}(k) e^{-ikx} |\uparrow, 0\rangle \\ \Phi_{-k; \downarrow, 1_\ell}^< &= \sqrt{\frac{1}{2\pi}} T_{\downarrow, 1_\ell}(k_\ell) e^{-ik_\ell x} |\downarrow, 1_\ell\rangle. \end{aligned}$$

For  $x > 0$ , these states can be calculated similar to the preceding subsection, although for the latter states of course contributions containing  $e^{-iq_\mu(k_\ell)x}$  have to be taken into account.

However, we are interested in states which asymptotically, for very early times  $t' \rightarrow -\infty$ , behave as free states incident from the left while detector spin and boson bath are in state  $|\uparrow, 0\rangle$ . To be more specific, if  $|\Psi_{t'}\rangle$  denotes the state of the complete system, spin, bath, and particle, at time  $t'$ , we are interested in states for which

$$|\Psi_{t'}\rangle \sim e^{-i\omega_0 t'/2} |\uparrow, 0\rangle \int_0^\infty dk \tilde{\psi}(k) e^{-i\hbar k^2 t'/2m} |k\rangle, \quad t' \rightarrow -\infty \quad (3.18)$$

holds, where  $|k\rangle$  with  $\langle x|k\rangle = \sqrt{1/2\pi} e^{ikx}$ ,  $k > 0$  is the free momentum eigenstate, and  $\tilde{\psi}$  is the momentum density of the incoming, asymptotically free state. These states belong to the subspace spanned by the  $|\Phi_k\rangle$  evaluated in the preceding subsection: For very early times  $|\Psi_{t'}\rangle$  is located very far on the left side,

$$\Psi_{t'}(x) = \langle x | \Psi_{t'} \rangle \rightarrow 0, \quad x > 0, \quad t' \rightarrow -\infty.$$

Consequently, being interested in the overlap of  $|\Psi_{t'}\rangle$  with the energy eigenstates  $|\Phi_k\rangle$ , we have

$$\begin{aligned} \langle \Phi_k | \Psi_{t'} \rangle &= \int_{-\infty}^\infty dx \overline{\Phi_k(x)} \Psi_{t'}(x) \\ &\sim \int_{-\infty}^\infty dx \overline{\Phi_k^<(x)} \Psi_{t'}(x) \sim \tilde{\psi}(k) e^{-iE_k t'/\hbar}, \quad t' \rightarrow -\infty, \end{aligned}$$



where  $\Phi_k^<$  is extended to the whole real axis, and  $E_k$  is given in Equation (3.8). Similarly, one has

$$\langle \Phi_{k; \downarrow 1_\ell} | \Psi_{t'} \rangle \sim \langle \Phi_{-k; \uparrow 0} | \Psi_{t'} \rangle \sim \langle \Phi_{-k; \downarrow 1_\ell} | \Psi_{t'} \rangle \sim 0, \quad t' \rightarrow -\infty.$$

Thus, at a very early time  $t'$  the asymptotically free state can be expanded into the states  $|\Phi_k\rangle$ ,

$$|\Psi_{t'}\rangle \sim \int_0^\infty dk |\Phi_k\rangle \langle \Phi_k | \Psi_{t'} \rangle = \int_0^\infty dk \tilde{\psi}(k) e^{-iE_k t'/\hbar} |\Phi_k\rangle, \quad t' \rightarrow -\infty. \quad (3.19)$$

Since the states  $|\Phi_k\rangle$  are eigenstates of the Hamiltonian the state  $|\Psi_t\rangle$  for all times remains in the subspace spanned by the  $|\Phi_k\rangle$ . From the expansion in Equation (3.19) the time development of the scattering state  $|\Psi_t\rangle$  is obtained by applying  $e^{-iH^{1,1d}(t-t')/\hbar}$ , yielding

$$|\Psi_t\rangle = \int_0^\infty dk \tilde{\psi}(k) |\Phi_k\rangle e^{-iE_k t/\hbar}. \quad (3.20)$$

Orthogonality and normalization of the eigenstates  $|\Psi_k\rangle$  can be calculated directly from Equations (3.7), (3.14), and (3.15), but are most easily seen by means of the asymptotic freedom of the scattering states. We consider two asymptotically free states,  $|\Psi_t^{(j)}\rangle$ ,  $j = 1, 2$  with

$$|\Psi_t^{(j)}\rangle = \int_0^\infty dk \tilde{\psi}^{(j)}(k) |\Phi_k\rangle e^{-iE_k t/\hbar}.$$

The overlap between these two states for very early times can be evaluated by means of the asymptotic freedom, i.e., by replacing  $|\Phi_k\rangle$  with the free momentum and spin-bath eigenstate  $|k\rangle |\uparrow 0\rangle$  [compare Equation (3.18)], yielding

$$\langle \Psi_t^{(1)} | \Psi_t^{(2)} \rangle \sim \int_0^\infty dk \overline{\tilde{\psi}^{(1)}(k)} \tilde{\psi}^{(2)}(k), \quad t \rightarrow -\infty.$$

For  $t = 0$  one finds

$$\langle \Psi_0^{(1)} | \Psi_0^{(2)} \rangle = \int_0^\infty dk dk' \overline{\tilde{\psi}^{(1)}(k)} \tilde{\psi}^{(2)}(k') \langle \Phi_k | \Phi_{k'} \rangle.$$

The two expressions must agree, due to the unitarity of the time development, and since this argument is independent of the choice of the functions  $\tilde{\psi}^{(j)}$  we have

$$\langle \Phi_k | \Phi_{k'} \rangle = \delta(k - k').$$

### 3.2.3 Jaynes-Cummings approach

Already for a rather modest number of boson modes  $N \sim \mathcal{O}(10)$ , solving the coupled Equations (3.17) will typically require a numerical treatment. Some insight can be obtained, however, from an analytical treatment of a simple



model with  $N = 1$ , similar to the Jaynes-Cummings model of quantum optics [JC63]<sup>5</sup>.

We take the coupling constants to be of the form  $g_\ell = -i|g_\ell|$  (as will also be done in Sections 3.2.5 and 3.2.6 investigating numerically examples with several, discrete boson modes). For  $N = 1$  the space of detector-bath states with excitation number 1 is two-dimensional, and we choose the basis

$$|\uparrow \ 0\rangle \triangleq \begin{pmatrix} 1 \\ 0 \end{pmatrix}, \quad |\downarrow \ 1_\ell\rangle \triangleq \begin{pmatrix} 0 \\ 1 \end{pmatrix}.$$

The eigenvalue Equation (3.10) can then be written as

$$\left[ \omega_\ell \begin{pmatrix} 1 & 0 \\ 0 & 1 \end{pmatrix} + \begin{pmatrix} \omega_0 - \omega_\ell & -2i|g_\ell| \\ 2i|g_\ell| & -(\omega_0 - \omega_\ell) \end{pmatrix} \right] \begin{pmatrix} \mu_1 \\ \mu_2 \end{pmatrix} = \Omega_\mu \begin{pmatrix} \mu_1 \\ \mu_2 \end{pmatrix}.$$

We introduce the notations

$$\Delta := \omega_0 - \omega_\ell \quad \text{and} \quad \Re := \sqrt{\Delta^2 + 4|g_\ell|^2}. \quad (3.21)$$

Thus,  $\Delta$  denotes the detuning of the boson mode with respect to the transition frequency  $\omega_0$  of the spin, and  $\Re$  corresponds to the ‘Rabi flopping frequency’ of quantum optics. Then, the eigenvalues are given by

$$\Omega_\pm = \omega_\ell \pm \Re$$

with corresponding eigenvectors

$$|\Omega_-\rangle = \begin{pmatrix} \cos \vartheta \\ i \sin \vartheta \end{pmatrix} \quad \text{and} \quad |\Omega_+\rangle = \begin{pmatrix} i \sin \vartheta \\ \cos \vartheta \end{pmatrix},$$

where

$$\cos \vartheta := \frac{\Re - \Delta}{\sqrt{(\Re - \Delta)^2 + 4|g_\ell|^2}} \quad \text{and} \quad \sin \vartheta := \frac{2|g_\ell|}{\sqrt{(\Re - \Delta)^2 + 4|g_\ell|^2}}.$$

In the sequel we will further assume the boson mode to be in resonance with the transition frequency of the spin,  $\omega_\ell = \omega_0$ , i.e.,

$$\Delta \equiv 0, \quad \text{consequently} \quad \Re \equiv 2|g_\ell|. \quad (3.22)$$

In this case one simply has

$$\Omega_\pm = \omega_0 \pm 2|g_\ell|$$

and

$$|\Omega_-\rangle = \sqrt{\frac{1}{2}} \begin{pmatrix} 1 \\ i \end{pmatrix}, \quad |\Omega_+\rangle = \sqrt{\frac{1}{2}} \begin{pmatrix} i \\ 1 \end{pmatrix}. \quad (3.23)$$

---

<sup>5</sup>For a review of the Jaynes-Cummings model and its impact on quantum optics see, e.g., the review article Reference [SK93], containing an extensive list of references up to 1993.



Further, in case of resonance one has  $k_\ell(k) = k$ , by Equation (3.8). Equations (3.17) hence can easily be solved, yielding

$$\alpha_-(k) = \frac{k\sqrt{2}}{k + q_-(k)} \quad \text{and} \quad \alpha_+(k) = -\frac{ik\sqrt{2}}{k + q_+(k)}, \quad (3.24)$$

where [see Equation (3.13)]

$$q_\pm(k) = \sqrt{k^2 + \frac{m}{\hbar}(\omega_0 - \Omega_\pm)} = \sqrt{k^2 \mp \frac{2m}{\hbar}|g_\ell|}. \quad (3.25)$$

From Equations (3.16) one finally obtains the reflection coefficients in the eigenstate for  $x < 0$ ,  $\Phi_k^<$  [see Equation (3.7)],

$$\begin{aligned} R_0(k) &= k \left( \frac{1}{k + q_-(k)} + \frac{1}{k + q_+(k)} \right) - 1 \\ R_\ell(k) &= ik \left( \frac{1}{k + q_-(k)} - \frac{1}{k + q_+(k)} \right). \end{aligned} \quad (3.26)$$

We note that the coefficient for reflection without detection,  $R_0(k)$ , indeed depends on  $k$ , leading to deviations of the ‘measured’ arrival-time density with respect to ‘ideal’ quantities, as remarked earlier.

From Equations (3.26) together with Equation (3.25) one easily finds the limits of the reflection coefficients for very small and very high energies and coupling constants:

$$\begin{aligned} \lim_{k \rightarrow \infty} R_\ell(k) = 0 &= \lim_{|g_\ell| \rightarrow 0} R_\ell(k) & \lim_{k \rightarrow 0} R_\ell(k) = 0 &= \lim_{|g_\ell| \rightarrow \infty} R_\ell(k) \\ \lim_{k \rightarrow \infty} R_0(k) = 0 &= \lim_{|g_\ell| \rightarrow 0} R_0(k) & \lim_{k \rightarrow 0} R_0(k) = -1 &= \lim_{|g_\ell| \rightarrow \infty} R_0(k). \end{aligned} \quad (3.27)$$

The last limit is particularly interesting. It states that for very slow particles as well as for very strong spin-bath coupling the particle under consideration will be reflected with probability close to 1 while spin and bath remain unaffected. One sees that there is a back-reaction on the particle, including the possibility of reflection, which for an unsuitable choice of parameters may render the measurement useless. In the framework of the limit of continuous boson modes we will discuss optimization schemes for the detection of wave packets of a given energy range, see Section 5.2.3.

The eigenstate  $\Phi_k^>$  for  $x > 0$  is obtained by inserting  $\alpha_\pm(k)$ ,  $q_\pm(k)$ , and  $|\Omega_\pm\rangle$  from Equations (3.24), (3.25), and (3.23), into Equation (3.14), yielding

$$\begin{aligned} \Phi_k^>(x) &= \sqrt{\frac{1}{2\pi}} \frac{k}{[k + q_-(k)][k + q_+(k)]} \\ &\quad \left( \begin{aligned} &e^{iq_-(k)x} [k + q_+(k)] + e^{iq_+(k)x} [k + q_-(k)] \\ &ie^{iq_-(k)x} [k + q_+(k)] - ie^{iq_+(k)x} [k + q_-(k)] \end{aligned} \right). \end{aligned}$$

We consider a limit of weak coupling,

$$\frac{2m}{\hbar^2} |g_\ell| \ll k^2.$$



By means of the Taylor series expansion

$$q_{\pm}(k) = k \mp \frac{m}{\hbar k} |g_{\ell}| + \mathcal{O}\left(\frac{(2m|g_{\ell}|/\hbar)^2}{k^3}\right)$$

one finds for the ratio of population

$$\frac{|\langle x \uparrow 0 | \Phi_k^{\rangle} \rangle|^2}{|\langle x \downarrow 1_{\ell} | \Phi_k^{\rangle} \rangle|^2} \approx \left| \frac{[2k - (m|g_{\ell}|/\hbar k)] + e^{-i(2m|g_{\ell}|/\hbar k)x} [2k + (m|g_{\ell}|/\hbar k)]}{[2k - (m|g_{\ell}|/\hbar k)] - e^{-i(2m|g_{\ell}|/\hbar k)x} [2k + (m|g_{\ell}|/\hbar k)]} \right|^2.$$

In particular, for  $x = 0$  one has

$$\frac{|\langle x = 0, \uparrow 0 | \Phi_k^{\rangle} \rangle|^2}{|\langle x = 0, \downarrow 1_{\ell} | \Phi_k^{\rangle} \rangle|^2} \approx \frac{4k^4}{(m|g_{\ell}|/\hbar)^2} \gg 1.$$

This ratio is inverted at

$$x = \pi \frac{\hbar k}{2m|g_{\ell}|}.$$

Indeed, the ratio of population is oscillating with respect to  $x$ ,

$$\frac{|\langle x \uparrow 0 | \Phi_k^{\rangle} \rangle|^2}{|\langle x \downarrow 1_{\ell} | \Phi_k^{\rangle} \rangle|^2} = \frac{|\langle x + \lambda_x \uparrow 0 | \Phi_k^{\rangle} \rangle|^2}{|\langle x + \lambda_x \downarrow 1_{\ell} | \Phi_k^{\rangle} \rangle|^2}$$

with

$$\lambda_x(k) = \pi \frac{\hbar k}{m|g_{\ell}|}.$$

Thus, when a wave packet of the form (3.18) has entered the detector region  $x > 0$  and propagates forward along the  $x$  axis, population in the spin-bath space will be transferred back and forth between the states  $|\uparrow 0\rangle$  and  $|\downarrow 1_{\ell}\rangle$ . We consider the case that the wave packet is sharply peaked around  $k_0$  in momentum space,  $\Delta k/k_0 \ll 1$ , and sufficiently fast such that  $\Delta x/\lambda_x(k_0) \sim \hbar/2k_0\Delta k \ll 1$  holds. Then, all momentum components of the wave packet essentially ‘see’ the same spatial oscillation length  $\lambda_x(k_0)$  and at a time  $t > 0$  after entering the interaction region  $x > 0$  the wave packet is located essentially at a position  $x(t) = \hbar k_0 t/m$ . In this case, the population number integrated over  $x$  will oscillate in time with period

$$T = \frac{\lambda_x(k_0)}{\hbar k_0/m} = \frac{\pi}{|g_{\ell}|},$$

yielding a circular frequency

$$\frac{2\pi}{T} = \mathfrak{R}, \quad (3.28)$$

where  $\mathfrak{R}$  is the ‘Rabi flopping frequency’ from Equations (3.21) and (3.22). If the wave packet, however, is broad in momentum space,  $\Delta k \gtrsim k_0$ , and/or in position space,  $\Delta x \gtrsim \lambda_x(k_0)$ , the oscillation in the population number integrated over  $x$  will (partly) be washed out. This is similar to the oscillations in



occupation number investigated in Reference [NEMH03b] for a two-level system with center-of-mass motion in the presence of a laser field.

Equation (3.28) states that (for a sufficiently fast and peaked wave packet) the population in the spin-bath state flops back and forth between the states  $|\uparrow 0\rangle$  and  $|\downarrow 0\rangle$  with flopping frequency  $\mathfrak{R}$ . This is consistent with the results obtained for the Jaynes-Cummings model of quantum optics, considering a two-level system at rest coupled to a single photon mode. It has been shown in that context that for a large but finite number of field modes the population in the excited state shows a complicated sequence of collapses and revivals. This is due to the interference of the floppings associated with the several bath modes. In the limit of a continuum of modes the population of the excited state finally shows exponential and irreversible decay. This indicates that also in the present detector model it will be necessary to go to a continuum limit for the boson bath in order to prevent revivals  $|\downarrow 1_\ell\rangle \rightarrow |\uparrow 0\rangle$ , and thus to truly relate the spin flip and the associated boson creation to the first detection of the particle. This will be the aim of Chapter 4.

### 3.2.4 Detection of a wave packet

We return to the model with many discrete boson modes and discuss the detection of a wave packet in this model. Let the state of the complete system, spin, bath, and particle, at time  $t$  be denoted by  $|\Psi_t\rangle$ . The probability of finding the bath in some boson state  $|1_\ell\rangle$  (and hence the spin in state  $|\downarrow\rangle$ ) at time  $t$  is given by integration over the modulus square of the respective component of  $|\Psi_t\rangle$ ,

$$\begin{aligned} P_1^{\text{disc}}(t) &= \sum_\ell \int_{-\infty}^{\infty} dx |\langle x \downarrow 1_\ell | \Psi_t \rangle|^2 \\ &= 1 - \int_{-\infty}^{\infty} dx |\langle x \uparrow 0 | \Psi_t \rangle|^2 =: 1 - P_0^{\text{disc}}(t), \end{aligned}$$

where the superscript ‘disc’ distinguishes the discrete model from the continuum limit discussed in Chapter 4. As long as no revivals occur, i.e., no transitions  $|\downarrow 1_\ell\rangle \mapsto |\uparrow 0\rangle$ , one can regard

$$w_1^{\text{disc}}(t) = \frac{d}{dt} P_1^{\text{disc}}(t) = -\frac{d}{dt} P_0^{\text{disc}}(t).$$

as the probability density for a spin flip (i.e., for a detection) at time  $t$ .

For examples with  $N = 20$  and  $N = 40$  boson modes the probability density for detection will be evaluated numerically in the subsequent subsections and will be compared to the probability density obtained from the corresponding continuum limit of Chapter 4. This comparison is a test of the validity of the approximations made in the derivation of this limit. It further gives an idea to which extent the continuum limit provides a good approximation to the discrete case, even for modest numbers of  $N = 20$  or  $N = 40$  bath modes. This is interesting since in some cases as, e.g., in cavity QED, one actually has to deal with discrete boson baths. The numerical investigation of continuum limit, though, typically is far less time consuming than that of the discrete case.



### 3.2.5 Examples with constant density of states

As an example we consider a maximal boson frequency  $\omega_M$  and a constant density of states,

$$\begin{aligned}\omega_\ell &= \omega_M n/N \quad n = 1, \dots, N \\ g_\ell &= -iG\sqrt{\omega_\ell/N}.\end{aligned}\tag{3.29}$$

We start with detector and bath in state  $|\uparrow 0\rangle$  as described in Section 3.1.3. As particle we consider a cesium atom. The particle is prepared in the remote past very far away from the detector as an asymptotically free state [see Equation (3.18)]. The momentum density is chosen such that the corresponding free packet (i.e., in the absence of the detector) at  $t = 0$  would be a Gaussian minimal uncertainty packet around  $x = 0$  with width  $\Delta p$  in momentum space and average velocity  $v_0$ . Decomposing this into the eigenstates of  $H$ , the wave packet at time  $t$  is given by (see Section 10)

$$|\Psi_t\rangle = \int_0^\infty dk \tilde{\psi}(k) |\Phi_k\rangle e^{-iE_k t/\hbar}\tag{3.20}$$

with

$$\tilde{\psi}(k) = \left(\frac{\hbar}{\Delta p \sqrt{2\pi}}\right)^{1/2} \exp\left(-\frac{\hbar^2}{4(\Delta p)^2} (k - mv_0/\hbar)^2\right),\tag{3.30}$$

where the parameters  $v_0$ ,  $\Delta p$  will be chosen such that  $\tilde{\Psi}(k) \approx 0$  for  $k \leq 0$ .

Two numerical illustrations of  $w_1^{\text{disc}}$  are given in Figure 3.2 (with  $N = 40$ ) and in Figure 3.3 (with  $N = 20$ ). The average velocity  $v_0$  of the incident wave packet is the same in both figures. The main difference between the two figures is the width of the wave packet in momentum space,  $\Delta p = 20 \mu m^{-1} \times \hbar$  in Figure 3.2 and  $\Delta p = 2 \mu m^{-1} \times \hbar$  in Figure 3.3. This difference in  $\Delta p$  has important consequences: We note that if  $\Delta x$  is the width of the wave packet in position space, then the width of the probability density for detection is at least of the order of  $\Delta x/v_0$  since it takes some time for the wave packet to enter the detection region. (Further broadening of the detection density arises from the width of the delay of the first spin flip once the particle is inside the detector.) Consequently, wave packets with small  $\Delta p$  and thus large  $\Delta x$  yield rather broad detection densities, as is seen in Figure 3.3. As soon as a significant part of the wave function overlaps with the detector, though, the time scale of the revivals is essentially determined by the properties of the detector and the bath and by their coupling. The detector and bath parameters are of the same order of magnitude in both figures, and hence in both figures the time scales for the revivals are similar. This time scale is sufficient to obtain a reasonable resolution of the probability density for detection in the case of the wave packet with larger  $\Delta p$  in Figure 3.2. In the case of wave packets with small  $\Delta p$  as in Figure 3.3 longer recurrence times would be needed to obtain a good resolution of the typically broad detection densities. This would require a significantly larger number of bath modes. Already for the present examples with  $N = 20$  and  $N = 40$ , however, the numerical calculation is quite



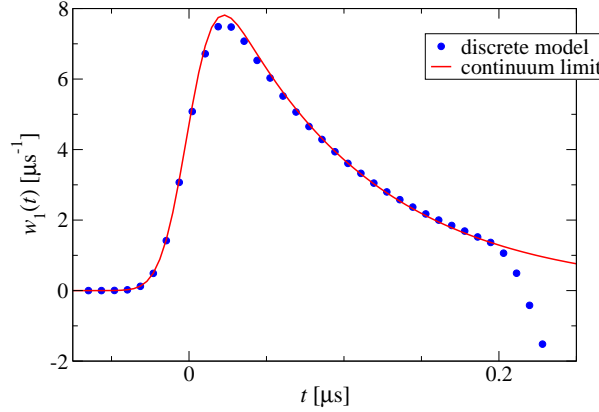


**Figure 3.2:** Dots: spin-flip probability density  $w_1^{\text{disc}}(t)$  for an incoming Gaussian wave packet of Equations (3.20, 3.30) with  $\Delta p = 20 \mu\text{m}^{-1} \times \hbar$  and  $v_0 = 1.79 \text{ m/s}$ ;  $\omega_\ell$  as in Equation (3.29),  $\omega_0 = 2.39 \times 10^8 \text{ s}^{-1}$ ,  $\omega_M = 4.6 \omega_0$ ,  $G = 2.782 \times 10^3 \text{ s}^{-1/2}$ ,  $N = 40$ . Solid line:  $w_1(t)$  from Equation (4.21) for the corresponding continuum limit. In the continuum limit, the flip rate of the excited spin state in the presence of the particle is  $A = 1.057 \times 10^7 \text{ s}^{-1}$ , and the ‘line shift’ is  $\delta_{\text{shift}} = -1.979 \times 10^7 \text{ s}^{-1}$  [see Equations (4.23)]. Up to the time of revivals,  $|\downarrow 1_\ell\rangle \mapsto |\uparrow 0\rangle$  (due to the discrete nature of the bath), the discrete and continuum probability densities are in good agreement.

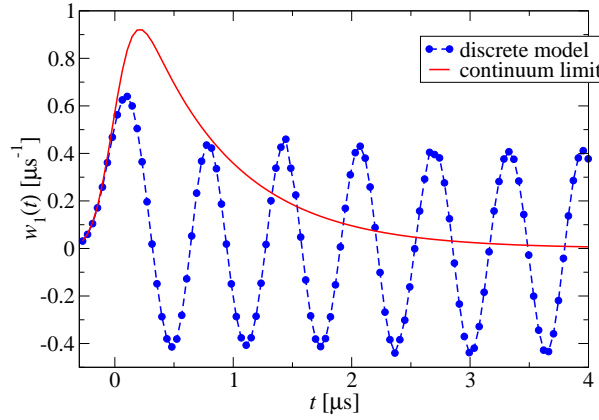


**Figure 3.3:** Dots: spin-flip probability density  $w_1^{\text{disc}}(t)$  for an incoming Gaussian wave packet of Equations (3.20, 3.30) with  $v_0 = 1.79 \text{ m/s}$  as in Figure 3.2, but with  $\Delta p = 2 \mu\text{m}^{-1} \times \hbar$ ;  $\omega_0 = 2.39 \times 10^8 \text{ s}^{-1}$ ,  $\omega_M = 2.3 \omega_0$ ,  $G = 6.955 \times 10^2 \text{ s}^{-1/2}$ ,  $N = 20$ . Solid line:  $w_1(t)$  from Equation (4.21) for the corresponding continuum limit. In the continuum limit, the flip rate of the excited spin state in the presence of the particle is  $A = 1.321 \times 10^6 \text{ s}^{-1}$ , and the ‘line shift’ is  $\delta_{\text{shift}} = -1.078 \times 10^6 \text{ s}^{-1}$  [see Equations (4.23)]. The time scale for the revivals is similar as in Figure 3.2, but as explained in the text the probability density is much broader and thus is not reasonably resolved in the discrete case. Up to the time of revivals in the discrete case, however, the discrete and continuum probability densities again are in good agreement.



time consuming since the Equations (3.17) have to be solved for every  $k$  in the course of the integration. The numerical calculation in the continuous case with the quantum jump approach, discussed in the Chapter 4, is much faster. In addition, there are no revivals in the continuum limit. We further note that for more complicated incident wave packets as, e.g., the coherent superposition of several Gaussian wave packets with different mean velocities, the probability density exhibits a more complicated structure due to the self-interference of the wave function.

### 3.2.6 Example with non-constant density of states

As an example for a non-constant density of states we consider a maximal boson frequency  $\omega_M$  as before, but

$$\omega_\ell = \left(\frac{n}{N}\right)^2 \omega_M, \quad n = 1, \dots, N. \quad (3.31)$$

Again, we set  $g_\ell = -iG\sqrt{\omega_\ell/N}$ . A numerical illustration of  $w_1^{\text{disc}}$  is given in Figure 3.4 for the same incoming wave packet as in Figure 3.2. As in that figure, the discrete and the continuum probability density are in good agreement up to revivals in the discrete case.

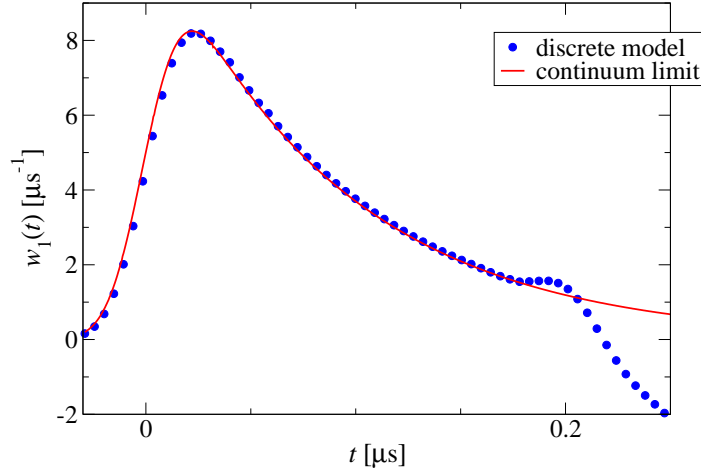


**Figure 3.4:** Dots: spin-flip probability density  $w_1^{\text{disc}}(t)$  for an incoming Gaussian wave packet of Equations (3.20, 3.30). The parameters  $\Delta p$  and  $v_0$  for the wave packet and  $\omega_0$ ,  $\omega_M$ ,  $G$ ,  $N = 40$  for the boson bath are the same as in Figure 3.2, but the frequencies  $\omega_\ell$  now are given by Equation (3.31). Solid line:  $w_1(t)$  from Equation (4.21) for the corresponding continuum limit. In the continuum limit, the flip rate of the excited spin state in the presence of the particle is  $A = 1.134 \times 10^7 \text{ s}^{-1}$ , and the ‘line shift’ is  $\delta_{\text{shift}} = -1.183 \times 10^7 \text{ s}^{-1}$  [see Equations (4.24)]. Up to the time of revivals,  $|\downarrow 1_\ell\rangle \mapsto |\uparrow 0\rangle$  (due to the discrete nature of the bath), the discrete and continuum probability densities are in good agreement.







## Chapter 4

# The continuum limit and the quantum jump approach

The application of the spin-boson detector model of Chapter 3 to arrival-time measurements is investigated by means of the so called ‘quantum jump approach’. This approach uses continuous bath modes as a limit, so there are no revivals, in contrast to the discrete case of Chapter 3. It is easily generalized to multiple spins, and it is more accessible to analytic treatment. The bath modes are eliminated, but in contrast to Bloch equations one can work with a (conditional or effective) Hamiltonian and has reduced dimensions. In the derivation of the continuum limit we assume that the Markov property holds. Analytical expressions are derived for the ‘conditional Hamiltonian’, governing the time development up to the detection of the first boson, and for the probability density for detection. The probability density for the first boson detection is compared numerically to the density obtained in Chapter 3 for the case of discrete boson modes, and the presented examples show a good agreement. Further, examples for arrival time-measurements with smooth sensitivity functions are presented. Finally, we briefly comment on the internal dynamics of the detector.

### 4.1 The quantum jump approach: Conditional time development

To measure truly the first appearance of a boson, implying the first spin flip and thus detection as remarked in Section 3.1.3, one would have to observe the bath continuously. In standard quantum mechanics with the simple von Neumann measurement theory (see Chapter V.1 of Reference [vN32]) this leads to difficulties due to the quantum Zeno effect [BN67, Kha68, MS77]. This is very similar to problems in quantum optics, where one is interested, e.g., in measuring the appearance of the first fluorescence photon from an atom. In that context the so called ‘quantum jump approach’ has been developed by Hegerfeldt and co-workers<sup>1</sup> [HW92, Heg93, HS96, Heg03]; for a review see, e.g.,

---

<sup>1</sup>The quantum jump approach is essentially equivalent to the Monte-Carlo wave-function approach by Dalibard, Castin, and Mølmer [DCM92], and to the quantum trajectories of



[PK98]. In this chapter the extension of the quantum jump approach to the spin-boson detector model is investigated.

The general idea of the quantum jump approach is to circumvent the problems related to a continuous measurement by observations which are coarse-grained in time, and by employing a coarse-grained time scale. The continuous measurement is replaced by repeated, instantaneous measurements, separated by a time  $\Delta t$ . For a Markovian system with correlation time  $\tau_c$  [see Equation (4.14)], one takes  $\Delta t \gg \tau_c$  to avoid the quantum Zeno effect, but  $\Delta t$  much shorter than the lifetime of the excited state  $|\uparrow_1 \dots \uparrow_D\rangle$  in order to obtain a good time resolution. Typical numbers for quantum optical models are  $\Delta t \simeq 10^{-13}\text{s} \dots 10^{-10}\text{s}$ . To find *no boson until*  $t = n\Delta t$  means that no boson has been found in the first  $n$  measurements. We will sketch in this section how to evaluate the probability for this to happen.

Let the complete system (bath, detector, and particle) at  $t = 0$  be prepared in the state

$$|\Psi_0\rangle = |0\rangle |\uparrow_1 \dots \uparrow_D\rangle |\psi_0\rangle,$$

where  $|\psi_0\rangle$  denotes the spatial wave function of the particle. If no boson is found at the first measurement then, by the von Neumann-Lüders reduction rule<sup>2</sup> [vN32, Lüd51], the state right after the measurement is given up to normalization by projecting with  $|0\rangle\langle 0|$ ,

$$|\Psi_{\text{cond}}^{\Delta t}\rangle \equiv |0\rangle\langle 0| U(\Delta t, 0) |0\rangle |\uparrow_1 \dots \uparrow_D\rangle |\psi_0\rangle, \quad (4.1)$$

where  $U(t, t')$  denotes the time development operator of the complete system. The probability for no boson detection,  $P_0(\Delta t)$ , is the norm squared of the vector in Equation (4.1),

$$P_0(\Delta t) = \|\langle 0| \langle 0| U(\Delta t, 0) |0\rangle |\uparrow_1 \dots \uparrow_D\rangle |\psi_0\rangle\|^2.$$

The state then develops with  $U(2\Delta t, \Delta t)$  until the next measurement, and so on. The state after the  $n^{\text{th}}$  consecutive no-boson measurement,  $|\Psi_{\text{cond}}^{n\Delta t}\rangle$ , is given up to normalization by

$$\begin{aligned} |\Psi_{\text{cond}}^{n\Delta t}\rangle &= |0\rangle\langle 0| U(n\Delta t, [n-1]\Delta t) |0\rangle \dots \\ &\dots \langle 0| U(\Delta t, 0) |0\rangle |\uparrow_1 \dots \uparrow_D\rangle |\psi_0\rangle. \end{aligned} \quad (4.2)$$

The probability of finding the bath in the state  $|0\rangle$  in *all* of the first  $n$  measurements,  $P_0(n\Delta t)$ , is given by its norm squared,

$$P_0(n\Delta t) = \langle \Psi_{\text{cond}}^{n\Delta t} | \Psi_{\text{cond}}^{n\Delta t} \rangle. \quad (4.3)$$

Note that  $\langle 0| U(\nu\Delta t, [\nu-1]\Delta t) |0\rangle$  is an operator in the particle-detector Hilbert space which does not rotate  $|\uparrow_1 \dots \uparrow_D\rangle$ , by excitation number conservation mentioned in Remark 3.1.2. Thus, one can introduce a ‘conditionally developed’

---

Carmichael [Car93].

<sup>2</sup>We note that the projection postulate as commonly used nowadays is due to Lüders [Lüd51]. His formulation differs from that by von Neumann [vN32] if one considers observables with degenerate eigenvalues.



spatial wave function  $|\psi_{\text{cond}}^t\rangle$  of the particle by writing  $|\Psi_{\text{cond}}^t\rangle$  from Equation (4.2) in the form

$$|\Psi_{\text{cond}}^{n\Delta t}\rangle =: |0\rangle |\uparrow_1 \dots \uparrow_D\rangle |\psi_{\text{cond}}^t\rangle, \quad (4.4)$$

where  $t = n\Delta t$ . It is of particular importance to note that  $|\psi_{\text{cond}}^t\rangle$  denotes the spatial wave function developed in time *not* freely but under the condition that no boson has been found in all of the repeated measurements on the bath *until*  $t$ ; this is called the ‘conditional time development’. Therefore, the norm of  $|\psi_{\text{cond}}^t\rangle$  is not conserved but decreases due to the repeated projections  $|0\rangle\langle 0|$ . Since  $|0\rangle$  and  $|\uparrow_1 \dots \uparrow_D\rangle$  are normalized states, Equation (4.3) can be written

$$P_0(t) = \langle \psi_{\text{cond}}^t | \psi_{\text{cond}}^t \rangle. \quad (4.5)$$

This is the probability that no transition  $|0\rangle \rightarrow |1_{\mathbf{t}}\rangle$ , i.e., that no detection occurs *until* the time  $t$ . We note that Equation (4.5) gives this probability solely in terms of the conditionally developed wave function of the particle. Detector and bath contribute only implicitly via the conditional time development. The probability for the first detection to occur at the next measurement is just given by

$$P_0(t) - P_0(t + \Delta t) =: w_1(t)\Delta t. \quad (4.6)$$

The crucial point now is to calculate the conditional time development of  $|\psi_{\text{cond}}^t\rangle$ , i.e., to calculate the time development ‘under the condition that no detection occurs’. For this one has to evaluate  $\langle 0 | U(\nu\Delta t, [\nu-1]\Delta t) | 0 \rangle |\uparrow_1 \dots \uparrow_D\rangle$ . This will be the aim of Section 4.2.

## 4.2 Conditional Hamiltonian and probability density for detection

### 4.2.1 A simplified model

For greater clarity, we first investigate the simplified model introduced in Section 3.2.1. The generalization to the full model will be discussed in Section 4.2.4.

We use the interaction picture with respect to

$$H_0^{1,1d} = H^{1,1d} - H_{\text{coup}}^{1,1d},$$

and calculate

$$U_I(t, t') := e^{iH_0^{1,1d}t/\hbar} U(t, t') e^{-iH_0^{1,1d}t'/\hbar}$$

in second order perturbation theory with respect to  $H_{\text{coup}}^{1,1d}$ ,

$$U_I(t, t') = \mathbb{1} - \frac{i}{\hbar} \int_{t'}^t dt_1 H_I(t_1) - \frac{1}{\hbar^2} \int_{t'}^t dt_1 \int_{t'}^{t_1} dt_2 H_I(t_1) H_I(t_2) + \dots \quad (4.7)$$

with

$$H_I(t) := e^{iH_0^{1,1d}t/\hbar} H_{\text{coup}}^{1,1d} e^{-iH_0^{1,1d}t/\hbar}.$$



One arrives at

$$\langle 0 | U_I(\nu\Delta t, [\nu-1]\Delta t) | 0 \rangle | \uparrow \rangle = | \uparrow \rangle \left( \mathbf{1} - \int_{[\nu-1]\Delta t}^{\nu\Delta t} dt_1 \int_{[\nu-1]\Delta t}^{t_1} dt_2 \sum_{\ell} \chi_{\mathcal{I}_d}(\hat{x}(t_1)) \chi_{\mathcal{I}_d}(\hat{x}(t_2)) |g_{\ell}|^2 e^{i(\omega_0 - \omega_{\ell})(t_1 - t_2)} \right), \quad (4.8)$$

where  $\hat{x}(t) = \hat{x} + \hat{p}t/m$  is the time development of the operator  $\hat{x}$  in the Heisenberg picture of the free particle. The phases  $f_{\ell}$  in the coupling terms have canceled; even if one would assume these phases to be dependent on the particle's position,  $f_{\ell} = f_{\ell}(x)$ , this would be the case to very good approximation since  $\Delta t$  is very small and thus  $\hat{x}(t_1) \approx \hat{x}(t_2)$  for  $|t_1 - t_2| < \Delta t$  [Heg03]. We introduce the correlation function

$$\kappa(\tau) := \sum_{\ell} |g_{\ell}|^2 e^{-i(\omega_{\ell} - \omega_0)\tau} \quad (4.9)$$

and write Equation (4.8) in the form

$$\langle 0 | U_I(\nu\Delta t, [\nu-1]\Delta t) | 0 \rangle | \uparrow \rangle = | \uparrow \rangle \left( \mathbf{1} - \int_{[\nu-1]\Delta t}^{\nu\Delta t} dt_1 \int_{[\nu-1]\Delta t}^{t_1} dt_2 \chi_{\mathcal{I}_d}(\hat{x}(t_1)) \chi_{\mathcal{I}_d}(\hat{x}(t_2)) \kappa(t_1 - t_2) \right). \quad (4.10)$$

To have irreversible decay we go to the continuum limit as follows. At first the bath modes are indexed by ‘wave numbers’

$$\ell = \frac{2\pi n}{L_{\text{bath}}}, \quad n = 1, 2, \dots,$$

and  $\omega_{\ell}$  is chosen as

$$\omega_{\ell} = c(\omega_{\ell}) \ell,$$

so that

$$\Delta\omega = \frac{c(\omega)^2}{c(\omega) - \omega c'(\omega)} \Delta\ell = \frac{c(\omega)^2}{c(\omega) - \omega c'(\omega)} \frac{2\pi}{L_{\text{bath}}}. \quad (4.11)$$

The coupling constants are taken to be of the form

$$g_{\ell} = [\Gamma(\omega_{\ell}) + \mathcal{O}(L_{\text{bath}}^{-1})] \sqrt{\frac{\omega_{\ell}}{L_{\text{bath}}}}, \quad (4.12)$$

where  $\Gamma(\omega_{\ell})$  does not depend on  $L_{\text{bath}}$ . One then goes to the limit of continuous bath modes,  $L_{\text{bath}} \rightarrow \infty$ . By Equations (4.9) and (4.11) one finds that

$$\kappa(\tau) = \frac{1}{2\pi} \int_0^{\infty} d\omega \frac{c(\omega) - \omega c'(\omega)}{c(\omega)^2} \omega |\Gamma(\omega)|^2 e^{-i(\omega - \omega_0)\tau}. \quad (4.13)$$



We assume  $\Gamma(\omega)$  to be of such a form that the Markov property holds, i.e.,

$$\kappa(\tau) \approx 0 \quad \text{if} \quad \tau > \tau_c \quad (4.14)$$

for some small correlation time  $\tau_c$ . This is the case, e.g., for  $\Gamma(\omega) \equiv \Gamma$  as in quantum optics. In the double integral of Equation (4.10) then only times with  $t_1 - t_2 \leq \tau_c$  contribute, and if  $\tau_c$  is small enough one can write

$$\chi_{x_d}(\hat{x}(t_1)) \chi_{x_d}(\hat{x}(t_2)) \approx \chi_{x_d}(\hat{x}(t_1))^2. \quad (4.15)$$

With a change of variables  $\tau := t_1 - t_2$  and  $t' = t_1 - [\nu - 1]\Delta t$ , the double integral of Equation (4.10) then becomes

$$\begin{aligned} & \int_{[\nu-1]\Delta t}^{\nu\Delta t} dt_1 \int_{[\nu-1]\Delta t}^{t_1} dt_2 \chi_{x_d}(\hat{x}(t_1)) \chi_{x_d}(\hat{x}(t_2)) \kappa(t_1 - t_2) \\ & \approx \int_0^{\Delta t} dt' \chi_{x_d}(\hat{x}(t' + (\nu - 1)\Delta t))^2 \int_0^{t'} d\tau \kappa(\tau). \end{aligned}$$

With  $\Delta t \gg \tau_c$  the second integral can be extended to infinity, by the Markov property of Equation (4.14). Putting

$$A := 2 \operatorname{Re} \int_0^\infty d\tau \kappa(\tau) = \omega_0 \frac{c(\omega_0) - \omega_0 c'(\omega_0)}{c(\omega_0)^2} |\Gamma(\omega_0)|^2, \quad (4.16)$$

$$\delta_{\text{shift}} := 2 \operatorname{Im} \int_0^\infty d\tau \kappa(\tau) \quad (4.17)$$

one obtains

$$\begin{aligned} & \langle 0 | U_I(\nu\Delta t, [\nu - 1]\Delta t) | 0 \rangle |\uparrow\rangle \\ & = |\uparrow\rangle \left( \mathbb{1} - \frac{1}{2} (A + i\delta_{\text{shift}}) \int_{[\nu-1]\Delta t}^{\nu\Delta t} dt_1 \chi_{x_d}[\hat{x}(t_1)]^2 \right) \\ & = |\uparrow\rangle \exp \left\{ -\frac{1}{2} (A + i\delta_{\text{shift}}) \int_{[\nu-1]\Delta t}^{\nu\Delta t} dt_1 \chi_{x_d}[\hat{x}(t_1)]^2 \right\}, \end{aligned}$$

up to higher orders in  $\Delta t$ . Note that  $A$  is a decay rate of the upper spin level; in quantum optics  $A$  and  $\delta_{\text{shift}}$  correspond to the Einstein coefficient and to a line shift. Going back to the Schrödinger picture one then obtains by Equations (4.2) and (4.4)

$$|\psi_{\text{cond}}^t\rangle = e^{-iH_{\text{cond}}(t-t_0)/\hbar} |\psi_0\rangle \quad (4.18)$$

with the ‘conditional Hamiltonian’

$$H_{\text{cond}} \equiv \frac{\hat{p}^2}{2m} + \frac{\hbar}{2}(\delta_{\text{shift}} - iA)\chi_{x_d}(\hat{x})^2. \quad (4.19)$$



Note that this result is independent of the particular choice of  $\Delta t$  as long as  $\Delta t$  satisfies the above requirements. As a consequence, on a coarse-grained time scale in which  $\Delta t$  is small,  $t$  can be regarded as continuous and  $|\psi_{\text{cond}}^t\rangle$  obeys a Schrödinger equation with a complex potential,

$$i\hbar \frac{\partial}{\partial t} |\psi_{\text{cond}}^t\rangle = \left( \frac{\hat{p}^2}{2m} + \frac{\hbar}{2} [\delta_{\text{shift}} - iA] \chi_{\mathcal{I}_d}(\hat{x})^2 \right) |\psi_{\text{cond}}^t\rangle.$$

In this continuous, coarse-grained, time scale, Equation (4.6) yields for the probability density for the first detection,  $w_1(t)$ ,

$$w_1(t) = -\frac{dP_0(t)}{dt}. \quad (4.20)$$

With Equations (4.5) and (4.18) one easily finds

$$\begin{aligned} w_1(t) &= \frac{i}{\hbar} \left\langle \psi_{\text{cond}}^t \left| H_{\text{cond}} - H_{\text{cond}}^\dagger \right| \psi_{\text{cond}}^t \right\rangle \\ &= A \int_{-\infty}^{\infty} dx \chi_{\mathcal{I}_d}(x)^2 |\langle x | \psi_{\text{cond}}^t \rangle|^2. \end{aligned} \quad (4.21)$$

If  $\chi_{\mathcal{I}_d}(\hat{x})$  is the characteristic function of the interval  $[0, d]$  this is just the decay rate of the excited state of the detector multiplied by the probability that the particle is inside the detector but not yet detected — a physically very reasonable result.

#### 4.2.2 Example with constant density of states

As an example with a constant density of states we consider the continuum limit of the discrete model of Equations (3.29). In this case one has, with  $\omega_{\text{M}}$  the maximal frequency,

$$\begin{aligned} c(\omega) &\equiv c_0 \\ \omega_\ell &= \omega_{\text{M}} \frac{n}{N} \equiv c_0 \frac{2\pi n}{L_{\text{bath}}}, \quad n = 1, \dots, N \\ L_{\text{bath}} &\equiv \frac{2\pi c_0 N}{\omega_{\text{M}}} \\ g_\ell &= -iG \sqrt{\frac{\omega_\ell}{N}} \equiv -iG \sqrt{\frac{2\pi c_0}{\omega_{\text{M}}}} \sqrt{\frac{\omega_\ell}{L_{\text{bath}}}} \\ \Gamma(\omega) &= \begin{cases} -iG \sqrt{2\pi c_0 / \omega_{\text{M}}} \equiv \Gamma & \text{if } \omega \leq \omega_{\text{M}} \\ 0 & \text{else,} \end{cases} \end{aligned} \quad (4.22)$$

We are interested in the continuum limit,  $N$  or  $L_{\text{bath}} \rightarrow \infty$ . In order to obtain the correlation function  $\kappa$ , one can either insert the above equations into Equation (4.13) giving the general form of  $\kappa$  in the continuum limit. This yields

$$\kappa(\tau) = \int_0^{\omega_{\text{M}}} \frac{\omega d\omega}{2\pi c_0} \frac{2\pi c_0}{\omega_{\text{M}}} |G|^2 e^{-i(\omega - \omega_0)\tau}.$$



Or, one can insert Equations (3.29) into Equation (4.9) giving  $\kappa$  in the discrete case, and then calculate the continuum limit directly for this specific example. This yields

$$\begin{aligned}\kappa(\tau) &= \omega_M |G|^2 \sum_{n=1}^N \frac{1}{N} \frac{n}{N} e^{-i\omega_M \tau (n/N) + i\omega_0 \tau} \\ &\rightarrow \omega_M |G|^2 \int_0^1 d\xi \xi e^{-i\omega_M \tau \xi + i\omega_0 \tau} \quad \text{for } N \rightarrow \infty.\end{aligned}$$

From both approaches one obtains in the case  $\omega_M > \omega_0$

$$\kappa(\tau) = \frac{|G|^2}{\omega_M} \frac{(1 + i\omega_M \tau) e^{-i(\omega_M - \omega_0)\tau} - e^{i\omega_0 \tau}}{\tau^2}.$$

Consequently, from Equations (4.16) and (4.17),

$$\begin{aligned}A &= 2\pi |G|^2 \frac{\omega_0}{\omega_M} \\ \delta_{\text{shift}} &= 2 |G|^2 \left( \frac{\omega_0}{\omega_M} \ln \left[ \frac{\omega_0}{\omega_M - \omega_0} \right] - 1 \right),\end{aligned}\tag{4.23}$$

and  $\tau_c$  is of the order of  $\omega_0^{-1}$ . In the integral for  $w_1(t)$  in (4.21) one has

$$\chi_{\mathcal{I}_d}(x) = \Theta(x).$$

The resulting  $w_1(t)$  is plotted in Figures 3.2 and 3.3 for the same wave function and parameters as for  $w_1^{\text{disc}}(t)$  in the respective figure. The densities obtained from the discrete model and from the continuum limit are in good agreement up to the occurrence of revivals  $|\downarrow 1_\ell\rangle \mapsto |\uparrow 0\rangle$  in the discrete case. This agreement is seen most nicely in Figure 3.2. In the case depicted there both the discrete model and the continuum limit yield a reasonable resolution of the ‘measured’ arrival-time density. In the case of small  $\Delta p$ , depicted in Figure 3.3, the revivals distinguishing the discrete model from the continuum limit play a much more dominant role. Since their time scale is shorter than the width of the probability density for detection, the arrival-time measurement by the discrete model with only  $N = 20$  boson modes is rendered useless in that case. The continuum limit, where no revivals occur, can be applied without any problems.

### 4.2.3 Example with non-constant density of states

As an example with a non-constant density of states we consider the continuum limit of the example of Equation (3.31). In this case one has, with  $\omega_M$  the maximal boson frequency,

$$\begin{aligned}c(\omega) &= c_0 \sqrt{\frac{\omega_\ell}{\omega_M}} \\ \omega_\ell &= \left( \frac{n}{N} \right)^2 \omega_M \equiv c(\omega_\ell) \frac{2\pi n}{L_{\text{bath}}} = c_0 \frac{2\pi n^2}{N L_{\text{bath}}}, \quad n = 1, \dots, N.\end{aligned}$$



$L_{\text{bath}}$ ,  $g_\ell$  and  $\Gamma(\omega)$  have the same form as in Equations (4.22). In contrast to the preceding section we have  $c'(\omega) \neq 0$ , and hence Equation (4.13) yields a more complicated form for the correlation function,

$$\kappa(\tau) = \frac{|G|^2}{2\sqrt{\omega_M}} \int_0^{\omega_M} d\omega \sqrt{\omega} e^{-i(\omega-\omega_0)\tau}.$$

In order to evaluate the decay rate  $A$  and the ‘line shift’  $\delta_{\text{shift}}$  it is convenient to change the order of integration,

$$\begin{aligned} \frac{1}{2}(A + i\delta_{\text{shift}}) &= \int_0^\infty d\tau \kappa(\tau) \\ &= \frac{|G|^2}{2\sqrt{\omega_M}} \int_0^{\omega_M} d\omega \sqrt{\omega} \int_0^\infty d\tau e^{-i(\omega-\omega_0)\tau} \\ &= \frac{|G|^2}{2\sqrt{\omega_M}} \left( \pi\sqrt{\omega_0} + i\mathcal{P} \int_0^{\omega_M} d\omega \frac{\sqrt{\omega}}{\omega_0 - \omega} \right), \end{aligned}$$

where  $\mathcal{P}$  denotes the principal value of the integral. One finally obtains

$$\begin{aligned} A &= \pi|G|^2 \sqrt{\frac{\omega_0}{\omega_M}} \\ \delta_{\text{shift}} &= |G|^2 \left[ \sqrt{\frac{\omega_0}{\omega_M}} \ln \left( \frac{\sqrt{\omega_M/\omega_0} + 1}{\sqrt{\omega_M/\omega_0} - 1} \right) - 2 \right]. \end{aligned} \quad (4.24)$$

The resulting  $w_1(t)$  is plotted in Figure 3.4 for the same wave function and parameters as for  $w_1^{\text{disc}}$  in the discrete case. Again, the densities obtained from the discrete case and from the continuum limit are in good agreement up to revivals  $|\downarrow 1_\ell\rangle \mapsto |\uparrow 0\rangle$  in the discrete case.

The agreement between the quantum jump approach and the discrete case of Chapter 3 is quite interesting. It indicates that the continuum limit of the quantum jump approach may provide a good approximation to situations where one is faced with a discrete boson bath as, e.g., in cavity QED, up to the time of revivals. This will surely be useful since the explicit handling even of a modest number of bath modes,  $N \approx 10 \dots 100$ , makes a numerical investigation rather time consuming. But already for such modest boson numbers the discrete model is well approximated by the continuum limit of the quantum jump approach, up to the occurrence of revivals, as the examples show. We note that this continuum limit was derived under the assumption that the Markov property Equation (4.14) holds, and that in all examples  $\tau_c \ll 1/A$ . The latter inequality is a necessary assumption in the derivation of the quantum jump approach, as indicated in Section 4.1.

#### 4.2.4 The three-dimensional model with several spins

The continuum limit and quantum jump approach for the full three-dimensional, multiple-spin model introduced in Section 3.1 are quite similar until Equation (4.8). Analogously to Section 4.2.1 we use the interaction picture with



respect to

$$H_0 = H - (H_{\text{spn}} + H_{\text{coup}}).$$

In second order perturbation theory with respect to  $H_{\text{coup}} + H_{\text{spn}}$  one obtains

$$\begin{aligned} \langle 0 | U_I(\nu \Delta t, [\nu - 1] \Delta t) | 0 \rangle | \uparrow_1 \dots \uparrow_D \rangle &= | \uparrow_1 \dots \uparrow_D \rangle \left( \mathbb{1} \right. \\ &- \sum_{j, \ell} \int_{[\nu-1]\Delta t}^{\nu \Delta t} dt_1 \int_{[\nu-1]\Delta t}^{t_1} dt_2 \exp \left\{ i \left( \omega_0^{(j)} - \sum_{\substack{k \\ k \neq j}} \omega_J^{(kj)} - \omega_\ell \right) (t_1 - t_2) \right\} \\ &\times \overline{\left( \chi^{(j)}(\hat{\mathbf{x}}(t_1)) g_\ell^{(j)} + \gamma_\ell^{(j)} \right)} \left( \chi^{(j)}(\hat{\mathbf{x}}(t_2)) g_\ell^{(j)} + \gamma_\ell^{(j)} \right) \Bigg), \quad (4.25) \end{aligned}$$

which generalizes Equation (4.8) to the three-dimensional, multi-spin case. The phases  $f_\ell^{(j)}$  have canceled similar to the single-spin case since only products of the form  $\hat{a}_\ell \hat{\sigma}_+^{(j)} \hat{a}_\ell^\dagger \hat{\sigma}_-^{(j)}$  contribute to the second order, and consequently the contributions from different spins do not mix.

We introduce ‘modified resonance frequencies’

$$\tilde{\omega}_0^{(j)} := \omega_0^{(j)} - \sum_{\substack{k \\ k \neq j}} \omega_J^{(kj)} \quad (4.26)$$

taking into account the ferromagnetic spin-spin coupling. This definition can be rephrased by saying that  $\hbar \tilde{\omega}_0^{(j)}$  is the energy gap between  $| \uparrow_1 \dots \uparrow_D \rangle$  and  $| \uparrow_1 \dots \downarrow_j \dots \uparrow_D \rangle$ . We further define correlation functions analogously to Equation (4.9),

$$\kappa_{\bar{g}g}^{(j)}(\tau) := \sum_{\ell} |g_\ell|^2 e^{-i(\omega_\ell - \tilde{\omega}_0^{(j)})\tau}, \quad (4.27)$$

and similarly for  $\kappa_{\bar{g}\gamma}^{(j)}$ ,  $\kappa_{\bar{\gamma}g}^{(j)}$  and  $\kappa_{\bar{\gamma}\gamma}^{(j)}$ . With these definitions one can write Equation (4.25) as

$$\begin{aligned} \langle 0 | U_I(\nu \Delta t, [\nu - 1] \Delta t) | 0 \rangle | \uparrow_1 \dots \uparrow_D \rangle &= | \uparrow_1 \dots \uparrow_D \rangle \left( \mathbb{1} \right. \\ &- \sum_j \int_{[\nu-1]\Delta t}^{\nu \Delta t} dt_1 \int_{[\nu-1]\Delta t}^{t_1} dt_2 \left[ \chi^{(j)}(\hat{\mathbf{x}}(t_1)) \chi^{(j)}(\hat{\mathbf{x}}(t_2)) \kappa_{\bar{g}g}^{(j)}(t_1 - t_2) \right. \\ &\left. + \chi^{(j)}(\hat{\mathbf{x}}(t_1)) \kappa_{\bar{g}\gamma}^{(j)}(t_1 - t_2) + \chi^{(j)}(\hat{\mathbf{x}}(t_2)) \kappa_{\bar{\gamma}g}^{(j)}(t_1 - t_2) + \kappa_{\bar{\gamma}\gamma}^{(j)}(t_1 - t_2) \right] \Bigg). \quad (4.28) \end{aligned}$$



In analogy to (4.12), the coupling constants are taken in the form

$$\begin{aligned} g_{\boldsymbol{\ell}}^{(j)} &= \left[ \Gamma^{(j)}(\omega_{\ell}, \mathbf{e}_{\boldsymbol{\ell}}) + \mathcal{O}(L_{\text{bath}}^{-1}) \right] \sqrt{\frac{\omega_{\ell}}{L_{\text{bath}}^3}}, \\ \gamma_{\boldsymbol{\ell}}^{(j)} &= \left[ \Gamma_{\text{spon}}^{(j)}(\omega_{\ell}, \mathbf{e}_{\boldsymbol{\ell}}) + \mathcal{O}(L_{\text{bath}}^{-1}) \right] \sqrt{\frac{\omega_{\ell}}{L_{\text{bath}}^3}} \end{aligned} \quad (4.29)$$

with  $\omega_{\ell} = c(\omega_{\ell})\ell$  as before,  $\mathbf{e}_{\boldsymbol{\ell}} = \boldsymbol{\ell}/\ell$ , and

$$\left| \Gamma^{(j)}(\omega_{\ell}, \mathbf{e}_{\boldsymbol{\ell}}) \right|^2 \gg \left| \Gamma_{\text{spon}}^{(j)}(\omega_{\ell}, \mathbf{e}_{\boldsymbol{\ell}}) \right|^2. \quad (4.30)$$

Again the Markov property Equation (4.14) is assumed to hold for the correlation functions in the continuum limit. The several integrals in Equation (4.28) can then be evaluated analogously to the single-spin case of Section 4.2.1. Again, one obtains a conditional Schrödinger Equation (4.18), but now with the conditional Hamiltonian

$$H_{\text{cond}} = \frac{\hat{\mathbf{p}}^2}{2m} + \frac{\hbar}{2} [\delta_{\text{shift}}(\hat{\mathbf{x}}) - iA(\hat{\mathbf{x}})], \quad (4.31)$$

with  $A(\mathbf{x})$  given by

$$\begin{aligned} A(\mathbf{x}) &= 2 \operatorname{Re} \sum_j \int_0^\infty d\tau \{ \kappa_{g\gamma}^{(j)}(\tau) \chi^{(j)}(\mathbf{x})^2 + \kappa_{\bar{\gamma}\gamma}^{(j)}(\tau) \} \\ &= \sum_j \left( \tilde{\omega}_0^{(j)} \right)^3 \left[ \frac{c \left( \tilde{\omega}_0^{(j)} \right) - \tilde{\omega}_0^{(j)} c' \left( \tilde{\omega}_0^{(j)} \right)}{c \left( \tilde{\omega}_0^{(j)} \right)^4} \right] \int \frac{d\Omega_{\mathbf{e}}}{(2\pi)^2} \\ &\quad \times \left( \left| \Gamma^{(j)} \left( \tilde{\omega}_0^{(j)}, \mathbf{e} \right) \right|^2 \chi^{(j)}(\mathbf{x})^2 + \left| \Gamma_{\text{spon}}^{(j)} \left( \tilde{\omega}_0^{(j)}, \mathbf{e} \right) \right|^2 \right) \end{aligned} \quad (4.32)$$

generalizing Equation (4.16). In Equation (4.32) the  $d\Omega_{\mathbf{e}}$  integral is taken over the unit sphere; the contributions from  $\kappa_{g\gamma}^{(j)}$ ,  $\kappa_{\bar{\gamma}g}^{(j)}$  have been neglected, due to Equation (4.30). The terms have the familiar form of the Einstein coefficients in quantum optics, where there would also be a sum over polarizations. The real part of the potential contribution to  $H_{\text{cond}}$ , the ‘line shift’  $\delta_{\text{shift}}(\mathbf{x})$  is given by

$$\delta_{\text{shift}}(\mathbf{x}) = 2 \operatorname{Im} \sum_j \int_0^\infty d\tau \{ \kappa_{g\gamma}^{(j)}(\tau) \chi^{(j)}(\mathbf{x})^2 + \kappa_{\bar{\gamma}\gamma}^{(j)}(\tau) \}. \quad (4.33)$$

Since the  $\kappa_{\bar{\gamma}\gamma}$  term leads to a constant it just gives an overall phase factor and can therefore be omitted. We note that  $A$  and  $\delta_{\text{shift}}$  depend on the modified resonance frequencies  $\tilde{\omega}_0^{(j)}$ , through  $\kappa_{g\gamma}^{(j)}$  and  $\kappa_{\bar{\gamma}\gamma}^{(j)}$ , rather than on  $\omega_0^{(j)}$ . This is as one would expect since the ferromagnetic coupling between the spins results in a decreased energy gap between  $|\uparrow_1 \dots \uparrow_D\rangle$  and  $|\uparrow_1 \dots \downarrow_j \dots \uparrow_D\rangle$  when compared to the single spin states  $|\uparrow\rangle$  and  $|\downarrow\rangle$ .



The probability density for the first detection, on the continuous, coarse-grained time-scale on which  $\Delta t$  is small, is obtained from Equations (4.6), (4.5), and Equation (4.18), together with Equation (4.31), and is again similar to Equation (4.21),

$$\begin{aligned} w_1(t) &= \frac{i}{\hbar} \left\langle \psi_{\text{cond}}^t \left| H_{\text{cond}} - H_{\text{cond}}^\dagger \right| \psi_{\text{cond}}^t \right\rangle \\ &= \int d^3x A(\mathbf{x}) |\langle \mathbf{x} | \psi_{\text{cond}}^t \rangle|^2. \end{aligned} \quad (4.34)$$

This is an average of the position dependent decay rate of the detector, weighted with the probability density for the particle to be at position  $\mathbf{x}$ , and to be undetected yet.

### 4.3 Example: Detector with smooth sensitivity function

#### 4.3.1 General setup

So far, the examples considered numerically always employed Heaviside's  $\Theta$  function as sensitivity function of the detector spin. In this section we consider a further example of an arrival-time measurement by means of the continuum limit of the spin-boson detector model, but now with a smooth sensitivity function. For simplicity, we will stick in this section to the simplified, one-dimensional model introduced in Section 3.2.1. As outlined in Section 3.1.3 we again assume that spin and bath are initially in state  $|\uparrow 0\rangle$ . Furthermore, we again assume that the Markov property Equation (4.14) holds, and so the analysis of the previous sections applies. According to Equation (4.18), the conditional time development in the continuum limit thus is governed by the conditional Hamiltonian

$$H_{\text{cond}} = \frac{\hat{p}^2}{2m} + \frac{\hbar}{2}(\delta_{\text{shift}} - iA)\chi_{\mathcal{I}_d}(\hat{x})^2, \quad (4.19)$$

containing a complex potential.  $A$  and  $\delta_{\text{shift}}$  are defined in Equations (4.16) and (4.17), and  $\chi_{\mathcal{I}_d}$  now is assumed to be smooth.

We note that in contrast to typical problems in scattering theory it will not be sufficient to investigate the asymptotic behavior, for  $t \rightarrow \pm\infty$ , of a wave packet subject to scattering off the potential

$$V(x) = \frac{\hbar}{2}(\delta_{\text{shift}} - iA)\chi_{\mathcal{I}_d}(x)^2.$$

In order to investigate the probability density for detection we need to calculate the complete time development of the wave packet, and in particular need to calculate the behavior of the wave packet just at those times when it hits the potential describing the detector.

We first aim at evaluating the eigenstates of the Hamiltonian of Equation (4.19) with smooth sensitivity function  $\chi_{\mathcal{I}_d}$ . The conditional time development of a given wave packet is then obtained as usual by means of a decomposition of the wave packet into these eigenstates.



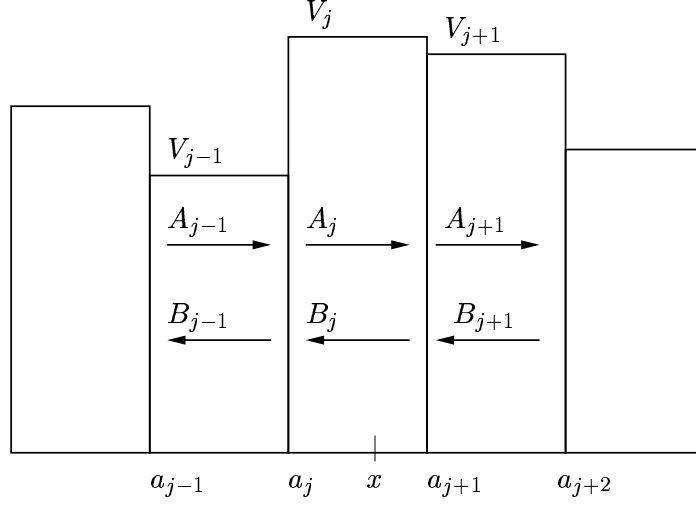


**Figure 4.1:** A piecewise constant potential. The eigenfunctions of the corresponding Hamiltonian are given piecewise in Equation (4.35). In any interval  $[a_j, a_{j+1}]$  an eigenfunction is given by a superposition on plane waves  $e^{\pm ik_j x}$  with the possibly complex wave number  $k_j$  defined in Equation (4.36), and with coefficients  $A_j$  for right-going waves and coefficients  $B_j$  for left-going waves.

### 4.3.2 Eigenfunctions

Although the physical model under consideration is the continuum limit of the spin-boson detector model or rather its simplification described in Section 3.2.1, we stress that the reasoning outlined in this subsection is valid for all smooth potentials  $V(x)$ , independent of their physical interpretation.

#### Starting point: Piecewise constant potential

We start our reasoning from a piecewise constant potential, from which the smooth potential will be obtained as a limit. Let  $\chi_{[a_j, a_{j+1}]}$ ,  $a_j < a_{j+1}$ , be the characteristic function of the interval  $[a_j, a_{j+1}]$ ,

$$\chi_{[a_j, a_{j+1}]}(x) = \begin{cases} 1 & \text{if } a_j < x < a_{j+1} \\ 0 & \text{else} \end{cases},$$

and let a piecewise constant potential  $V$  be defined by

$$V(x) = \sum_j V_j \chi_{[a_j, a_{j+1}]}(x),$$

see Figure 4.1. The eigenfunctions of the corresponding Hamiltonian

$$H_V = \frac{\hat{p}^2}{2m} + V(x),$$



to energy eigenvalue  $E_k$ , are given by

$$\Phi_k(x) = \sqrt{\frac{1}{2\pi}} \sum_j \left( A_j e^{ik_j x} + B_j e^{-ik_j x} \right) \chi_{[a_j, a_{j+1}]}(x) \quad (4.35)$$

with

$$k_j = \sqrt{\frac{2m}{\hbar^2} (E_k - V_j)}. \quad (4.36)$$

The coefficients  $A_j$ ,  $B_j$ ,  $j = 1, 2, \dots$  are related via the usual matching condition that both  $\Phi_k$  and its derivative with respect to  $x$  must be continuous. Introducing the matrix

$$\mathcal{M}_j(x) := \begin{pmatrix} e^{ik_j x} & e^{-ik_j x} \\ k_j e^{ik_j x} & -k_j e^{-ik_j x} \end{pmatrix},$$

this matching condition can be written as

$$\mathcal{M}_{j-1}(a_j) \begin{pmatrix} A_{j-1} \\ B_{j-1} \end{pmatrix} = \mathcal{M}_j(a_j) \begin{pmatrix} A_j \\ B_j \end{pmatrix}. \quad (4.37)$$

### Smooth potential limit

From Equation (4.37) one finds that the coefficients on the left and on the right side of the interval  $[a_j, a_{j+1}]$  are related by

$$\begin{aligned} \begin{pmatrix} A_{j+1} \\ B_{j+1} \end{pmatrix} &= \mathcal{M}_{j+1}^{-1}(a_{j+1}) \mathcal{M}_j(a_{j+1}) \mathcal{M}_j^{-1}(a_j) \mathcal{M}_{j-1}(a_j) \begin{pmatrix} A_{j-1} \\ B_{j-1} \end{pmatrix} \\ &=: \widetilde{\mathcal{M}}_j \begin{pmatrix} A_{j-1} \\ B_{j-1} \end{pmatrix}. \end{aligned} \quad (4.38)$$

It is convenient to introduce the notations

$$\Delta x := a_{j+1} - a_j, \quad \Delta k := k_{j+1} - k_{j-1}, \quad \text{and} \quad D_{\pm}^{j'} := k_{j'} \pm k_j, \quad j' = j \pm 1.$$

With these definitions the ‘transfer matrix’  $\widetilde{\mathcal{M}}_j$  reads

$$\widetilde{\mathcal{M}}_j = \frac{1}{4k_j k_{j+1}} \begin{pmatrix} m_{11} & m_{12} \\ m_{21} & m_{22} \end{pmatrix} \quad (4.39)$$

with

$$\begin{aligned} m_{11} &= e^{-ia_j \Delta k} \left( D_+^{j-1} D_+^{j+1} e^{-iD_-^{j+1} \Delta x} - D_-^{j-1} D_-^{j+1} e^{-iD_+^{j+1} \Delta x} \right) \\ m_{12} &= e^{-i(k_{j-1} + k_{j+1})a_j} \left( D_+^{j-1} D_-^{j+1} e^{-iD_+^{j+1} \Delta x} - D_-^{j-1} D_+^{j+1} e^{-iD_-^{j+1} \Delta x} \right) \\ m_{21} &= e^{i(k_{j-1} + k_{j+1})a_j} \left( D_+^{j-1} D_-^{j+1} e^{iD_+^{j+1} \Delta x} - D_-^{j-1} D_+^{j+1} e^{iD_-^{j+1} \Delta x} \right) \\ m_{22} &= e^{ia_j \Delta k} \left( D_+^{j-1} D_+^{j+1} e^{iD_-^{j+1} \Delta x} - D_-^{j-1} D_-^{j+1} e^{iD_+^{j+1} \Delta x} \right). \end{aligned} \quad (4.40)$$



We are interested in the limit of a smooth potential, i.e., in the limit

$$a_{j+1} \rightarrow a_j \quad \text{and} \quad k_{j-1} \rightarrow k_j \leftarrow k_{j+1}.$$

In this case one has

$$\begin{aligned} D_+^{j-1} D_+^{j+1} &\approx 4k_j^2, \\ D_+^{j-1} D_-^{j+1} - D_-^{j-1} D_+^{j+1} &\approx 2k_j \Delta k, \end{aligned}$$

and

$$\left| D_-^{j-1} D_-^{j+1} \right| \sim \mathcal{O}([\Delta k]^2).$$

Keeping only terms linear in  $\Delta x$ ,  $\Delta k$ , the transfer matrix  $\widetilde{\mathcal{M}}_j$  defined in Equations (4.39) and (4.40) simplifies to

$$\widetilde{\mathcal{M}}_j \approx \begin{pmatrix} 1 - ia_j \Delta k & e^{-2ik_j a_j} \Delta k / 2k_j \\ e^{2ik_j a_j} \Delta k / 2k_j & 1 + ia_j \Delta k \end{pmatrix},$$

and with Equation (4.38) one finds

$$\begin{aligned} \begin{pmatrix} A_{j+1} \\ B_{j+1} \end{pmatrix} - \begin{pmatrix} A_{j-1} \\ B_{j-1} \end{pmatrix} &= (\widetilde{\mathcal{M}}_j - \mathbb{1}) \begin{pmatrix} A_{j-1} \\ B_{j-1} \end{pmatrix} \\ &= \Delta k \begin{pmatrix} -ia_j & e^{-2ik_j a_j} / 2k_j \\ e^{2ik_j a_j} / 2k_j & ia_j \end{pmatrix} \begin{pmatrix} A_{j-1} \\ B_{j-1} \end{pmatrix}, \end{aligned}$$

up to higher orders in  $\Delta x$ ,  $\Delta k$ . We divide both sides of this equation by  $\Delta x$  and then consider the limit  $\Delta x \rightarrow 0$  and  $\Delta k \rightarrow 0$  which yields a smooth potential. With Equations (4.35) and (4.36) we find that in the limit of a smooth potential an eigenfunction for energy eigenvalue  $E_k$  is given by

$$\Phi_k(x) = \sqrt{\frac{1}{2\pi}} \left( A(x) e^{ik(x)x} + B(x) e^{-ik(x)x} \right), \quad (4.41)$$

where

$$k(x) = \sqrt{\frac{2m}{\hbar^2} [E_k - V(x)]},$$

and the coefficients  $A(x)$ ,  $B(x)$  fulfill a kind of ‘continuous matching condition’

$$\begin{pmatrix} A'(x) \\ B'(x) \end{pmatrix} = k'(x) \begin{pmatrix} -ix & e^{-2ik(x)x} / 2k(x) \\ e^{2ik(x)x} / 2k(x) & ix \end{pmatrix} \begin{pmatrix} A(x) \\ B(x) \end{pmatrix}. \quad (4.42)$$

We note that for this result to be valid it is necessary that  $k(x) \neq 0$  and

$$k'(x) = -\frac{mV'(x)/\hbar^2}{\sqrt{\frac{2m}{\hbar^2} (E_k - V(x))}}$$

exists. This condition will be fulfilled for all  $x \in \mathbb{R}$  in the examples discussed in Section 4.3.3, where  $V$  will always be smooth and  $\text{Im } V(x) \neq 0$  for all  $x \in \mathbb{R}$ .



### Boundary conditions: Asymptotic behavior

Similar to scattering theory, one will typically be interested in somehow ‘localized’ potentials,

$$\lim_{|x| \rightarrow \infty} V(x) = 0.$$

One then considers a wave packet which has been prepared in the remote past, far away from the potential, as a superposition of plane waves. Say, the wave packet is prepared far away on the left side, and contains only positive momenta. Such a wave packet can be decomposed into eigenfunctions  $\Phi_k$  given by Equation (4.41) with

$$\begin{aligned} \lim_{x \rightarrow -\infty} \begin{pmatrix} A(x) \\ B(x) \end{pmatrix} &= \begin{pmatrix} N \\ R(k) N \end{pmatrix} \\ \lim_{x \rightarrow \infty} \begin{pmatrix} A(x) \\ B(x) \end{pmatrix} &= \begin{pmatrix} T(k) N \\ 0 \end{pmatrix}. \end{aligned} \quad (4.43)$$

Such an eigenstate corresponds to a plane wave incident from the left, with a normalization constant  $N$ , together with a reflected part with a coefficient  $R(k)$  and a transmitted part with a coefficient  $T(k)$ .

We note that one prescribes the normalization  $N$  of the incident wave and also  $\lim_{x \rightarrow \infty} B(x) = 0$  which indicates that no wave is incident from the right. The coefficients  $R(k)$  and  $T(k)$ , though, are not prescribed from the start but are evaluated from Equation (4.42). Hence, the asymptotic behavior neither on the far left nor on the far right provides a suitable boundary value for a numerical integration of Equation (4.42). One can, however, integrate Equation (4.42) for

$$\lim_{x \rightarrow \infty} \begin{pmatrix} \tilde{A}(x) \\ \tilde{B}(x) \end{pmatrix} = \begin{pmatrix} 1 \\ 0 \end{pmatrix},$$

yielding a solution  $\begin{pmatrix} \tilde{A}(x) & \tilde{B}(x) \end{pmatrix}^T$ . Due to the linearity of Equation (4.42), the correct solution with the asymptotic behavior of Equation (4.43) is then given by

$$\begin{pmatrix} A(x) \\ B(x) \end{pmatrix} = \frac{N}{\left[ \lim_{x \rightarrow -\infty} \tilde{A}(x) \right]} \begin{pmatrix} \tilde{A}(x) \\ \tilde{B}(x) \end{pmatrix}.$$

#### 4.3.3 Numerical example

As a numerical example we consider similar to Sections 3.2.5, 3.2.6 and 4.2.2, 4.2.3 a cesium atom. The wave packet is prepared in the remote past far away from the detector such that the corresponding free packet (i.e., in the absence of the detector) at  $t = 0$  would be a Gaussian minimal uncertainty packet around  $x = x_0$  with width  $\Delta p$  in momentum space, and with an average velocity  $v_0$ . The conditional time development of the wave packet is obtained from



the decomposition into eigenstates (4.41) of the conditional Hamiltonian (4.19) with smooth sensitivity function  $\chi_{\mathcal{I}_d}$ ,

$$\langle x | \psi_{\text{cond}}^t \rangle = \int_0^\infty dk \tilde{\psi}(k) \Phi_k(x) e^{-i\hbar k^2 t/2m} \quad (4.44)$$

with a momentum distribution

$$\tilde{\psi}(k) = \left( \frac{\hbar}{\Delta p \sqrt{2\pi}} \right)^{1/2} \exp \left( -\frac{\hbar^2}{4(\Delta p)^2} (k - mv_0/\hbar)^2 + ikx_0 \right). \quad (4.45)$$

The parameters  $v_0$ ,  $\Delta p$  will be chosen such that  $\tilde{\Psi}(k) \approx 0$  for  $k \leq 0$ . The probability density for detection is given by

$$\begin{aligned} w_1(t) &= \frac{i}{\hbar} \left\langle \psi_{\text{cond}}^t \left| H_{\text{cond}} - H_{\text{cond}}^\dagger \right| \psi_{\text{cond}}^t \right\rangle \\ &= A \int_{-\infty}^\infty dx \chi_{\mathcal{I}_d}(x)^2 |\langle x | \psi_{\text{cond}}^t \rangle|^2, \end{aligned} \quad (4.21)$$

see Section 4.2.1.

In the sequel we will neglect the ‘line shift’  $\delta_{\text{shift}}$ ; negligible  $\delta_{\text{shift}}$  can be obtained, e.g., in the example of Sections 3.2.5 and 4.2.2 by choosing a maximal boson frequency<sup>3</sup>  $\omega_{\text{M}} \approx 1.278 \omega_0$ . The sensitivity function  $\chi_{\mathcal{I}_d}$  in Equation (4.19) is taken as a Gaussian around  $x = 0$ ,

$$\chi_{\mathcal{I}_d}(x) = e^{-x^2/4b^2}, \quad (4.46)$$

In Figure 4.2 two examples with the same incident wave packet are plotted, but with different decay rates  $A$  and with different widths  $b$  of the sensitivity function. Also plotted is Kijowski’s arrival time density  $\Pi_K$  at  $x = 0$  for the same wave packet [see Section 2.3 and in particular Equation (2.6)]. In both examples reflection from the absorbing potential, i.e., reflection without detection does not play a significant role. In the example with the broad and only weakly absorbing potential, however, about 5% of the wave packet are transmitted through the potential rather than being absorbed, i.e., detected. We also note that this broad detector yields a broad detection density (dashed line) which exhibits strong deviations when compared to Kijowski’s arrival-time density at  $x = 0$  (dots). In contrast to this it is seen that the probability density from the spin-boson detector model with narrow sensitivity function (solid line) is in excellent agreement with Kijowski’s axiomatically predicted density  $\Pi_K$ . The distinctive point is that in this case the width  $b$  of the sensitivity function is small compared to the relevant length scales of the wave packet and thus provides a useful tool to detect the arrival at a specific position.

<sup>3</sup>We note that  $\delta_{\text{shift}}$  given by Equation (4.23) is exactly zero for  $\omega_{\text{M}} = [W(1/e) + 1] \omega_0$ , where  $W$  denotes Lambert’s ‘ $W$  function’. The  $W$  function solves  $W(y) e^{W(y)} = y$ ; for a discussion of the  $W$  function, including a number of practical applications, see Reference [CGH<sup>+</sup>96]. The decay rate  $A$  is independent of  $\omega_{\text{M}}$  as long as  $\omega_{\text{M}} > \omega_0$ .



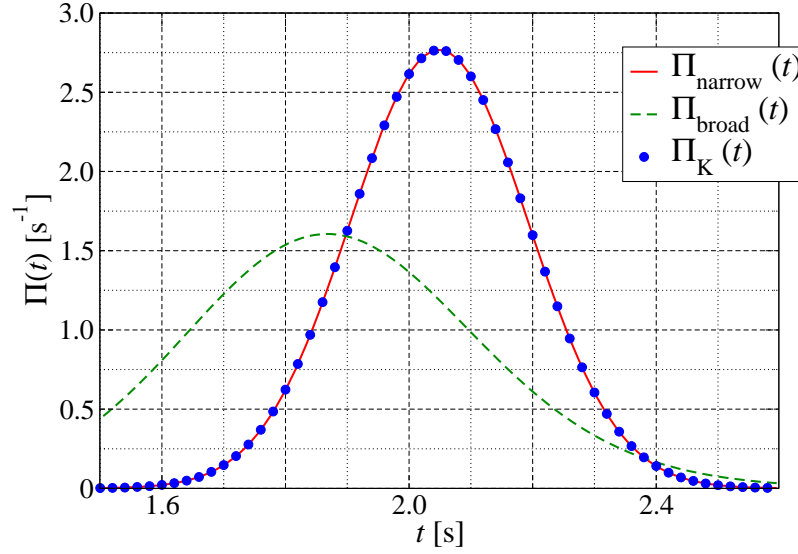


**Figure 4.2:** Solid line: spin-flip probability density  $w_1(t)$  for an incoming Gaussian wave packet of Equations (4.44) and (4.45) with  $v_0 = 0.903$  cm/s,  $x_0 = -18.5$  mm, and  $\Delta p = 0.38$  mm $^{-1} \times \hbar$ . The detector is described by its continuum limit with a decay rate  $A = 2.84 \times 10^5$  s $^{-1}$  and with a smooth sensitivity function of Equation (4.46) with width  $b = 0.27$   $\mu$ m. Dashed line: spin-flip probability density  $w_1(t)$  for the same incident wave packet, but now for detector parameters  $A = 1.69 \times 10^1$  s $^{-1}$  and  $b = 2$  mm. The density obtained from the detector with narrow sensitivity function is in excellent agreement with Kijowski's axiomatically predicted arrival-time density (dots).

#### 4.4 Detector dynamics: false positives, detection, and domino effect

In Section 4.2 we have derived all the necessary formulas to briefly comment on the detector dynamics. We note, however, that we do not aim at a complete analysis of the detector dynamics. Rather, the main features of the detector shall be made plausible. For a detailed analysis see References [GS90, Sch91, Sch97].

We start with the likelihood of a spontaneous first spin flip in the absence of the particle, a ‘false positive’. We note that the spin flip rate  $A(\mathbf{x})$  of Equation (4.32) can be written as

$$\begin{aligned}
 & A(\mathbf{x}) \\
 &= A_0 + \sum_j \left( \tilde{\omega}_0^{(j)} \right)^3 \left[ \frac{c \left( \tilde{\omega}_0^{(j)} \right) - \tilde{\omega}_0^{(j)} c' \left( \tilde{\omega}_0^{(j)} \right)}{c \left( \tilde{\omega}_0^{(j)} \right)^4} \right] \int \frac{d\Omega_{\mathbf{e}}}{(2\pi)^2} \left| \Gamma^{(j)} \left( \tilde{\omega}_0^{(j)}, \mathbf{e} \right) \right|^2 \chi^{(j)}(\mathbf{x})^2
 \end{aligned} \tag{4.32'}$$



with

$$A_0 = \sum_j \left( \tilde{\omega}_0^{(j)} \right)^3 \left[ \frac{c \left( \tilde{\omega}_0^{(j)} \right) - \tilde{\omega}_0^{(j)} c' \left( \tilde{\omega}_0^{(j)} \right)}{c \left( \tilde{\omega}_0^{(j)} \right)^4} \right] \int \frac{d\Omega_{\mathbf{e}}}{(2\pi)^2} \left| \Gamma_{\text{spn}}^{(j)} \left( \tilde{\omega}_0^{(j)}, \mathbf{e} \right) \right|^2. \quad (4.47)$$

We now consider the case that the particle's wave function has negligible overlap with all spins,

$$\left| \langle \mathbf{x} | \psi_{\text{cond}}^t \rangle \right|^2 \chi^{(j)}(\mathbf{x}) \approx 0, \quad j = 1, \dots, D.$$

Then, those parts of  $A(\mathbf{x})$  which are proportional to the squared sensitivity functions,  $\chi^{(j)}(\mathbf{x})^2$ , do not contribute to the spin-flip density  $w_1(t)$  given by Equation (4.34). Thus,  $A_0$  is regarded as spin flip rate in the absence of the particle. In this case the life time of the state  $|\uparrow_1 \dots \uparrow_D\rangle$  is simply given by

$$T_0 = \frac{1}{A_0}.$$

One sees from Equation (4.47) that  $T_0$  typically will be large, and false positives consequently will be rather unlikely, if the energy gap  $\hbar \tilde{\omega}_0^{(j)}$  between the states  $|\uparrow_1 \dots \uparrow_D\rangle$  and  $|\uparrow_1 \dots \downarrow_j \dots \uparrow_D\rangle$  is small for all  $j = 1, \dots, D$ , and the spin-bath coupling in the absence of the particle is weak.

But when the particle is close to the  $j^{\text{th}}$  spin, the enhanced spin-bath coupling according to  $\Gamma^{(j)}$  becomes valid as can be seen from Equations (4.32) and (4.34). The excited state  $|\uparrow\rangle_j$  hence decays much more quickly. As an example we consider the case that all spins are located in the same volume  $\mathcal{V}$ ,

$$\chi^{(j)}(\mathbf{x}) \equiv \chi_{\mathcal{V}}(\mathbf{x}).$$

Specializing Equation (4.32') to this case yields

$$A(\mathbf{x}) = A_0 + A_{\text{detection}} \chi_{\mathcal{V}}(\mathbf{x})^2$$

with

$$A_{\text{detection}} = \sum_j \left( \tilde{\omega}_0^{(j)} \right)^3 \left[ \frac{c \left( \tilde{\omega}_0^{(j)} \right) - \tilde{\omega}_0^{(j)} c' \left( \tilde{\omega}_0^{(j)} \right)}{c \left( \tilde{\omega}_0^{(j)} \right)^4} \right] \int \frac{d\Omega_{\mathbf{e}}}{(2\pi)^2} \left| \Gamma^{(j)} \left( \tilde{\omega}_0^{(j)}, \mathbf{e} \right) \right|^2.$$

One thus obtains from Equation (4.34) a probability density for the first spin flip reading

$$w_1(t) = A_0 + A_{\text{detection}} \int d^3x \chi_{\mathcal{V}}(\mathbf{x})^2 \left| \langle \mathbf{x} | \psi_{\text{cond}}^t \rangle \right|^2.$$

$A_{\text{detection}}$  is much larger than  $A_0$ , due to Equation (4.30), and its contribution to the spin-flip rate is proportional to the overlap of the wave function with the detector region  $\mathcal{V}$ . This is how a detector is supposed to work.

When the first spin has flipped, the ferromagnetic force experienced by its neighbors is strongly reduced, and thus these spins can flip rather quickly even



in the absence of the particle by means of the  $\gamma_{\ell}^{(j)}$ ; by a kind of ‘domino effect’, the whole array of spins will eventually flip, amplifying the first spin flip to a macroscopic event.

As an example we consider a ring of  $D$  identical spins with nearest-neighbor interaction,

$$\omega_0^{(j)} \equiv \omega_0 \quad \text{and} \quad \omega_J^{(jk)} \equiv \omega_J \delta_{j+1,k},$$

and  $j = D + 1$  identified with  $j = 1$ . For simplicity, we further assume  $c(\omega) \equiv c_0$  and  $\Gamma^{(j)}(\omega) \equiv \Gamma$ , accordingly for  $\Gamma_{\text{spn}}$ . We are interested in the further time development of the spin system after the first spin flip. The numbering of the spins is arbitrary, so we can assume that the spin which flipped first has the number 1. It has been argued in References [GS90, Sch91, Sch97] that, due to the relevant time scales, one may neglect processes of the kind of  $|\dots \uparrow_{j-1} \downarrow_j \dots\rangle \mapsto |\dots \downarrow_{j-1} \uparrow_j \dots\rangle$ . Consequently, we may calculate the flip rate of the neighboring spins, numbers 2 and  $D$ , under the assumption that all other spins are fixed. A calculation parallel to that outlined in Section 4.2 yields a flip rate for the spin number 2, reading

$$A_1(\mathbf{x}) = \left(\frac{\omega_0}{c_0}\right)^3 \int \frac{d\Omega_{\mathbf{e}}}{(2\pi)^2} \left( |\Gamma(\mathbf{e})|^2 \chi_{\nu}(\mathbf{x})^2 + |\Gamma_{\text{spn}}(\mathbf{e})|^2 \right). \quad (4.48)$$

The index 1 indicates that this is the decay rate under the assumption that spin number 1 has flipped already. As compared to Equation (4.32), the main difference is that  $\tilde{\omega}_0$  has been replaced with  $\omega_0$  since the ferromagnetic forces on this spin just cancel. One typically has  $\omega_0 \gg \tilde{\omega}_0$ , and thus  $A_1(\mathbf{x}) \gg A(\mathbf{x})$ . Even if we take into account only the weak spin-bath coupling according to  $\Gamma_{\text{spn}}$ , the spin still flips with a flip rate

$$A_{1,\text{spn}} = \left(\frac{\omega_0}{c_0}\right)^3 \int \frac{d\Omega_{\mathbf{e}}}{(2\pi)^2} \left| \Gamma_{\text{spn}}^{(j)}(\mathbf{e}) \right|^2 \gg A_0.$$

The same results also holds for the other neighboring spin, number  $D$ , and then in turn for *their* neighbors, and so on. Thus, even in the absence of the particle the whole ring flips, the average time needed for this given by

$$T_{\text{ring}} \approx \frac{D}{2A_{1,\text{spn}}}.$$

These results are in agreement with those obtained in References [GS90, Sch91, Sch97] by means of standard, unitary quantum mechanics. This illustrates the validity of the quantum jump approach. In the sequel, however, we will concentrate on the crucial event of the first spin flip.







## Chapter 5

# Application to arrival times: Discussion and extensions

The application of the spin-boson detector model to measurements of quantum arrival times is discussed, together with possible extensions. It is noted that the effective mathematical description (absorbing potential) is closely related to the one-channel limit of the fluorescence model. This relation between physically different models may help to illuminate the physical background of otherwise heuristically introduced complex potentials. Further, possible optimization schemes are discussed.

### 5.1 Relation of the detector model to the fluorescence model

The fluorescence model for particle detection has been introduced in Section 2.5. Originally it is a two-channel model since excitation number is not conserved due to the pumping by means of the classical laser field. In a certain limit, however, it yields a one-channel model (see Section 2.5.4). In this one-channel model, the conditional time development is governed by a Schrödinger equation with a complex potential

$$V(x) = \frac{\hbar\Delta(x)\Omega(x)^2 - i\hbar\gamma\Omega(x)^2/2}{4\Delta(x)^2 + \gamma^2}. \quad (2.27)$$

For  $\Delta(x) \equiv 0$  (laser in resonance)  $V$  is a purely imaginary potential, similar to the spin-boson detector model when the ‘line shift’ contribution  $\delta_{\text{shift}}$  can be neglected<sup>1</sup>; only the physical interpretation of the height of this imaginary potential differs. In other words, the one-channel limit of the fluorescence model coincides with the full quantum mechanical spin-boson detector model from Section 3.1 when considering the conditional time development for the particle until the first detection. In this way, the fully quantum mechanical detector model of Section 3.1 justifies the fluorescence model for quantum arrival times,

---

<sup>1</sup>For the possibility of neglecting  $\delta_{\text{shift}}$  see the remarks preceding Equation (4.46) in Section 4.3.3.



at least in the limit of Equation (2.24). Further, one can conversely immediately carry over the results of the fluorescence model to the detector model. The investigation of the fluorescence model (see Section 2.5) has shown that the essential features like reflection and delay [DEHM02], and main results like, e.g., linking Kijowski's arrival-time density to a particular measuring process [HSM03], can be obtained from the full two-channel model as well as from its one-channel limit. Hence these results immediately carry over to the present detector model.

This close relation is seen as a result of the careful analysis of both the models which yields in both cases a description by means of a complex potential. It is not at all obvious from the start since the models are physically quite different. We note that the derivation of a complex potential model for particle detection from two different physical models, viz. the fluorescence model and the spin-boson detector model, indicates the importance, and relevance of complex potentials.

Differences between the spin-boson detector model and the fluorescence model arise, however, when the models are applied to more complicated measurements than that of arrival time. An example for such an application showing differences between the models is the application to passage times, which will be investigated in Part II of the present thesis. In contrast to an arrival-time measurement the measurement of passage times requires knowledge about the particle's state after the first detection, the so called 'reset state'. This reset state is not the same in the two models.

## 5.2 Attempts to reduce the back-reaction

### 5.2.1 General remarks

The detector model introduced in Chapter 3 has three ingredients, viz. a particle in whose spatial properties one is interested, a 'detector' based on spins, and a bath of bosons, originally in the ground state. There is neither a direct measurement on the particle of interest nor on the detector but only on the bath, which is checked for bosons. In this way one can hope to keep the disturbance of the particle by the measurement to a minimum. However, the spin-boson detector model, in the limit of continuous boson modes, yields an effective description by a complex potential, just as the fluorescence model of Section 2.5 does. In Reference [Hal99] this has also been seen for a simplified spin-boson model. Thus, the spin-boson detector model shows the typical unwanted features mentioned in Section 2.2: There is a detection delay, due to the finite spin decay or flip rate, and there is also necessarily the possibility that the particle is reflected by the detector without the detection of a boson, due to the increased spin-bath coupling caused by the particle's wave function inside the detector. Due to this reflection without boson detection the probability density for the first detection,  $w_1(t)$  given by Equation (4.34), in general will not be normalized. A similar effect arises from the transmission of the particle without boson detection.



In order to reduce the detection delay one may be tempted to increase the spin-bath coupling in the presence of the particle, that is, to increase the coupling constants  $g_{\ell}^{(j)}$  in Equation (3.2). As a by-product this would also decrease transmission without detection. But the increase of this spatially dependent coupling means an increase of the complex potential  $(\hbar/2) [\delta_{\text{shift}}(\mathbf{x}) - iA(\mathbf{x})]$  [see Equations (4.32) and (4.33)], and this will also increase the reflection without boson detection. In the limit of infinite coupling, finally, everything is reflected while nothing is detected. This is in agreement with the explicit results obtained in the Jaynes-Cummings approximation of the detector model, see Section 3.2.3 and in particular Equations (3.26) and (3.27). The same phenomenon occurs in the fluorescence model [DEHM02] and is a typical feature of complex potentials, as already noted by Allcock [All69a, All69b, All69c].

### 5.2.2 Large number of spins, weak coupling

One might also try to reduce the influence of the spin-bath system on the particle and thus the latter's disturbance by decreasing the coupling of the individual spin to the boson-bath and simultaneously increasing the number of spins located in a given region. This seems promising because it is the flip of a single spin which gives rise to the detection. The reduced coupling of the individual spin could be expected to result in a reduced disturbance on the particle, while the increased number of spins compensates for the weaker coupling. To investigate this idea quantitatively we consider  $D$  spins, later to be taken to the limit  $D \rightarrow \infty$ , in the same volume  $\mathcal{V}$  and  $\chi^{(j)}(\mathbf{x}) \equiv \chi_{\mathcal{V}}(\mathbf{x})$  for all  $j$ . The coupling constants are taken in the form [compare Equation (4.29)]

$$g_{\ell}^{(j)} \equiv g_{\ell} = \frac{\Gamma(\omega_{\ell}, \mathbf{e}_{\ell}) + \mathcal{O}(L_{\text{bath}}^{-1})}{\sqrt{D}} \sqrt{\frac{\omega_{\ell}}{L_{\text{bath}}^3}},$$

and similarly for  $\gamma_{\ell}^{(j)}$ . Further, the ferromagnetic force experienced by the individual spin is assumed not to grow with increasing  $D$  such as for nearest neighbor interaction. Then (4.32) becomes

$$\begin{aligned} A(\mathbf{x}) &= \sum_{j=1}^D (\tilde{\omega}_0)^3 \left[ \frac{c(\tilde{\omega}_0) - \tilde{\omega}_0 c'(\tilde{\omega}_0)}{c(\tilde{\omega}_0)^4} \right] \\ &\quad \times \int \frac{d\Omega_{\mathbf{e}}}{(2\pi)^2} \frac{|\Gamma(\tilde{\omega}_0, \mathbf{e})|^2 \chi_{\mathcal{V}}(\mathbf{x})^2 + |\Gamma_{\text{spon}}(\tilde{\omega}_0, \mathbf{e})|^2}{D} \\ &= (\tilde{\omega}_0)^3 \left[ \frac{c(\tilde{\omega}_0) - \tilde{\omega}_0 c'(\tilde{\omega}_0)}{c(\tilde{\omega}_0)^4} \right] \\ &\quad \times \int \frac{d\Omega_{\mathbf{e}}}{(2\pi)^2} \left( |\Gamma(\tilde{\omega}_0, \mathbf{e})|^2 \chi_{\mathcal{V}}(\mathbf{x})^2 + |\Gamma_{\text{spon}}(\tilde{\omega}_0, \mathbf{e})|^2 \right), \end{aligned}$$

which is just the decay rate for a single spin in  $\mathcal{V}$ , with resonance frequency  $\tilde{\omega}_0$  and the coupling as for  $D = 1$ . A similar result holds for  $\delta_{\text{shift}}(\mathbf{x})$ , defined in (4.33).



Thus, simply increasing the number of spins  $D$  and scaling the coupling constants with  $\sqrt{1/D}$  leaves  $A$  and  $\delta_{\text{shift}}$  invariant and thus does not change the dynamics until the first detection (spin flip). In particular, it does not help to avoid reflection without detection. Any other scaling power of  $D$ , however, would not lead to a reasonable detector model in the limit  $D \rightarrow \infty$  since then  $A$  and  $\delta_{\text{shift}}$  would either go to zero or to infinity<sup>2</sup>. It is interesting to note that, although it is the flip of one single spin which triggers the detection, it is the totality of all spins located in  $V$  which determines the conditional time evolution.

### 5.2.3 Optimized detectors

It has been shown in the framework of complex potentials that one can deal with the delay/transmission-versus-reflection problem by means of an appropriate choice of the shape of the potential. In Reference [NEMH03a] a rather simple idea was investigated in the framework of the fluorescence model to optimize the reflection and transmission properties. This idea is easily applied to the present spin-boson model.

For simplicity we consider only one dimension, but several spins. The sensitivity functions  $\chi^{(j)}$  of the spins are assumed to be characteristic functions of the intervals  $\mathcal{G}^{(j)}$  where the respective spins are located, and these intervals are assumed not to overlap,  $\mathcal{G}^{(j)} \cap \mathcal{G}^{(k)} = \emptyset$  if  $j \neq k$ . Each spin is allowed to have its own coupling constants, i.e., we allow  $g_\ell^{(j)} \neq g_\ell^{(k)}$ ,  $j \neq k$ . We neglect  $H_{\text{spn}}$  in view of Equation 3.3, and accordingly neglect the possibility of spontaneous spin flips (false positives). We further assume that the model can be described by the continuum limit of Chapter 4. Since the contributions of different spins to the conditional time development do not mix, as was argued in Section 4.2.4, the analysis of Section 4.2.1 for the one-dimensional case is easily generalized to many spins. Analogously to Equations (4.16) and (4.17) we put

$$A^{(j)} = \tilde{\omega}_0^{(j)} \frac{c(\tilde{\omega}_0^{(j)}) - \tilde{\omega}_0^{(j)} c'(\tilde{\omega}_0^{(j)})}{c(\tilde{\omega}_0^{(j)})^2} \left| \Gamma^{(j)}(\tilde{\omega}_0^{(j)}) \right|^2$$

and

$$\delta_{\text{shift}}^{(j)} = 2 \operatorname{Im} \int_0^\infty d\tau \kappa_{gg}^{(j)}(\tau).$$

The conditional Hamiltonian then reads

$$H_{\text{cond}} = \frac{\hat{p}^2}{2m} + \frac{\hbar}{2} \sum_j \left[ \delta_{\text{shift}}^{(j)} - i A^{(j)} \right] \chi^{(j)}(\hat{x}). \quad (5.1)$$

Since the  $\chi^{(j)}$  are assumed to be characteristic functions of non-overlapping intervals this notation emphasizes that the potential contained in  $H_{\text{cond}}$  is piece-

---

<sup>2</sup>We mention, based on unpublished calculations by Hegerfeldt et al., that similar results also hold for the quantum optical fluorescence model of Section 2.5.



wise constant, as depicted in Figure 4.1. The height of each rectangular potential barrier in Equation 5.1 can be adjusted independently of the other barriers by adjusting the model parameters of the respective spin.

We assume that the detector consists of  $D$  spins, the first spin being located in the open interval  $\mathcal{G}^{(1)} = (x_1, x_2)$  and the last spin being located in  $\mathcal{G}^{(D)} = (x_D, x_{D+1})$ . As in Section 4.3.3 before taking the smooth-potential limit, the eigenstates of  $H_{\text{cond}}$ , to energy eigenvalue  $E_k$ , have the form

$$\Phi_k(x) = \sqrt{\frac{1}{2\pi}} \sum_j \left( A_j e^{ik_j x} + B_j e^{-ik_j x} \right) \chi_{[a_j, a_{j+1}]}(x) \quad (4.35)$$

with  $k$  given by Equation (4.36). We assume that the particle is incident from the left, i.e., the coefficients on the left of the detector have the form

$$\begin{pmatrix} A_0 \\ B_0 \end{pmatrix} = \begin{pmatrix} N \\ R(k) N \end{pmatrix},$$

and those on the right of the detector have the form

$$\begin{pmatrix} A_{D+1} \\ B_{D+1} \end{pmatrix} = \begin{pmatrix} T(k) N \\ 0 \end{pmatrix},$$

where  $N$  is the normalization constant of the incident plane wave. The coefficients  $A_j$  and  $B_j$ , and in particular  $B_0 = R(k) N$  and  $A_{D+1} = T(k) N$ , can be evaluated by the transfer-matrix method sketched in Section 4.3 (without the smooth-potential limit). The probability for reflection is given by  $|R(k)|^2$ , and the probability for transmission is given by  $|T(k)|^2$ . Consequently, the probability for non-detection is given by

$$P_{RT}(k) := |R(k)|^2 + |T(k)|^2.$$

For given  $k$  the probability  $P_{RT}(k)$  depends on the heights of the several rectangular potential barriers. If one considers a model with  $D$  barriers at fixed locations, minimizing  $P_{RT}(k)$  thus is an optimization problem with  $2D$  variables (real and imaginary part of each barrier) which can be solved numerically by standard routines. This procedure can be extended to a finite range of wave numbers  $k$ : One discretizes this range by choosing a finite number of  $k_i$ ,  $i = 1, \dots, N$ , and then minimizes the weighted average with weights  $\mathbf{w} = (w_1, \dots, w_N)$ ,

$$\langle P_{RT} \rangle_{\mathbf{w}} = \sum_{i=1}^N w_i P_{RT}(k_i).$$

As an example we consider a cesium atom incident from the left, and optimize  $\langle P_{RT} \rangle_{\mathbf{w}}$  for a range  $k = mv_0/\hbar$  with  $v_0 = 2 \dots 10$  cm/s with equal weights  $w_i = 1/D$ . The detector is assumed to be described by eight rectangular potential barriers with equal widths, located between  $x = 0$  and  $x = 1 \mu\text{m}$ . We neglect the real part of the potential,  $\delta_{\text{shift}}^{(j)}$  (see the corresponding remarks in Section 4.3.3, in particular the footnote there), and minimize the non-detection



probability with respect to the  $A^{(j)}$ . The optimized potential is depicted in Figure 5.1, and the non-detection probability  $P_{RT}(k)$  for the individual  $k$  obtained for the optimal choice of the  $A^{(j)}$  is shown in Figure 5.2. It is seen that it is possible to construct detectors such that neither reflection nor transmission without detection play a role for a given energy range of the incident particles.

More elaborated optimization techniques for general and in particular smooth complex potentials have been studied in References [MBM95, PMS98]. It has been shown that it is possible to absorb nearly the complete wave packet in a very short spatial interval; given a wave packet with a specific energy range, an appropriate complex potential can be constructed by means of inverse scattering techniques. Again, these results immediately carry over to the continuum limit of the spin-boson detector model. We stress that there is no such a thing as *the* optimal imaginary potential for all wave packets, but the construction of the optimized potential requires *a priori* information about energy range of the wave packet under consideration.

### 5.3 Outlook: Application to passage times

In Part II of the present thesis a more complicated application of the spin-boson detector model will be discussed: The measurement of quantum passage times. Like quantum arrival times, quantum passage times (and the related dwell, reflection, and tunnel times) are an extensively and sometimes controversially discussed topic. We investigate a particular measurement scheme which mimicks the way a passage-time measurement is typically performed by an experimentalist. The spin-boson detector model is used to model the individual particle detections during the measurement process.



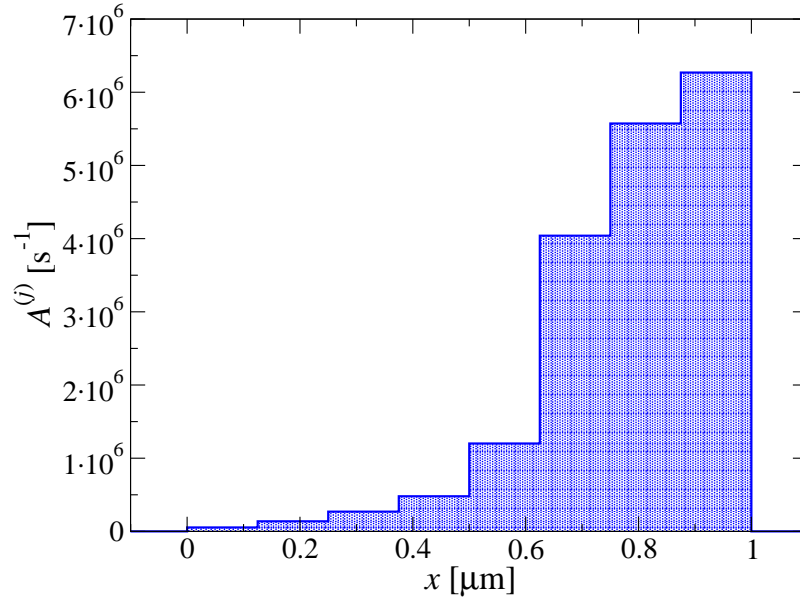


**Figure 5.1:** Optimal choice of decay rates  $A^{(j)}$  when the detector is described by eight rectangular, imaginary barriers with equal widths, located between  $x = 0$  and  $x = 1 \mu\text{m}$ ; optimized for cesium atoms incident from the left with velocities  $v = 2 \dots 10 \text{ cm/s}$ .

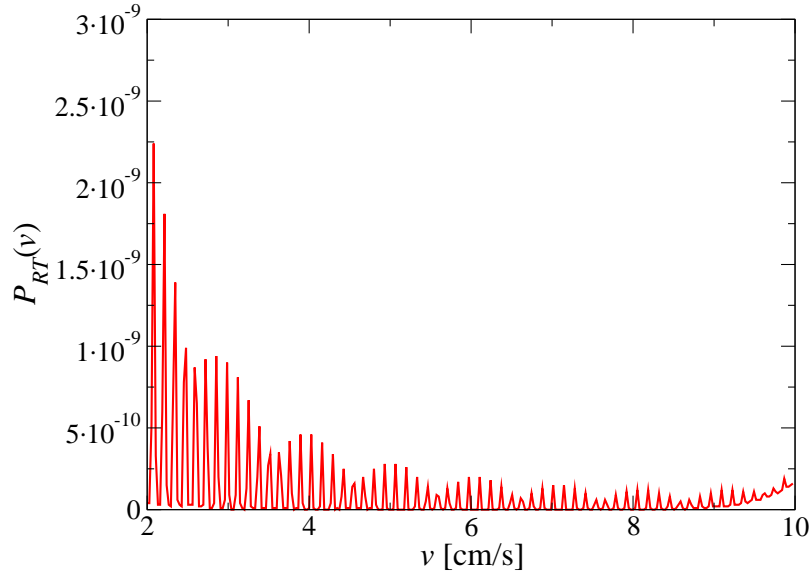


**Figure 5.2:** Non-detection probability  $P_{RT}$  as a function of the velocity  $v = \hbar k/m$  for a cesium atom incident from the left on the detector depicted in Figure 5.1. Over most of the range, the non-detection probability is less than  $10^{-9}$ .







## **Part II**

### **Application to passage times**







## Chapter 6

# Passage times: Introduction

Some approaches to quantum passage and related times are briefly sketched. This is *not* meant to be a complete review of the extensive literature on this topic. In order to give a first idea about quantum dwell and passage times, we just present two examples for ‘ideal’ approaches and briefly discuss their conceptual differences, and one example for an ‘operational’ approach. Idea and results of the latter example will later be compared to the measurement scheme investigated in Chapters 7 and 8. For a more exhaustive and detailed review (with main focus on tunneling times) see, e.g., References [HS89, LM94]. Further, an outline of Part II is given.

### 6.1 Quantum passage times

The arrival time discussed in Part I is, of course, not the only possible time observable in quantum mechanics. Preparing a particle at  $t = 0$  with localized but extended wave function as before, one may also ask for the time this particle spends in some given region of space. Repeating this experiment would yield a ‘dwell-time density’ or ‘sojourn-time density’. Again the question poses itself, how to measure the dwell time, and what to expect the resulting density to look like? One may also ask similar but more detailed questions than that concerning dwell times: Discriminating between those particles which eventually transmit the region of interest and those which are reflected, one may separately consider ‘passage times’ and ‘reflection times’. Related to the passage time is the ‘tunneling time’ when in the region of interest there is a barrier which classically cannot be traversed by the particle.

Similar to the approaches to arrival time, the approaches to dwell and related times may be separated into those aiming at ‘ideal’ quantities depending on the system of interest alone, and ‘operational’ ones coupling the system of interest to some kind of ‘measurement device’. Examples for the first class of approaches are the average dwell time for the stationary case by Smith [Smi60], the dwell-time operator by Ekstein and Siegert [ES71] (see Section 6.2), the approach via Feynman path integrals by Sokolovski and Baskin, yielding complex valued passage times [SB87], and the dwell time for a localized wave packet and its separation into passage and reflection times by Jaworski and Wardlaw



[JW88], e.g., or by Muga, Brouard, and Sala [MBS92]. Examples for the latter class of approaches are the Lamor clock approaches by Baz' and Rybachenko [Baz67, Ryb67], further investigated and related to Smith's ideal dwell time by Büttiker [Büt83], or the experimental approach by means of optical tunneling by Balcou and Dutriaux yielding both real and imaginary part of complex passage time [BD97]. Another model based on the particle's coupling to a clock is due to Salecker and Wigner [SW58], elaborated further by Peres [Per80], and extended to semi-continuous particle-clock coupling by Alonso, Sala, and Muga [ASM03] (see Section 6.4).

## 6.2 The dwell-time operator by Ekstein and Siegert

In the early 70ies, Ekstein and Siegert put forward a 'dwell-time operator' [ES71]: Consider first an ensemble of particles with time dependent position density  $\varrho_t(x)$ . The average time a particle spends between the position  $x = a$  and  $x = b$ ,  $L := b - a > 0$ , is given by

$$\tau_D^{\text{classical}}(a, b) = \int_{-\infty}^{\infty} dt \int_a^b dx \varrho_t(x). \quad (6.1)$$

The quantum mechanical counterpart of this classical average dwell time is formally<sup>1</sup> found to be [JW88, MBS92]

$$\tau_D(a, b) = \int_{-\infty}^{\infty} dt \int_a^b dx |\psi_t(x)|^2, \quad (6.2)$$

where  $\psi_t$  is the wave function of the particle. This 'quantum average dwell time' can be written as

$$\tau_D(a, b) = \langle \psi_0 | \hat{\tau}_D(a, b) | \psi_0 \rangle,$$

where  $\langle x | \psi_0 \rangle = \psi_0(x)$  is the initial wave function, and the dwell-time operator  $\hat{\tau}_D$  is defined by

$$\hat{\tau}_D(a, b) := \int_{-\infty}^{\infty} dt e^{iHt/\hbar} \mathbb{P}_{[a,b]} e^{-iHt/\hbar} \quad (6.3)$$

with the Hamiltonian  $H$  and the projector on the interval  $[a, b]$ ,

$$\mathbb{P}_{[a,b]} := \int_a^b dx |x\rangle \langle x|.$$

In order to sketch some basic properties of  $\hat{\tau}_D$  we consider the free case, i.e.,  $H = \hat{p}^2/2m$ . It can be shown [DEMN04] that  $\hat{\tau}_D$  is essentially self-adjoint;

<sup>1</sup>Note that in the standard interpretation of quantum mechanics there are no particle trajectories, and thus the interpretation of Equation (6.2) as 'average dwell time' is not quite straightforward. However, arguments for the extension of Equation (6.1) to the quantum case can be found, e.g., by means of the Feynman integral approach to quantum mechanics [Fey48], see Reference [SC92].



further, it commutes with  $H$ , and hence these operators can be diagonalized simultaneously. Expanding the eigenstates of  $\hat{\tau}_D$  into momentum eigenstates  $|k\rangle$ ,  $\langle x|k\rangle = \sqrt{1/2\pi} e^{ikx}$ , yields

$$|\tau_k^\pm\rangle = \sqrt{\frac{1}{2}} \left( |k\rangle \pm e^{ik(a+b)} |-k\rangle \right), \quad k > 0, \quad (6.4)$$

and the corresponding eigenvalues are

$$\tau_k^\pm = \frac{mL}{\hbar k} \left( 1 \pm \frac{\sin(kL)}{kL} \right). \quad (6.5)$$

Note that

$$\frac{1}{2} (\tau_k^+ + \tau_k^-) = \frac{mL}{\hbar k}$$

is the classical dwell time of a free particle with momentum  $p = \hbar k$ . In the limit  $k \rightarrow 0$  one finds  $\tau_k^+ \rightarrow \infty$ , but  $\tau_k^- \rightarrow 0$ . Since  $\hat{\tau}_D$  is essentially self-adjoint its eigenstates are complete,

$$\int_0^\infty dk (|\tau_k^+\rangle \langle \tau_k^+| + |\tau_k^-\rangle \langle \tau_k^-|) = \mathbb{1},$$

and thus by means of Equations (6.4) and (6.5) the dwell-time density for a given initial state  $|\psi_0\rangle$  is calculated to be

$$\begin{aligned} \Pi_D(\tau) &= \langle \psi_0 | \delta(\hat{\tau}_D(a, b) - \tau) | \psi_0 \rangle \\ &= \int_0^\infty dk \left( |\langle \tau_k^+ | \psi_0 \rangle|^2 \delta(\tau_k^+ - \tau) + |\langle \tau_k^- | \psi_0 \rangle|^2 \delta(\tau_k^- - \tau) \right) \\ &= \int_0^\infty dk \sum_j \left( |\langle \tau_k^+ | \psi_0 \rangle|^2 \frac{\delta(k_j^+[\tau] - k)}{|F'_+(k_j^+[\tau])|} \right. \\ &\quad \left. + |\langle \tau_k^- | \psi_0 \rangle|^2 \frac{\delta(k_j^-[\tau] - k)}{|F'_-(k_j^-[\tau])|} \right), \end{aligned} \quad (6.6)$$

where  $k_j^\pm[\tau]$  for given  $\tau$  denotes the zeros of the transcendental function

$$F_\pm(k) = \frac{mL}{\hbar k} \left( 1 \pm \frac{\sin(kL)}{kL} \right) - \tau,$$

and the prime denotes the derivative with respect to  $k$ . This dwell-time density exhibits a resonance structure since the denominators are given by the modulus of one of the derivatives

$$F'_\pm(k) = -\frac{mL}{\hbar k^2} \pm \frac{mL}{\hbar k^2} \cos(kL) \mp \frac{m}{\hbar k^3} \sin(kL),$$

and either  $F'_+$  or  $F'_-$  vanishes at  $k = n\pi/L$ ,  $n = 1, 2, \dots$ . Hence,  $\Pi_D$  diverges whenever  $k_j^\pm[\tau] = n\pi/L$  and  $\langle k_j^\pm[\tau] | \psi_0 \rangle \neq 0$ . We note that for  $k = n\pi/L$  one finds degenerate eigenvalues  $\tau_k^+ = \tau_k^-$ .



### 6.3 The passage time as difference of arrival times

The dwell-time operator  $\hat{\tau}_D$  introduced in the preceding section does not discriminate between transmitted and reflected particles. Now we turn to passage time, i.e., to the time spent in some given region by those particles which eventually are transmitted through this region. The typical way to measure such a passage time in a time-of-flight experiment is not to continuously observe the particle. Instead, the particle is detected upon entering the region of interest and upon exit, and the time interval between these signals is regarded as passage time. In the present section we treat the ‘passage time as difference of arrival times’ as ideal quantity determined by the properties of the particle’s wave function alone. An operational approach based on a particular detector model, viz. the spin-boson detector model introduced in Chapter 3, will be investigated in Chapters 7 and 8.

In case of free particles, an operator for the difference of arrival times at positions  $x = a$  and  $x = b$ ,  $L := b - a > 0$  can be constructed by means of the respective arrival-time operators [see Section 2.4 and in particular Equation (2.16)],

$$\hat{\tau}_{\text{passage}}(a, b) := |\hat{t}_b - \hat{t}_a| = mL |\hat{p}|^{-1}. \quad (6.7)$$

One immediately sees that the momentum eigenstates  $|k\rangle$  are eigenstates of  $\hat{\tau}_{\text{passage}}(a, b)$ , the eigenvalue  $mL/\hbar k$  being twofold degenerate,

$$\hat{\tau}_{\text{passage}}(a, b) |\pm k\rangle = \frac{mL}{\hbar k} |\pm k\rangle, \quad k > 0.$$

The corresponding passage-time density is calculated by means of the completeness relation of the momentum eigenstates as

$$\begin{aligned} \Pi_{\text{passage}}(\tau) &= \langle \psi_0 | \delta(\hat{\tau}_{\text{passage}} - \tau) | \psi_0 \rangle \\ &= \int_0^\infty dk \left( |\langle k | \psi_0 \rangle|^2 + |\langle -k | \psi_0 \rangle|^2 \right) \delta\left(\frac{mL}{\hbar k} - \tau\right) \\ &= \frac{mL}{\hbar \tau^2} \left( \left| \left\langle k = \frac{mL}{\hbar \tau} \middle| \psi_0 \right\rangle \right|^2 + \left| \left\langle k = -\frac{mL}{\hbar \tau} \middle| \psi_0 \right\rangle \right|^2 \right); \end{aligned}$$

this is just the passage-time density for an ensemble of classical particles with momentum density

$$\varrho_0(p) = |\langle p | \psi_0 \rangle|^2, \quad p = \hbar k.$$

In contrast to the dwell-time density  $\Pi_D$  of the preceding section, the passage-time density  $\Pi_{\text{passage}}$  does not exhibit a resonance structure. This difference is interesting to note since we investigated both operators,  $\hat{\tau}_D$  as well as  $\hat{\tau}_{\text{passage}}$ , in the free case. Classically, one would argue that in this case there is no reflection and thus dwell time and passage time should be identical. In quantum mechanics, however, we see that it is not that easy. We note that the ideas behind the two operators are different: The dwell-time operator  $\hat{\tau}_D(a, b)$  defined in Equation (6.3) can be understood as checking continuously the probability density for the particle to be in  $[a, b]$  and then integrating this density



over the time. From this point of view  $\hat{\tau}_D$  is the abstract image of one continuous measurement, or one continuous observation of the probability density  $|\psi(x, t)|^2$  inside  $[a, b]$ . In contrast to this,  $\hat{\tau}_{\text{passage}}$  can be seen as abstract image of a passage-time measurement based on two distinct measurements at the positions  $x = a$  and  $x = b$  while the probability density  $|\psi(x, t)|^2$  inside  $[a, b]$  is not directly observed. As seen above, the quantum mechanical operators related to these two different ideas yield different densities although the classical picture would suggest agreement. This illustrates that in quantum mechanics one has to be very careful to clarify the measurement by which a particular observable is to be obtained. It thus appears indeed useful to not merely rely on mathematical approaches aiming at ‘ideal’ passage, dwell, or related times. As in the case of arrival times, these approaches should be complemented by ‘operational’ approaches, i.e., by the formulation and investigation of particular *Gedanken* experiments aiming at the ‘measurement’ of the observable under consideration.

## 6.4 Clock models

Already in 1958, Wigner and Salecker made a proposal for a ‘quantum clock’ based on eigenstates of the angular momentum [SW58]. The application of this clock to the measurement of the duration of several physical processes, and in particular to the measurement of dwell time, was investigated by Peres [Per80].

### 6.4.1 The quantum clock of Wigner and Salecker

The idea of the quantum clock reads as follows. The clock’s Hamiltonian is given by

$$H_{\text{clock}} = \omega \hat{J}_z \hat{=} -i\hbar\omega \frac{\partial}{\partial \varphi},$$

where  $\omega$  is an angular frequency,  $\varphi \in [0, 2\pi[$ , and  $\hat{J}_z \hat{=} -i\hbar\partial/\partial\varphi$  is the  $z$ -component of the canonical angular momentum. Normalized and orthogonal<sup>2</sup> eigenstates of  $H_{\text{clock}}$  are given by  $|u_n\rangle$  with

$$\langle \varphi | u_n \rangle = \frac{1}{\sqrt{2\pi}} e^{in\varphi}, \quad n \in \mathbb{Z}.$$

The corresponding eigenvalue to  $|u_n\rangle$  is  $\hbar\omega n$ ,

$$H_{\text{clock}} |u_n\rangle = \hbar\omega n |u_n\rangle. \quad (6.8)$$

Now consider a coherent superposition

$$|v_0\rangle = \frac{1}{\sqrt{N}} \sum_{n=-j}^j |u_n\rangle, \quad N = 2j + 1.$$

---

<sup>2</sup>Here, ‘orthogonal’ is meant with respect to  $\langle f|g \rangle = \int_0^{2\pi} d\varphi \overline{f(\varphi)} g(\varphi)$ .



One has

$$\langle \hat{\varphi} \rangle_0 := \langle v_0 | \hat{\varphi} | v_0 \rangle = 0,$$

and from Equation (6.8) the time development of the initial state  $|v_0\rangle$  is found to be

$$\langle \varphi | v_t \rangle = \left\langle \varphi \left| e^{-iH_{\text{clock}}t/\hbar} \right| v_0 \right\rangle = \langle \varphi - \omega t | v_0 \rangle. \quad (6.9)$$

Thus,

$$\langle \hat{\varphi} \rangle_t := \langle v_t | \hat{\varphi} | v_t \rangle$$

can serve as a hand of a clock, indicating time as

$$t = \frac{\langle \hat{\varphi} \rangle_t}{\omega},$$

which is unique for  $0 \leq t < 2\pi/\omega$ . The overlap between states at different times,  $v_t$  and  $v_{t'}$ , is calculated as

$$\langle v_t | v_{t'} \rangle = \frac{\sin([N/2]\omega[t-t'])}{N \sin(\omega[t-t']/2)}.$$

Consequently, two states at different times  $t, t'$  are orthogonal, and thus can be clearly distinguished by a single measurement, if

$$|t - t'| = n \frac{2\pi}{N\omega}, \quad n \in \mathbb{N} \setminus \{0\}.$$

The smallest time difference for which such a clear distinction is possible,

$$\Delta_t = \frac{2\pi}{N\omega}, \quad (6.10)$$

is called the ‘hand width’ and indicates the precision of the quantum clock.

#### 6.4.2 Applications to dwell times

In order to measure by means of this clock the dwell time of a particle in an interval  $\mathcal{I}_d = [0, d]$  one couples the particle to the clock when being in the interval. If the particle is free up to the coupling to the clock, the corresponding Hamiltonian reads

$$H = \frac{\hat{p}^2}{2m} + \chi_{\mathcal{I}_d}(\hat{x}) \omega \hat{J}_z$$

with the characteristic function

$$\chi_{\mathcal{I}_d}(x) = \begin{cases} 1 & \text{if } 0 \leq x \leq d \\ 0 & \text{else} \end{cases}.$$

In case of interaction, the interaction potential  $V(x)$  would be added to the Hamiltonian. The particle, as long as it is in  $\mathcal{I}_d$ , is continuously coupled to the clock, and no distinction is made between transmitted and reflected particles. This is in line with the understanding of the dwell-time operator  $\hat{\tau}_D$ , as it has been outlined at the end of Section 6.3.



Since  $H$  and  $\hat{J}$  commute one has

$$H |\psi\rangle |u_n\rangle = \left( \frac{\hat{p}^2}{2m} + \chi_{\mathcal{I}_d}(\hat{x}) \hbar \omega n \right) |\psi\rangle |u_n\rangle, \quad (6.11)$$

where  $|\psi\rangle$  is the state of the moving particle. Consequently, the initial state  $|\psi_0\rangle |v_0\rangle$  develops according to

$$e^{-iHt/\hbar} |\psi_0\rangle |v_0\rangle = \frac{1}{\sqrt{N}} \sum_{n=-j}^j |\psi_t^{(n)}\rangle |u_n\rangle$$

with

$$|\psi_t^{(n)}\rangle = e^{-i(\hat{p}^2/(2m) + \chi_{\mathcal{I}_d}(\hat{x}) \hbar \omega n)t/\hbar} |\psi_0\rangle.$$

In other words,  $|\psi_t^{(n)}\rangle$ , which may be regarded as a kind of partial wave, behaves as if scattered by a rectangular potential of height (or depth, resp.)

$$V_n = \hbar \omega n, \quad n = -j, \dots, j, \quad (6.12)$$

due to the coupling to the clock.

We consider an incident plane wave,  $\langle x|k\rangle = \sqrt{1/2\pi} e^{ikx}$ , with wave number  $k = \sqrt{2mE_k}/\hbar$ ,  $E_k$  being the kinetic energy. The wave number inside the potential barrier  $V_n$  is  $k' = \sqrt{2m(E_k - V_n)}/\hbar$ . Consequently, for  $|V_n| \ll E_k$  ('small disturbance') the phase shift caused by this barrier is given by

$$(k' - k) d = -\frac{V_n}{\hbar} d \sqrt{\frac{m}{2E_k}} = -n\omega d \sqrt{\frac{m}{2E_k}} =: -n\omega\tau_d,$$

up to higher orders in  $V/E_k^{1/2}$ . There,  $\tau_d = d(2E_k/m)^{-1/2}$  is the classical dwell time of a free particle with kinetic energy  $E_k$  in the interval  $\mathcal{I}_d$ . Thus, if the incident wave packet is sharply peaked around wave number  $k$ ,  $|\psi_0\rangle \sim |k\rangle |v_0\rangle$ , the outgoing state after passing through the barrier will be [compare Equation (6.9)]

$$|\Psi_{\text{final}}\rangle \sim \frac{1}{\sqrt{N}} |k\rangle \sum_{j=-N}^N e^{-in\omega\tau_d} |u_n\rangle = |k\rangle |v_{\tau_d}\rangle,$$

the clock's hand pointing at the classically expected dwell time.

The hand width of the clock is the smaller the more eigenstates  $|u_n\rangle$  are coherently superposed in the clock's initial state  $|v_0\rangle$ , as can be seen from Equation (6.10). For given kinetic energy  $E_k$  of the incident particle, though, the number  $N = 2j + 1$  of superposed eigenstates is limited by the small disturbance condition  $|V_n| \ll E_k$  for all  $n = -j, \dots, j$ . This limits the hand width of the clock and thus the accuracy of the measurement scheme to [see Equations (6.10) and (6.12)]

$$\Delta_t \gg \frac{\pi \hbar}{E_k}. \quad (6.13)$$



Alonso, Sala, and Muga in Reference [ASM03] replaced the continuous coupling to the clock, Equation (6.11), by a pulsed coupling with a time  $T$  between the pulses,

$$H_{\text{pulsed}} = \frac{\hat{p}^2}{2m} + \omega T \left( \sum_{n=-\infty}^{\infty} \delta(t - nT) \right) \chi_{\mathcal{I}_d}(\hat{x}) \hat{J}_z.$$

They argued that even if Equation (6.13) is violated a dwell-time measurement fulfilling some kind of small disturbance condition is possible provided  $T > \Delta_t(2j+1)/j$  and

$$T \gg \frac{2\pi\hbar}{E_k}.$$

Since the dwell time is measured by the number of ‘kicks’ the clock’s hand experiences while the particle is inside  $\mathcal{I}_d$ , the accuracy again is proportional to  $E_k^{-1}$ , although the clock’s hand width may be smaller than the limit set by Equation (6.13). One might be tempted to conjecture that this limitation in precision is directly due to some kind of ‘time-energy uncertainty relation’, but this is not the case. In Chapter 7 we will present a measurement scheme for passage times based on the detection of the particle upon entering and exiting the region of interest, much like a time-of-flight experiment is typically performed. For the individual detections we employ the spin-boson detector model introduced and investigated in Part I of the present thesis. The accuracy of this measurement scheme will be estimated in Section 8.2. Under optimal conditions it behaves like  $E_k^{-3/4}$ , thus for low velocities breaking the  $E_k^{-1}$  behavior.

## 6.5 Plan of Part II

Part II is organized as follows. In Chapter 7 the measurement scheme is sketched (Section 7.1), and the quantities necessary for its investigation are derived. In particular, in Section 7.3 we calculate the ‘reset state’, i.e., the state immediately after the detection of the first boson. For some examples the reset state is calculated numerically for the case of a discrete boson bath as well as for the corresponding limit of continuous boson modes, and the results are compared. Further, a formula for the ‘measured’ passage-time density is derived in Section 7.6. In Chapter 8 properties of the passage-time density are discussed. In Section 8.1.1 three examples with different detector accuracies are investigated numerically. Mechanisms for the broadening of the obtained densities are discussed in Section 8.1.2, where a classical broadening mechanism for slowly responding detectors is distinguished from a quantum mechanism in the case of detectors responding quickly to the presence of the particle. The width of the passage-time density is estimated, and its optimization is discussed in Section 8.2.



## Chapter 7

# Application of the spin-boson detector model

A *Gedanken* experiment is described, aiming at the measurement of the passage-time density for a spread-out quantum particle to traverse a specific region. The measurement employs the detector model investigated in Part I. The continuum limit of the model is treated, under the assumption of the Markov property, and the particle state immediately after the first detection is calculated. Two explicit examples with 15 boson modes show excellent agreement between the discrete model and the continuum limit. Analytical expressions for the passage-time density are presented.

### 7.1 Measurement scheme

We investigate passage-time densities by means of a measurement scheme which mimicks the way an actual time-of-flight experiment is typically performed. The measurement scheme involves two measurements of arrival time, one upon entering the region of interest and one when exiting, see Figure 7.1. For the

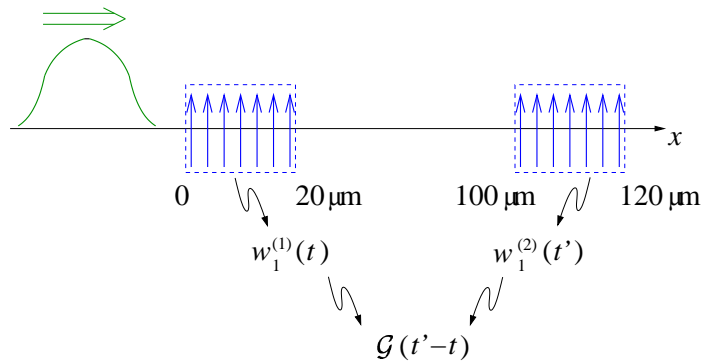


**Figure 7.1:** The first detector detects the particle upon entry into the region of interest, the second one when exiting. From the correlation of these two arrival-time densities,  $w_1^{(j)}$ , the passage-time density  $\mathcal{G}$  is obtained. The  $x$ -positions correspond to the numerical examples discussed in Chapter 8.



two measurements of arrival time the spin-boson detector model introduced in Section 3.1 and investigated in Part I of the present thesis is used. Between the two measurements the particle state develops freely. This scheme is in contrast to the scheme sketched in Section 6.4 which was based on the (semi-) continuous coupling of the particle under consideration to a ‘clock’. Due to the reduced interaction, the present measurement scheme can be expected to distort the particle’s wave function less than that scheme.

## 7.2 Quantum jump approach: The reset operation

For the intended application of the spin-boson detector model we need more than the time development up to the first detection, which was investigated in Part I. In particular, we require knowledge about the particle state immediately after the first boson detection. A similar problem arises in quantum optics when one wants to simulate fluorescence trajectories of a multi-level system interacting with a bath of photon modes and possibly a pumping laser. Then, knowledge is required about the state of the multi-level system after each individual photon detection. In the framework of the quantum jump approach, this state is called the ‘reset state’, and is obtained by means of the so called ‘reset operation’ [Heg93]. In the present context, the main idea reads as follows.

Let the complete system (bath, detector, particle) be described at a particular time by a density matrix of the form

$$\varrho \equiv |0\rangle |\uparrow_1 \dots \uparrow_D\rangle \varrho_p \langle \uparrow_1 \dots \uparrow_D| \langle 0|.$$

There,  $\varrho_p$  denotes the particle density matrix, the boson bath is in its vacuum state, and all spins are in the excited state. According to the quantum jump approach the bath is checked for bosons not continuously but by means of instantaneous measurements separated by a time  $\Delta t$  (see Section 4.1). Until the next measurement the system develops freely, and a time  $\Delta t$  later it is in the state

$$\varrho(\Delta t) = U(\Delta t, 0) \varrho U^\dagger(\Delta t, 0)$$

with the free time-development operator  $U(t, t')$ . Now, let a boson be found in the broadband boson measurement at  $\Delta t$ . The density matrix for the corresponding subensemble is obtained by sandwiching the above expression with the projector onto the one-boson space,

$$\mathbb{P}_1 \equiv \sum_{\ell} |1_\ell\rangle \langle 1_\ell|,$$

by the von Neumann-Lüders reduction rule [vN32, Lüd51]. The trace gives the probability for this event. The subsystem consisting solely of the particle, after the detection of a boson, is described by a partial trace,

$$\text{tr}_{\text{det}} \text{tr}_{\text{bath}} \mathbb{P}_1 U(\Delta t, 0) \varrho U^\dagger(\Delta t, 0) \mathbb{P}_1 =: \mathcal{R}(\Delta t) \varrho_p. \quad (7.1)$$

In general, the reset operation  $\mathcal{R}(\Delta t)$  must be expected to depend on the choice of  $\Delta t$ . When treating the limit of continuous bath modes, however, we will



in the sequel always choose  $\Delta t$  small enough so that in Equation (7.1) only contributions at most linear in  $\Delta t$  have to be taken into account. In that case one can define

$$\mathcal{R}(\Delta t)\varrho_p =: \hat{\mathcal{R}}_{\varrho_p} \Delta t + \mathcal{O}([\Delta t]^2), \quad (7.2)$$

as will explicitly be seen in Equation (7.14). The state  $\hat{\mathcal{R}}_{\varrho_p}$  is called the ‘reset state’. We will numerically justify this linear approximation for an example in Section 7.3.4. An abstract justification in the framework of photon-statistics, valid also for systems with more than two levels, has been given in Reference [HS96].

### 7.3 Evaluation of the reset state

#### 7.3.1 The general result

The aim of the present section is the evaluation of the reset state. We split the model Hamiltonian introduced in Section 3.1 into two parts,  $H = H_0 + H_1$  with

$$\begin{aligned} H_0 &:= H - (H_{\text{coup}} + H_{\text{spon}}) = H_{\text{part}} + H_{\text{det}} + H_{\text{bath}} \\ H_1 &:= H_{\text{coup}} + H_{\text{spon}} \end{aligned}$$

as in Chapter 4, and again use standard second-order perturbation theory for

$$U_I(t, t') := e^{iH_0 t/\hbar} U(t, t') e^{-iH_0 t'/\hbar},$$

compare Equation (4.7). The zeroth order does not contribute to Equation (7.1), neither does the first order since  $\mathbb{P}_1$  acts once on  $|0\rangle$ . Only the second order term with  $H_1$  on the left and on the right survives in second-order perturbation theory, and one thus obtains

$$\begin{aligned} \mathcal{R}(\Delta t)\varrho_p &= \text{tr}_{\text{det}} \text{tr}_{\text{bath}} \mathbb{P}_1 e^{-iH_0 \Delta t/\hbar} \left( -\frac{i}{\hbar} \right) \int_0^{\Delta t} dt_1 e^{iH_0 t_1/\hbar} H_1 e^{-iH_0 t_1/\hbar} \varrho \\ &\quad \times \left( \frac{i}{\hbar} \right) \int_0^{\Delta t} dt_2 e^{iH_0 t_2/\hbar} H_1 e^{-iH_0 t_2/\hbar} e^{iH_0 \Delta t/\hbar} \mathbb{P}_1. \quad (7.3) \end{aligned}$$

For later use it will be convenient to split the rectangular integration area into two triangles,

$$\int_0^{\Delta t} dt_1 \int_0^{\Delta t} dt_2 = \int_0^{\Delta t} dt_1 \int_0^{t_1} dt_2 + \int_0^{\Delta t} dt_2 \int_0^{t_2} dt_1.$$

We note that the two double integrals in this decomposition of the right hand side of Equation (7.3) are a complex conjugate of each other. Thus, one has

$$\begin{aligned} \mathcal{R}(\Delta t)\varrho_p &= 2 \text{Re} e^{-iH_{\text{part}} \Delta t/\hbar} \sum_{\ell, j} \int_0^{\Delta t} dt_1 \int_0^{t_1} dt_2 e^{i(\omega_\ell - \tilde{\omega}_0^{(j)})(t_1 - t_2)} \\ &\quad \times \left[ \gamma_\ell^{(j)} + g_\ell^{(j)} \chi^{(j)}(\hat{\mathbf{x}}(t_1)) \right] \varrho_p \left[ \overline{\gamma_\ell^{(j)} + g_\ell^{(j)} \chi^{(j)}(\hat{\mathbf{x}}(t_2))} \right] e^{iH_{\text{part}} \Delta t/\hbar}, \quad (7.4) \end{aligned}$$



where  $\hat{\mathbf{x}}(t) = \hat{\mathbf{x}} + \hat{\mathbf{p}}t/m$  is the free time development of  $\hat{\mathbf{x}}$  in the Heisenberg picture as in Chapter 4, and the modified resonance frequencies  $\tilde{\omega}_0^{(j)}$  have been defined in Equation (4.26). The phases  $f_\ell^{(j)}$  in  $H_1$  have canceled since we are taking the trace over detector states.

### 7.3.2 Examples with constant and non-constant density of states

As an example we again consider the simplified model with only one spatial dimension and only one spin introduced in Section 3.2.1. Again we take  $\chi(x) = \Theta(x)$ , and as particle we consider a cesium atom. The initial state at  $t = 0$  now is assumed to be a pure state,  $\varrho_p = |\psi_0\rangle\langle\psi_0|$ . When it comes to actual calculations [below Equation (7.7)], we will specify that  $|\psi_0\rangle$  is a Gaussian minimal uncertainty package around position  $x = 0$ , with width  $\Delta x$  in position space and with mean velocity  $v_0$ ,

$$\langle x | \psi_0 \rangle = \sqrt{\frac{1}{\Delta x \sqrt{2\pi}}} e^{-x^2/4(\Delta x)^2} e^{i(mv_0/\hbar)x}. \quad (7.5)$$

With the above simplifications the first line of Equation (7.3) yields

$$\begin{aligned} & \langle x | \mathcal{R}(\Delta t) \varrho_p | x \rangle \\ &= \sum_\ell |g_\ell|^2 \int_0^{\Delta t} dt_1 \int_0^{\Delta t} dt_2 e^{i(\omega_\ell - \omega_0)(t_1 - t_2)} \\ & \quad \times \left\langle x \left| e^{-iH_{\text{part}}\Delta t/\hbar} \Theta(\hat{x}(t_1)) \right| \psi_0 \right\rangle \left\langle \psi_0 \left| \Theta(\hat{x}(t_2)) e^{iH_{\text{part}}\Delta t/\hbar} \right| x \right\rangle \\ &= \sum_\ell \left| g_\ell \int_0^{\Delta t} dt e^{i(\omega_\ell - \omega_0)t} \left\langle x \left| e^{-iH_{\text{part}}(\Delta t - t)/\hbar} \Theta(\hat{x}) e^{-iH_{\text{part}}t/\hbar} \right| \psi_0 \right\rangle \right|^2. \quad (7.6) \end{aligned}$$

The contribution  $\langle x | \cdots | \psi_0 \rangle$  has an intuitive explanation: The initial state develops freely until  $t$  and is then projected onto the detector region. In an intuitive picture, the time  $t$  may be viewed as time of occurrence of a boson. Since a boson can only be created when the spin couples to the bath, the particle has to be inside the detector at  $t$ , hence the projection. Then the state continues to develop freely until  $\Delta t$ . The integration is understood as sum over all possible ‘paths’ satisfying the above picture, i.e., as sum over all times  $t$ . This is similar to the path decomposition for multidimensional tunneling by Auerbach and Kivelson [AK85] (see also Reference [AKN84] by the same authors together with Nicole); there, a propagator is decomposed into parts valid ‘before’ and ‘after’ an event, and the full propagator is obtained by an integration over the time of occurrence of the discriminating event.

The evaluation of the second line of Equation (7.6) is somewhat involved due to the projector  $\Theta(\hat{x})$ . We proceed as follows. We first insert on the right side of the  $\Theta$  function a decomposition of the identity into eigenstates of the momentum and the position operator,

$$\mathbb{1} = \int_{-\infty}^{\infty} dx' |x'\rangle \langle x'| \int_{-\infty}^{\infty} dk |k\rangle \langle k| = \sqrt{\frac{1}{2\pi}} \int_{-\infty}^{\infty} dx' \int_{-\infty}^{\infty} dk e^{ikx'} |x'\rangle \langle k|.$$



This yields

$$\begin{aligned} \left\langle x \left| e^{-iH_{\text{part}}(\Delta t - t)/\hbar} \Theta(\hat{x}) e^{-iH_{\text{part}}t/\hbar} \right| \psi_0 \right\rangle \\ = \int_{-\infty}^{\infty} dx' \left\langle x \left| e^{-iH_{\text{part}}(\Delta t - t)/\hbar} \Theta(\hat{x}) \right| x' \right\rangle \\ \times \sqrt{\frac{1}{2\pi}} \int_{-\infty}^{\infty} dk e^{ikx'} \left\langle k \left| e^{-iH_{\text{part}}t/\hbar} \right| \psi_0 \right\rangle. \end{aligned} \quad (7.7)$$

The integral over  $k$  in the last line of Equation (7.7) describes the free time development of the Gaussian wave packet  $|\psi_0\rangle$  given in Equation (7.5). We evaluate this Gaussian integral and introduce the notation

$$\begin{aligned} \psi_t(x') &:= \sqrt{\frac{1}{2\pi}} \int_{-\infty}^{\infty} dk e^{ikx'} \left\langle k \left| e^{-iH_{\text{part}}t/\hbar} \right| \psi_0 \right\rangle \\ &= \sqrt{\frac{\Delta x}{\sqrt{2\pi}}} \left[ (\Delta x)^2 + i \frac{\hbar t}{2m} \right]^{-1/2} \\ &\quad \times e^{ik_0 x'} e^{-i\hbar k_0^2 t/2m} \exp \left\{ -\frac{[x' - \hbar k_0 t/m]^2}{4(\Delta x)^2 + 2i\hbar t/m} \right\}, \end{aligned} \quad (7.8)$$

where we have set  $k_0 := mv_0/\hbar$ .

In order to evaluate the integral over  $x'$  on the right hand side of Equation (7.7) we insert  $\mathbb{1} = \int_{-\infty}^{\infty} dk |k\rangle \langle k|$  on the left side of the  $\Theta$  function. With  $\psi_t(x')$  as introduced in Equation (7.8) one obtains

$$\begin{aligned} \left\langle x \left| e^{-iH_{\text{part}}(\Delta t - t)/\hbar} \Theta(\hat{x}) e^{-iH_{\text{part}}t/\hbar} \right| \psi_0 \right\rangle \\ = \int_{-\infty}^{\infty} dk \left\langle x \left| e^{-iH_{\text{part}}(\Delta t - t)/\hbar} \right| k \right\rangle \int_{-\infty}^{\infty} dx' \langle k | \Theta(\hat{x}) | x' \rangle \psi_t(x') \end{aligned} \quad (7.9)$$

The integral over  $x'$  can be evaluated by noting that

$$\langle k | \Theta(\hat{x}) | x' \rangle = \Theta(x') \sqrt{\frac{1}{2\pi}} e^{-ikx'}.$$

After a lengthy calculation one obtains

$$\begin{aligned} \int_{-\infty}^{\infty} dx' \langle k | \Theta(\hat{x}) | x' \rangle \psi_t(x') \\ = \frac{\sqrt{\Delta x}}{2(2\pi)^{1/4}} e^{-i\hbar k_0^2 t/2m} \exp \left\{ -\frac{(\hbar k_0 t/m)^2}{(\Delta x)^2 + 2i\hbar t/m} \right\} w(z), \end{aligned} \quad (7.10)$$

where we have introduced

$$z := \frac{[(\Delta x)^2 + 2i\hbar t/m]^{1/2}}{2} (k_0 - k) - i \frac{\hbar k_0 t/m}{[(\Delta x)^2 + 2i\hbar t/m]^{1/2}}. \quad (7.11)$$



The function  $w$  is defined by

$$w(z) := e^{-z^2} \operatorname{erfc}(-iz) \quad (7.12)$$

with the complimentary error function [AS68]

$$\operatorname{erfc}(z) = \frac{2}{\sqrt{\pi}} \int_z^\infty dt e^{-t^2} = 1 - \operatorname{erf}(z), \quad \operatorname{erf}(z) = \frac{2}{\sqrt{\pi}} \int_0^z dt e^{-t^2}.$$

We substitute Equation (7.10) into Equation (7.9) and note further that

$$\left\langle x \left| e^{-iH_{\text{part}}(\Delta t - t)/\hbar} \right| k \right\rangle = \sqrt{\frac{1}{2\pi}} e^{-i\hbar k^2(\Delta t - t)/2m} e^{ikx}.$$

Substituting Equation (7.9) into Equation (7.6) finally yields

$$\begin{aligned} & \langle x | \mathcal{R}(\Delta t) \varrho_{\text{p}} | x \rangle \\ &= \sum_{\ell} \left| g_{\ell} \int_0^{\Delta t} dt e^{i(\omega_{\ell} - \omega_0)t} \sqrt{\frac{1}{2\pi}} \int_{-\infty}^{\infty} dk e^{-i\hbar k^2(\Delta t - t)/2m} e^{ikx} \right. \\ & \quad \times \left. \frac{\sqrt{\Delta x}}{2(2\pi)^{1/4}} e^{-i\hbar k_0^2 t/2m} \exp \left\{ -\frac{(\hbar k_0 t/m)^2}{(\Delta x)^2 + 2i\hbar t/m} \right\} w(z) \right|^2, \end{aligned}$$

where  $z$  has been defined in Equation (7.11) and the function  $w$  has been introduced in Equation (7.12). The remaining two integrals and the summation over  $\ell$  can be evaluated numerically.

As an example with a constant density of states we consider the example investigated in Section 3.2.5 with a maximal boson frequency  $\omega_{\text{M}}$  and  $N$  boson modes,

$$\begin{aligned} \omega_{\ell} &= \omega_{\text{M}} n/N \quad n = 1, \dots, N \\ g_{\ell} &= -iG \sqrt{\omega_{\ell}/N}. \end{aligned} \quad (3.29)$$

A numerical illustration of  $\langle x | \mathcal{R}(\Delta t) \varrho_{\text{p}} | x \rangle / \Delta t$  for  $N = 15$  bosons modes is given in Figure 7.2 (dots). [Note the division by  $\Delta t$  as compared to Equations (7.3) and (7.4) or Equation (7.6).] As an example with a non-constant density of states we consider the example investigated in Section 3.2.6 with a maximal boson frequency  $\omega_{\text{M}}$  and  $N$  boson modes,

$$\omega_{\ell} = \left( \frac{n}{N} \right)^2 \omega_{\text{M}}, \quad n = 1, \dots, N. \quad (3.31)$$

A numerical illustration of  $\langle x | \mathcal{R}(\Delta t) \varrho_{\text{p}} | x \rangle / \Delta t$  for  $N = 15$  bosons modes in that case is given in Figure 7.3 (dots).



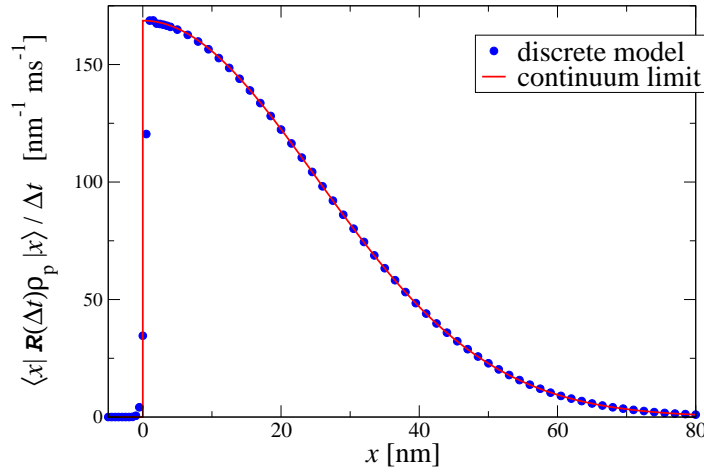


**Figure 7.2:** Dots: reset state  $\langle x | \mathcal{R}(\Delta t) \rho_p | x \rangle / \Delta t$  for a pure state  $\rho_p = |\psi_0\rangle \langle \psi_0|$  with  $|\psi_0\rangle$  being the Gaussian wave packet of Equation (7.5),  $\Delta x = 50$  nm and  $v_0 = 1.79$  m/s;  $\omega_\ell$  as in Equation (3.29),  $\omega_0 = 2.38 \times 10^{12} \text{ s}^{-1}$ ,  $\omega_M = 4.6 \omega_0$ ,  $G = 2.782 \times 10^3 \text{ s}^{-1/2}$ ,  $N = 15$ , and  $\Delta t = 100 \omega_0^{-1} = 4.185 \times 10^{-11} \text{ s}$ . Solid line: spatial probability density of the reset state,  $A |\langle x | \Theta(\hat{x}) | \psi_0 \rangle|^2$ , from Equation (7.16) for the corresponding continuum limit. Up to small deviations around  $x = 0$ , the reset states from the discrete and the continuum model are in very good agreement.

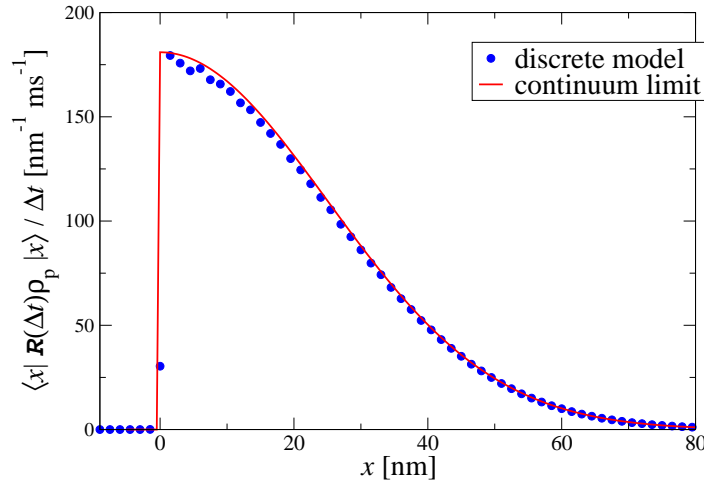


**Figure 7.3:** Dots: reset state  $\langle x | \mathcal{R}(\Delta t) \rho_p | x \rangle / \Delta t$  for a pure state  $\rho_p = |\psi_0\rangle \langle \psi_0|$  with  $|\psi_0\rangle$  being the Gaussian wave packet of Equation (7.5);  $\Delta t = 75 \omega_0^{-1}$ , all other parameters as in Figure 7.2, but  $\omega_\ell$  now given by Equation (3.31). Solid line: spatial probability density of the reset state,  $A |\langle x | \Theta(\hat{x}) | \psi_0 \rangle|^2$ , from Equation (7.16) for the corresponding continuum limit. Up to small deviations around  $x = 0$ , the reset states from the discrete and the continuum model again are in good agreement.



### 7.3.3 The continuum limit

We return to the general expression in Equation (7.4). For simplicity, we will assume in the following that all  $D$  spins are located in the same volume  $\mathcal{V}$  and thus have same sensitivity function,

$$\chi^{(j)}(\mathbf{x}) \equiv \chi_{\mathcal{V}}(\mathbf{x}), \quad j = 1, \dots, D.$$

In view of Equation (3.3) we neglect the  $\gamma_{\ell}^{(j)}$  terms as long as no spin has flipped. In other words, we neglect the possibility of spontaneous spin flips before the first particle-induced spin flip; see the remarks about such ‘false positives’ in Section 4.4. We introduce the ‘collective correlation function’

$$\kappa_{\Sigma}(\tau) = \sum_j \kappa_{\bar{g}g}^{(j)}(\tau) = \sum_j \sum_{\ell} \left| g_{\ell}^{(j)} \right|^2 e^{-i(\omega_{\ell} - \tilde{\omega}_0^{(j)})\tau}, \quad (7.13)$$

where the  $\kappa_{\bar{g}g}^{(j)}$  have been defined in Equation (4.27). As in Chapter 4 we assume that the coupling constants are such that in the continuum limit the Markov property holds, i.e.,

$$\kappa_{\Sigma}(\tau) \approx 0 \quad \text{if} \quad \tau > \tau_c$$

for some small correlation time  $\tau_c$  [compare Equation (4.14)]. Thus, in the double integral of Equation (7.4) only times with  $t_1 - t_2 \leq \tau_c$  contribute, and if  $\tau_c$  is small enough one again can write

$$\chi_{\mathcal{V}}(\hat{\mathbf{x}}(t_1)) \approx \chi_{\mathcal{V}}(\hat{\mathbf{x}}(t_2)). \quad (4.15')$$

With these assumptions Equation (7.4) reads

$$\begin{aligned} \mathcal{R}(\Delta t) \varrho_{\text{p}} &= 2 \operatorname{Re} e^{-iH_{\text{part}}\Delta t/\hbar} \int_0^{\Delta t} dt_1 \chi_{\mathcal{V}}(\hat{\mathbf{x}}(t_1)) \varrho_{\text{p}} \chi_{\mathcal{V}}(\hat{\mathbf{x}}(t_1)) \\ &\quad \times \int_0^{t_1} dt_2 \kappa_{\Sigma}(t_1 - t_2) e^{iH_{\text{part}}\Delta t/\hbar}. \end{aligned}$$

Then, with a change of variable,  $\tau := t_1 - t_2$ , the integration over  $\tau$  can be extended to  $\infty$  if  $\tau_c \ll \Delta t$ , by the Markov property. Again, we take the coupling constants to be of the form given in Equation (4.29), so that the continuum limit can then be taken as in Chapter 4. Specializing the definition in Equation (4.32) to the case at hand, we put

$$\begin{aligned} A &= 2 \operatorname{Re} \int_0^{\infty} d\tau \kappa_{\Sigma}(\tau) \\ &= \sum_j \left( \tilde{\omega}_0^{(j)} \right)^3 \left[ \frac{c \left( \tilde{\omega}_0^{(j)} \right) - \tilde{\omega}_0^{(j)} c' \left( \tilde{\omega}_0^{(j)} \right)}{\left[ c \left( \tilde{\omega}_0^{(j)} \right) \right]^4} \right] \int \frac{d\Omega_{\mathbf{e}}}{(2\pi)^2} \left| \Gamma^{(j)} \left( \tilde{\omega}_0^{(j)}, \mathbf{e} \right) \right|^2. \end{aligned}$$

One then obtains

$$\begin{aligned} &\mathcal{R}(\Delta t) \varrho_{\text{p}} \\ &= A \int_0^{\Delta t} dt_1 e^{-iH_{\text{part}}(\Delta t - t_1)/\hbar} \chi_{\mathcal{V}}(\hat{\mathbf{x}}) e^{-iH_{\text{part}}t_1/\hbar} \varrho_{\text{p}} e^{iH_{\text{part}}t_1/\hbar} \chi_{\mathcal{V}}(\hat{\mathbf{x}}) e^{iH_{\text{part}}(\Delta t - t_1)/\hbar}. \end{aligned} \quad (7.14)$$



In general, it is cumbersome to work with the rather complicated full reset state given by Equation (7.14). For  $\Delta t$  small enough, however, it is sufficient to take into account only terms at most linear in  $\Delta t$ . This yields

$$\begin{aligned}\mathcal{R}(\Delta t)\varrho_p &= A\chi_{\mathcal{V}}(\hat{\mathbf{x}})\varrho_p\chi_{\mathcal{V}}(\hat{\mathbf{x}})\Delta t + \mathcal{O}\left([\Delta t]^2\right) \\ &=: \hat{\mathcal{R}}_{\varrho_p}\Delta t + \mathcal{O}\left([\Delta t]^2\right),\end{aligned}\quad (7.15)$$

compare Equation (7.2). If  $\varrho_p$  is a pure state, then the reset state  $\hat{\mathcal{R}}_{\varrho_p}$  is a pure state, too. We are particularly interested in the case  $\varrho_p = |\psi_{\text{cond}}^t\rangle\langle\psi_{\text{cond}}^t|$ , i.e.,  $\varrho_p$  originates from the conditional time development of the particle until the time  $t$ . Then, the reset state is given by

$$\hat{\mathcal{R}}_{\varrho_p} = |\psi_{\text{reset}}^t\rangle\langle\psi_{\text{reset}}^t|$$

with the pure reset state

$$|\psi_{\text{reset}}^t\rangle \equiv A^{1/2}\chi_{\mathcal{V}}(\hat{\mathbf{x}})|\psi_{\text{cond}}^t\rangle. \quad (7.16)$$

We note that this result is physically very reasonable. It means that if the particle has been detected by a detector located in the region  $\mathcal{V}$ , immediately afterwards it will be localized in  $\mathcal{V}$ . We also note that

$$\langle\psi_{\text{reset}}^t|\psi_{\text{reset}}^t\rangle = A \int d^3x \chi_{\mathcal{V}}(\mathbf{x})^2 |\langle\mathbf{x}|\psi_{\text{cond}}^t\rangle|^2 = w_1(t), \quad (7.17)$$

which is the probability density for the first detection at time  $t$  [see Equation (4.34)]. This is in line with the physical understanding of the conditional time development and the reset state: no boson detection *until* time  $t$ , but a boson detection a time  $\Delta t$  later which is small compared to the coarse grained time scale of the quantum jump approach.

#### 7.3.4 Continuum limit: Examples

In the preceding section  $\hat{\mathcal{R}}_{\varrho_p}$  has been obtained in the limit of continuous boson modes, under the assumptions that the Markov property Equation (4.14) holds and that only terms at most linear in  $\Delta t$  have to be taken into account. In contrast to this, in Section 7.3.2  $\langle x|\mathcal{R}(\Delta t)\varrho_p|x\rangle/\Delta t$  has been computed exactly for the discrete case. From Equation (7.15), however, it is seen that up to higher orders in  $\Delta t$  one has

$$\hat{\mathcal{R}} = \frac{\mathcal{R}(\Delta t)}{\Delta t}.$$

Thus, for  $\Delta t$  short enough the quantities  $\langle x|\mathcal{R}(\Delta t)\varrho_p|x\rangle/\Delta t$  and  $\langle x|\hat{\mathcal{R}}_{\varrho_p}|x\rangle$  should agree when computed for the same  $\varrho_p$ , provided that the approximations of the preceding section are valid and that the discrete case is well approximated by the continuum limit of the quantum jump approach.

We therefore apply Equation (7.16) to the continuum limit of the examples of Section 7.3.2. In that case of the simplified model introduced in Section 3.2.1,



there is no summation over  $j$  since we consider only one spin. The wave vector  $\ell$  is replaced by the wave number  $\ell$  in this one-dimensional example, and  $\tilde{\omega}_0^{(1)}$  may simply be written as  $\omega_0$ . Accordingly, the collective correlation function introduced in Equation (7.13) reduces to the correlation function of the simplified model, which is given in Equation (4.9). Thus, for  $\omega_M > \omega_0$  one obtains in the continuum limit in the case of the example with constant density of states [see Equation (3.29)]

$$\begin{aligned}\kappa(\tau) &= \frac{|G|^2}{\omega_M} \frac{(1 + i\omega_M \tau) e^{-i(\omega_M - \omega_0)\tau} - e^{i\omega_0\tau}}{\tau^2} \\ A &= 2\pi |G|^2 \frac{\omega_0}{\omega_M} \\ \delta_{\text{shift}} &= 2 |G|^2 \left( \frac{\omega_0}{\omega_M} \ln \left[ \frac{\omega_0}{\omega_M - \omega_0} \right] - 1 \right)\end{aligned}\quad (4.23)$$

as in Section 4.2.2, and in the case of the example with non-constant density of states [see Equation (3.31)]

$$\begin{aligned}\kappa(\tau) &= \frac{|G|^2}{2\sqrt{\omega_M}} \int_0^{\omega_M} d\omega \sqrt{\omega} e^{-i(\omega - \omega_0)\tau} \\ A &= \pi |G|^2 \sqrt{\frac{\omega_0}{\omega_M}} \\ \delta_{\text{shift}} &= |G|^2 \left[ \sqrt{\frac{\omega_0}{\omega_M}} \ln \left( \frac{\sqrt{\omega_M/\omega_0} + 1}{\sqrt{\omega_M/\omega_0} - 1} \right) - 2 \right]\end{aligned}\quad (4.24)$$

as in Section 4.2.3. In any case,  $\tau_c$  is of the order of  $\omega_0^{-1}$ . As in Section 7.3.2 we consider as initial state the pure state  $\varrho_p = |\psi_0\rangle \langle \psi_0|$  with  $|\psi_0\rangle$  given by Equation (7.5), and take  $\chi_v(x) = \Theta(x)$ . For the sake of comparison, the resulting spatial probability densities of the respective reset states,

$$\langle x | \hat{\mathcal{R}} \varrho_p | x \rangle = A |\langle x | \Theta(\hat{x}) | \psi_0 \rangle|^2,$$

are plotted in Figures 7.2 and 7.3 for the same parameters as in the discrete case. The plots are in very good agreement. This again indicates that the continuum limit of the quantum jump approach is a very good approximation to the discrete case and may help to find a way around the generally cumbersome numerical calculations in the latter case. We stress that we obtained the nice agreement in Figures 7.2 and 7.3 with as little as  $N = 15$  boson modes in the discrete case.

## 7.4 Short discussion of the reset state

Two basic properties of the reset state of Equation (7.16) have been noted already: First, right after a detection of the particle by a detector located in a specific region the particle is localized in that region; second, the squared



norm of the reset state,  $\langle \psi_{\text{reset}}^t | \psi_{\text{reset}}^t \rangle$ , gives the probability density for the first detection to occur at time  $t$  [see Equation (7.17)].

We further note that in the present model with phases  $f_{\mathbf{l}}^{(j)}$  independent of  $\mathbf{x}$  there is no explicit recoil on the particle from the created boson. This is in line with the original idea of a minimally invasive measurement. The absence of an explicit recoil distinguishes the present detector model from other models which are based on the direct interaction with the particle's internal degrees of freedom. In the case of the fluorescence model sketched in Section 2.5, e.g., the reset state after the detection of the first fluorescence photon explicitly incorporates a recoil due to the momentum of the emitted photon [Heg03]. It appears reasonable that in the present model no such recoil on the particle occurs: After all, the boson is not emitted by the particle but by the spin lattice. Hence, the recoil should be experienced by this lattice, rather than by the particle, similar to what occurs in the Mössbauer effect. We note, however, that although there is no recoil the particle's wave function still is changed by the detection, due the projection onto the detector region by means of the reset operation. This changes position and momentum density of the wave packet, as will be seen in the examples discussed in Chapter 8.

Finally, we note that Blanchard and Jadczyk [BJ93, Jad95] in the framework of Event Enhanced Quantum Theory described the detection of a particle by means of a sensitivity function of the detector,  $-iV(x)$  with  $V(x) > 0$ , and put

$$|\psi_{\text{detected}}\rangle = \sqrt{\frac{2V(\hat{\mathbf{x}})}{\hbar}} |\psi_{\text{undetected}}\rangle \quad (7.18)$$

as the particle's state immediately after the detection. In case of the spin-boson detector model we may define

$$V(\mathbf{x}) := \frac{\hbar}{2} A\chi_{\nu}(\mathbf{x})$$

and neglect the line-shift term  $\delta_{\text{shift}}$  for the moment (see the remarks in the Section 4.3.3 about the possibility of neglecting  $\delta_{\text{shift}}$ ). The conditional Hamiltonian of Equation (4.31) then takes the same form as the Hamiltonian in References [BJ93, Jad95], and the reset state of Equation (7.16) takes the form

$$|\psi_{\text{reset}}^t\rangle = \sqrt{\frac{2V(\hat{\mathbf{x}})}{\hbar}} |\psi_{\text{cond}}^t\rangle,$$

exactly as in Equation (7.18). Thus, the spin-boson detector model provides a microscopic justification for the rather phenomenological description of the detection process in References [BJ93, Jad95].

## 7.5 Subsequent time development

After detection of a boson, the further interaction of the particle with the detector depends on the particular choice of parameters of the detector model. The internal dynamics of the detector after the first spin flip was investigated



in detail in References [Sch97, GS90, Sch91], and a short account in the framework of the quantum jump approach has also been given in Section 4.4 of the present thesis. Based on these results, several choices are possible such that the amplification of the first spin flip will not significantly change the spatial wave function after the first spin flip,  $|\psi_{\text{reset}}^t\rangle$ . This means that effectively only one reset operation, associated with the very first spin flip, has to be performed on the spatial wave function. Such ‘minimally invasive’ detector models will be of interest if one is interested in actual quantum mechanical limitations of a passage-time measurement.

As a simple example we consider as in Section 4.4 a ring of  $D$  identical spins with nearest-neighbor interaction,

$$\omega_0^{(j)} \equiv \omega_0 \quad \text{and} \quad \omega_J^{(jk)} \equiv \omega_J \delta_{j+1,k}, \quad (7.19)$$

$\chi^{(j)}(\mathbf{x}) \equiv \chi_v(\mathbf{x})$  as before, and  $j = D + 1$  identified with  $j = 1$ . We choose  $\omega_0 \gg \tilde{\omega}_0$  and  $\Gamma, \Gamma_{\text{spn}}$  independent of  $\omega_\ell$  as well as  $c(\omega_\ell) \equiv c_0$ . The rate for the neighbors of the first-flipped spin to flip into *their* ground state is denoted by  $A_1(\mathbf{x})$  and is given by Equation (4.48). These flips can be rather fast since the ferromagnetic forces on these spins cancel and hence the energy gain for flipping can be very large. In other words, one has  $A_1 \gg A$  since the resonance frequency occurring in  $A_1$  is  $\omega_0$  instead of  $\tilde{\omega}_0$ , and  $\omega_0 \gg \tilde{\omega}_0$ . By a kind of domino effect the whole ring flips into the ground state; the mean time needed for this given by  $D/2A_1$  [Sch97, GS90, Sch91], see Section 4.4. If this time is very short compared to the time scale of the particle’s center-of-mass motion, as one can achieve by making  $\omega_0$  large (while  $\tilde{\omega}_0$  remains small to prevent spontaneous spin flips before the first particle-induced spin flip), the reset operations associated with these subsequent spin flips will not significantly change the particle’s state since the wave function has been projected onto the detector by the first reset operation already.

Another possibility to prevent the spatial wave function from being changed by the amplification process would be to couple only one spin to the particle, by choosing  $g_\ell^{(j)} = g_\ell \delta_{j,j_0}$  in Equation (3.2). (In fact, this is the *de facto* setup of the detector actually investigated in References [GS90, Sch91, Sch97]: Effectively only one spin couples to the particle, and subsequently the other spins flip spontaneously, i.e., without particle-enhanced spin-bath coupling.)

## 7.6 Passage-time density

By now, we have all ingredients to evaluate a passage-time density based on the measurement scheme sketched in Section 7.1. As described there, and depicted in Figure 7.1, we consider two spin-boson detectors separated by some distance. We assume in the sequel that the detectors can be described by the continuum limit of Chapter 4. We further assume that the detectors are separated much farther than the width of the wave packet when it is near to or inside the region of interest. Neglecting for the moment undetected transmission through the first detector, this means that we can neglect the presence of the second



detector until the particle has been detected by the first one. If the particle is not detected by the first detector, however, it will not at all contribute to the measured passage-time density. The above approximation thus remains valid even if one takes the possibility of transmission without detection into account. Thus, the probability density for the first spin flip in the first detector can be calculated as outlined in Chapter 4 for a single detector.

As indicated in Section 7.5, we assume that the amplification of the first spin flip to a macroscopic event is very fast<sup>1</sup> and does not change the spatial wave function. Thus, we take the probability density  $w_1(t)$  [Equation (4.34)] for the first spin flip to be the ‘measured arrival-time density’ and  $|\psi_{\text{reset}}^t\rangle$  [Equation (7.16)] as the particle’s state after the detection. Once the particle has been detected by the first detector, this detector is in its ground state. Since in the continuum limit there are no revivals the detector remains in its ground state and does not participate in the subsequent time development. The bosons have either been detected in a destructive measurement or have propagated away. In any case, we may assume that the bath is effectively in its vacuum state again, and calculate the probability density for detection by the second detector again as outlined in Chapter 4.

The joint probability density for the first detector to detect the particle at  $T$  and the second one to detect it at  $T + \tau$  is now given by

$$\mathcal{G}(T, T + \tau) = w_1^{(1)}(T; |\psi_0\rangle) w_1^{(2)}\left(\tau; \frac{|\psi_{\text{reset}}^T\rangle}{\| |\psi_{\text{reset}}^T\rangle \|}\right),$$

where the superscripts indicate the detector under consideration and the second argument is the initial state for which the respective probability density is calculated. Since  $w_1$  is bilinear in the wave function [see Equation (4.34)], this simplifies to

$$\mathcal{G}(T, T + \tau) = w_1^{(2)}(\tau; |\psi_{\text{reset}}^T\rangle)$$

by Equation (7.17). The desired measured passage-time density is then given by integration over the entry time  $T$ :

$$\mathcal{G}(\tau) = \int dT w_1^{(2)}(\tau; |\psi_{\text{reset}}^T\rangle). \quad (7.20)$$

---

<sup>1</sup>We note that it is actually not the length of the amplification process that leads to a problem in the passage-time measurement. If the time needed for the amplification of the first spin flip to a macroscopic, measurable event was identical in both the detectors, this amplification delay would cancel when one takes the difference of the measured arrival times. It is thus only the *spread* of the time needed for the amplification which would cause trouble.







## Chapter 8

# Discussion of the passage-time density

The passage-time density obtained in Chapter 7 is investigated numerically. Slowly responding detectors as well as quickly responding ones yield broad densities, while intermediate detectors yield narrower ones. The mechanisms of the density broadening are investigated by closely examining the first detection and the corresponding reset state. It is shown that the mechanism responsible for the broadening in the case of slowly responding detectors is different from that responsible in the case of quickly responding ones. In the latter case the broadening is shown to be a quantum effect. The precision of the measurement scheme is estimated and its optimization discussed. For slow particles, the precision in an optimized setup behaves like  $E^{-3/4}$ , which improves previous  $E^{-1}$  estimates, obtained with the quantum clock model sketched in Section 6.4.

### 8.1 Numerical investigation

#### 8.1.1 Three examples

In Chapter 7 a measurement scheme for passage times was sketched (Section 7.1), and the application of the spin-boson detector model to this scheme was investigated analytically. In particular, in Section 7.6 a formula was given for the ‘measured’ passage-time density  $\mathcal{G}$ , see Equation (7.20). But what does this density look like, and how does it depend on the detector properties, in particular on the decay rate  $A$ ? The aim of the present chapter is the investigation of basic features of the passage-time density  $\mathcal{G}$ .

We consider as a simple example a cesium atom in one dimension. The initial wave packet is prepared in the remote past far away from the detector such that the free wave packet (with no detectors present) would be described at  $t = 0$  by a Gaussian minimal uncertainty packet around  $x = 0$  with  $\Delta x = 1\mu\text{m}$  and average velocity  $v_0 = 0.717\text{cm/s}$ . Each of the two identical detectors is described in the continuum limit by an absorbing potential  $-iV = -i\hbar A/2$ , extending from 0 to  $20\mu\text{m}$  or  $100\mu\text{m}$  to  $120\mu\text{m}$ , resp. We consider three examples  $A = 1.4337 \times 10^3 \text{ s}^{-1}$ ,  $A = 2.3895 \times 10^3 \text{ s}^{-1}$ , and  $A = 2.3895 \times 10^4 \text{ s}^{-1}$ . These



parameters are chosen in such a way that transmission and reflection without detection, which are typical for imaginary potentials [AII69a, AII69b, AII69c] and have been extensively studied in the framework of quantum arrival times [DEHM02, HSM03, NEMH03a, DEHM03], play no significant role. Consequently, all densities shown in the following are normalized to 1 to a good approximation. The passage-time densities, calculated as described in Section 7.6, are shown in Figure 8.1. It is seen that small and large values of  $A$  give rise to rather broad densities, while the intermediate value yields a narrower one. The mechanisms for the broadening are discussed in Section 8.1.2.

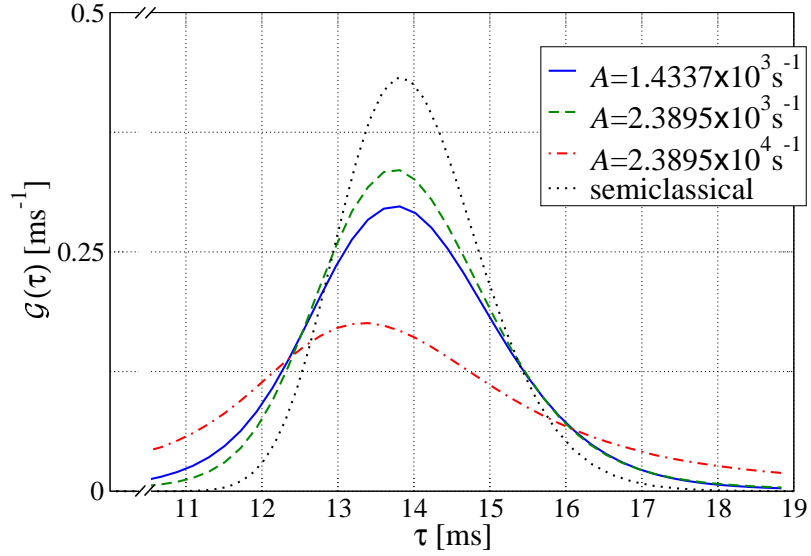


**Figure 8.1:** Passage-time densities calculated from the detector model in the continuum limit for three different values of the rate  $A$  for the first spin flip in the presence of the particle, all other parameters kept fixed. For comparison, the dotted line shows the passage-time density for an ensemble of classical particles which have the same momentum density as the initial wave packet; this classical passage-time density equals the density  $\Pi_{\text{passage}}$  which was obtained from the difference of two arrival-time operators in Section 6.3.

### 8.1.2 Broadening mechanisms

#### Small $A$ : slowly responding detectors

The reason for the broad density arising for small  $A$  can be understood by looking at the arrival-time density measured by the first detector, see Figure 8.2: It is already this density which is rather broad for small  $A$ . Physically, small  $A$  means that the detector is responding only slowly to the presence of the particle; the undetected amplitude  $|\psi_{\text{cond}}^t\rangle$  decays only slowly, yielding a broad arrival-time density at each of the two detectors. This broadening of the arrival-time density remains valid even if the particles are fast enough for their center-of-mass motion to be treated classically. We assume that such a classical, dot-like



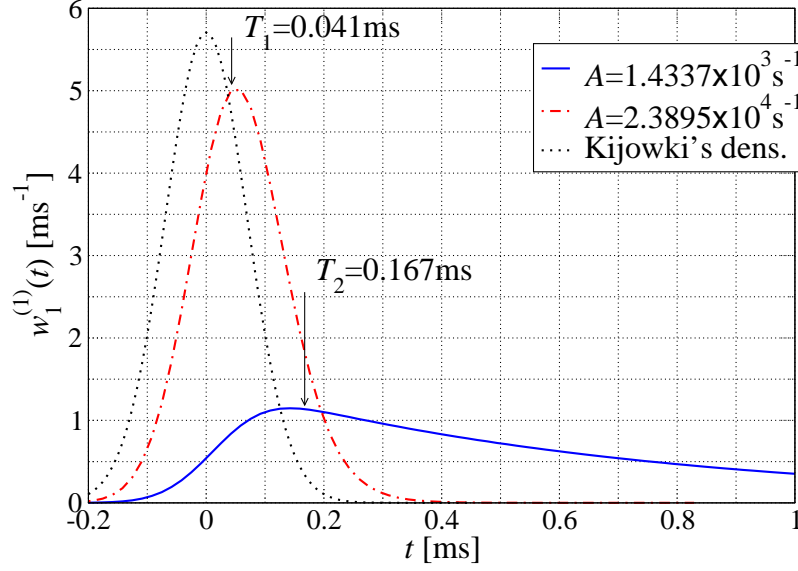


**Figure 8.2:** Arrival-time densities as obtained from the first detector. The detector with small  $A$  yields a broad density indicating poor quality of this measurement. Enlarging  $A$  carefully (to avoid reflection), one may approach Kijowski's axiomatically derived arrival-time density at  $x = 0$  (dotted line; see Section 2.3).

particle has entered the detector at  $t = 0$ . After the particle has entered the detector, the detector state  $|\uparrow_1 \dots \uparrow_D\rangle$  has a life time  $A^{-1}$ , i.e., the probability to find all spins in the excited state at a time  $t$  after the particle has entered the detector is given by

$$P_0^{\text{cl}}(t) = e^{-At}.$$

The probability density for the first spin flip at time  $t$  is thus given by

$$w_1^{\text{cl}}(t) = -\frac{dP_0^{\text{cl}}}{dt}(t) = Ae^{-At},$$

yielding an average waiting time or detection delay

$$\langle t_{\text{delay}}^{\text{cl}} \rangle = \int_0^\infty dt t w_1^{\text{cl}}(t) = \frac{1}{A}.$$

An identical delay in both detectors would cause no problems for the passage-time measurement but would cancel when taking the *difference* between their signals. The main problem is the width of this delay, which is given by

$$\Delta t_{\text{delay}}^{\text{cl}} = \left[ \int_0^\infty dt \left( \langle t_{\text{delay}}^{\text{cl}} \rangle - t \right)^2 w_1^{\text{cl}}(t) \right]^{1/2} = \frac{1}{A}$$

and thus is large for small decay rates  $A$ . This *width* of the delay yields broad arrival-time densities and in consequence broad passage-time densities.



We have thus identified a broadening mechanism for the measured passage-time density for small  $A$  which is not due to the quantum nature of the wave packet: The density is broadened by shortcomings of the detectors for the individual arrival-time measurements, in particular, by the width of the detection delay which broadens the measured arrival-time densities. This effect, however, can be reduced by making  $A$  large, which makes the detector respond faster to the presence of the particle and simultaneously reduces the width of the detection delay. This has to be done carefully in order to avoid reflection without detection, which becomes significant if  $A$  becomes too large. In Figure 8.2 it is seen, e.g., that for  $A = 2.3895 \times 10^4 \text{ s}^{-1}$  one comes much closer to Kijowski's arrival-time density  $\Pi_K$  [Kij74] discussed in Section 2.3. In Section 4.3.3 an example has been presented in which the measured arrival-time density from the spin-boson detector model with a smooth sensitivity function numerically agrees with  $\Pi_K$ . Kijowski's density in turn is known to have minimum standard deviation width among all those densities fulfilling the axioms outlined in Section 2.3, which were transferred to quantum mechanics from classical arrival-time densities. One thus may view the width the  $\Pi_K$  as determined solely by the quantum nature of wave packet under consideration and free from shortcomings of the detector as the width of the detection delay.

### Large $A$ : Quickly responding detectors

We now turn to the case of large  $A$ . In this case the  $A^{-1}$  contribution of the width of the detection delay can be neglected, and the broadening cannot be understood in the simple picture of classical particles which remain unaffected by the measurement. In the full quantum mechanical picture, however, it can be understood by looking at the reset state immediately after the detection by the first detector, evaluated in Section 7.3. Of course, the reset state depends on the instant of time when the detection took place; as examples we consider detection times  $T_1 = 0.041 \text{ ms}$  if  $A = 2.3895 \times 10^4 \text{ s}^{-1}$  and  $T_2 = 0.167 \text{ ms}$  if  $A = 1.4337 \times 10^3 \text{ s}^{-1}$ , which are close to the maximum of the respective probability density  $w_1(t)$  (see Figure 8.2). The reset states and the free packet at the respective times are shown in Figure 8.3. It is seen that the fast detection has a strong impact on the wave function. Large  $A$  means that  $|\psi_{\text{cond}}^t\rangle$ , in particular that part of  $|\psi_{\text{cond}}^t\rangle$  which overlaps with the detector, decays very fast. But since the reset state (7.16) immediately after the detection is essentially the projection of  $|\psi_{\text{cond}}^t\rangle$  onto the detector region the fast decay of this overlap yields a reset state which is very narrow in position space, located at the very beginning of the detector. Thus, by the Heisenberg uncertainty relation, the reset state in this case is very broad in momentum space as can be seen explicitly in Figure 8.4. It is intuitively clear that such a broad momentum density immediately after the measurement of the entry time by the first detector yields a broad passage-time density. Thus, the broad passage-time density in the case of large  $A$  is due to the strong distortion of the wave function by the first measurement. We stress that in the present spin-boson detector model there is no recoil from the created boson on the particle, as was discussed in Section 7.4. The change of the wave



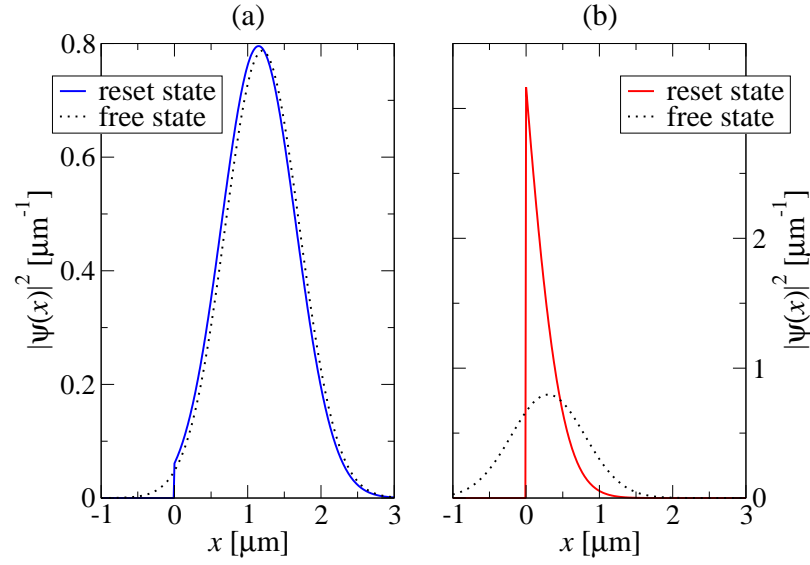


**Figure 8.3:** The normalized reset state in position space immediately after a detection at (a)  $T_2 = 0.167$  ms (with  $A = 1.4337 \times 10^3 \text{ s}^{-1}$ ) and at (b)  $T_1 = 0.041$  ms (with  $A = 2.3895 \times 10^4 \text{ s}^{-1}$ ), compared with the free wave packet at the respective instance of time (dotted line). The fast detection in case (b) has a strong impact on the wave function.

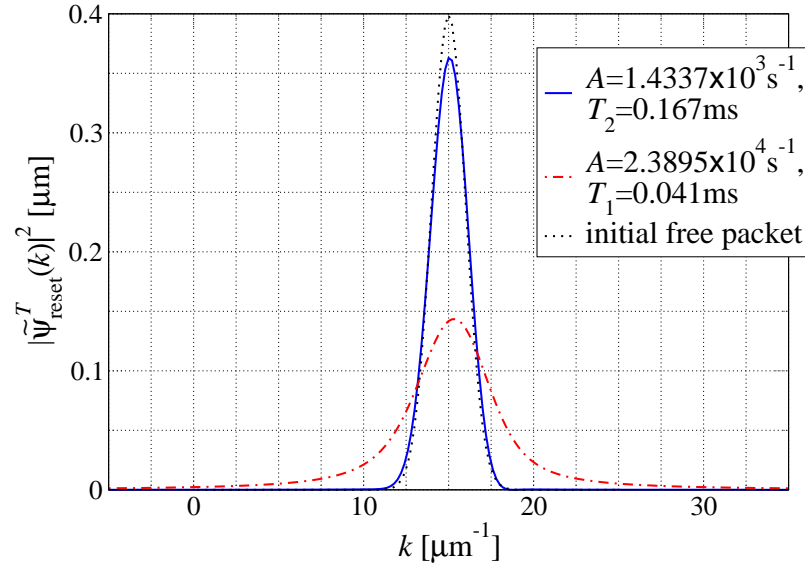


**Figure 8.4:** Momentum densities of reset states immediately after a detection at  $T_2 = 0.167$  ms (solid line, with  $A = 1.4337 \times 10^3 \text{ s}^{-1}$ ) and at  $T_1 = 0.041$  ms (dash-dotted line, with  $A = 2.3895 \times 10^4 \text{ s}^{-1}$ ), compared to the momentum density of the initial wave packet (dotted line). The fast detection in the latter case leads to a strong broadening of the momentum density.



packet in momentum space is a consequence solely of the projection in position space by the reset operation. Since the broad momentum density of the typical reset states in this case is enforced by the Heisenberg uncertainty relation, it is a pure quantum effect.

## 8.2 Width of the passage-time density

In Section 6.4 a measurement scheme for passage times was sketched, which had been investigated in References [Per80, ASM03]. This scheme is based on the (semi-) continuous coupling of the particle under consideration to a clock. It was argued that the precision of the measurement behaves like  $E^{-1}$ , where  $E$  denotes the kinetic energy of the particle. One now may wonder whether or not the  $E^{-1}$  behavior is a fundamental quantum limit for measuring passage times. In the present section it is argued that this is not the case since the present measurement scheme by means of two spatially separated spin-boson detectors yields, for optimal parameter choices, passage-time densities with widths behaving like  $E^{-3/4}$ . Thus, for low energies, we have an example which breaks the  $E^{-1}$  limitation of the clock model.

### 8.2.1 Estimating the precision

In this subsection we give an estimate for the width of the passage-time density obtained from the present measurement scheme. We assume that the detectors can be described by the continuum limit and that transmission and reflection without detection are negligible. This assumption is justified in the examples discussed in the preceding sections of the present chapter, which employed rectangular sensitivity functions. It can also be justified in general if one drops the restriction to rectangular sensitivity functions  $\chi(x)$ <sup>1</sup>.

Considering particles with mean velocity  $v_0$ , the detector is assumed to be constructed in such a way that the first detection occurs with high probability in a spatial interval of length  $L$ . The length  $L$  is related to  $A$  of Equation (4.16), an average detection rate,  $L$  being of the order of  $v_0/A$ . The length  $L$  imposes an upper limit on the width of the reset state in position space,

$$\Delta x_{\text{reset}} \leq L \approx \frac{v_0}{A}. \quad (8.1)$$

By the Heisenberg uncertainty relation, this immediately yields a lower bound for the width  $\Delta p_{\text{reset}}$  of the reset state in momentum space,

$$\Delta p_{\text{reset}} \geq \frac{\hbar}{2\Delta x_{\text{reset}}} \geq \frac{\hbar}{2L}. \quad (8.2)$$

---

<sup>1</sup>Given an energy range, an optimized absorbing potential can be constructed which almost completely absorbs wave packets of this energy range in a very short spatial interval; this was shown in References [MBM95, PMS98] by means of inverse scattering techniques, see also Section 5.2.3. Such a potential can then be considered as a continuum limit of a discrete spin-boson detector. Again, we stress that the optimization depends on the energy range under consideration, and that there is no such thing as *the* optimal detector for all energy ranges.



Note that this is only a very rough estimate, without taking into account details of the actual wave packet. If the incident wave packet is very narrow in position space, then  $\Delta x_{\text{reset}}$  also may be much smaller than  $L$ , and consequently  $\Delta p_{\text{reset}}$  may be much larger than  $\hbar/2L$ . Also, the reset state may be far from being a Gaussian, and then already the first inequality in Equation (8.2) may underestimate the width of  $\Delta p_{\text{reset}}$  seriously.

Let  $\Delta\tau$  denote the width of the measured passage-time density. There are several contributions to this width. First, a particle with velocity  $v_0$  takes the time  $\tau = d/v_0$  to travel the distance  $d$  between the two detectors, and therefore the width of the reset state in position space contributes

$$\Delta\tau_{\text{reset},x} = \frac{\Delta x_{\text{reset}}}{v_0} \quad (8.3)$$

to  $\Delta\tau$ . Second, the width in momentum space contributes according to

$$\Delta\tau_{\text{reset},p} = \frac{\Delta p_{\text{reset}}}{mv_0} \frac{d}{v_0} \geq \frac{\hbar}{2\Delta x_{\text{reset}}} \frac{d}{mv_0^2}. \quad (8.4)$$

Third, the width of the detection delay,  $\Delta\tau_{\text{delay}}$ , is roughly

$$\Delta\tau_{\text{delay}} = \frac{1}{A} \approx \frac{L}{v_0},$$

as was argued in Section 8.1.2. We note that  $\Delta\tau_{\text{delay}}$  contributes twice to  $\Delta\tau$  since it arises in both detectors. An estimate for the width of the passage-time density is given by the sum of these contributions,

$$\begin{aligned} \Delta\tau &= 2\Delta\tau_{\text{delay}} + \Delta\tau_{\text{reset},x} + \Delta\tau_{\text{reset},p} \\ &\gtrsim \frac{2}{A} + \frac{\Delta x_{\text{reset}}}{v_0} + \frac{\hbar d}{2mv_0^2 \Delta x_{\text{reset}}}. \end{aligned} \quad (8.5)$$

From this estimate it is again seen that both small as well as large values of  $A$ , i.e., both slow as well as fast detectors, lead to rather broad passage-time densities (due to  $\Delta\tau_{\text{delay}} \sim 1/A$  and  $\Delta\tau_{\text{reset},p} \sim 1/\Delta x_{\text{reset}} \sim 1/L \sim A$ , respectively).

### 8.2.2 Optimal parameters

Having established the general estimate for  $\Delta\tau$  in Equation (8.5), we now turn to the task of finding optimal parameters, minimizing  $\Delta\tau$ . We are interested in measuring the passage time through a spatial interval of length  $d$ , the distance between the starting points of the two detectors, which we regard as fixed. First, we consider given detectors, i.e., a given detection rate  $A$ . Again, particles with mean velocity  $v_0$  would be detected within an interval with length  $L$  given approximately by  $L \approx v_0/A$ . This means that the velocities must not be too large since in order to avoid undetected transmission  $L$  must not exceed the actual length of the detector (and in particular  $L$  must not exceed  $d$ ). Quantum effects, however, are expected to play a role for slow particles while fast particles may be treated classically, hence this is not a serious drawback.



We assume that the reset state is a Gaussian wave packet, or at least close to a Gaussian, so that in the second line of Equation (8.5) the approximate equality holds,

$$\Delta\tau \approx \frac{2}{A} + \frac{\Delta x_{\text{reset}}}{v_0} + \frac{\hbar d}{2mv_0^2 \Delta x_{\text{reset}}} . \quad (8.6)$$

We note that  $2/A$  is a purely detector-related quantity, viz. the width of the detection delay in each of the two detectors due to the finite decay rate  $A$ . The remaining contribution to  $\Delta\tau$  is determined by the shape of the reset state only. We will first optimize this latter quantity. For given particles with given mean velocity, i.e.,  $m$  and  $v_0$  fixed, this is minimal for

$$\Delta x_{\text{reset}}^{\text{opt}} = \sqrt{\frac{\hbar d}{2mv_0}} . \quad (8.7)$$

Substituting this into Equation (8.6) and writing  $E = mv_0^2/2$  for the kinetic energy of the incident particles yields

$$\Delta\tau_{\text{opt; reset}} \approx \frac{2}{A} + \sqrt{\hbar d \sqrt{m/2}} E^{-3/4} . \quad (8.8)$$

The subscript “opt; reset” indicates that only the reset state was optimized while the detection rate  $A$  was considered as a given quantity.

Aiming at optimizing also the detection rate  $A$  for minimal  $\Delta\tau$ , one would like to choose  $A$  as large as possible in order to reduce the  $2/A$  contribution to  $\Delta\tau$ . However, one has to take into account that the width of the reset state is bounded by Equation (8.1). Thus, given  $d$ ,  $m$ , and  $v_0$ , the decay rate must be at most of the order of  $v_0/\Delta x_{\text{reset}}^{\text{opt}}$  with  $\Delta x_{\text{reset}}^{\text{opt}}$  as in Equation (8.7). In fact, we may choose the incoming state such that it forms a Gaussian minimal uncertainty packet at the starting point of the first detector with width in position space

$$\Delta x = \Delta x_{\text{reset}}^{\text{opt}} = \sqrt{\frac{\hbar d}{2mv_0}} ,$$

and choose further  $A$  as large as possible in view of Equation (8.1) with  $\Delta x_{\text{reset}} = \Delta x_{\text{reset}}^{\text{opt}}$ , i.e.

$$A \approx \frac{v_0}{2\Delta x} = \sqrt{\frac{m}{2\hbar d}} v_0^{3/2} . \quad (8.9)$$

We note that, by this parameter choice, yet another requirement of a good measurement scheme is fulfilled: The detection by the first detector will not change the wave function too strongly. The reset operation after this detection is essentially a projection onto the detector region, and the detection is slow enough that at typical detection times most of the wave packet overlaps with the detector, hence the projection does not change the wave function too much. Thus, the reset state will be close to a Gaussian wave packet with width  $\Delta x = \Delta x_{\text{reset}}^{\text{opt}}$ . Substituting Equation (8.9) into Equation (8.8) finally yields

$$\Delta\tau_{\text{opt}} \approx \sqrt{5\hbar d \sqrt{m/2}} E^{-3/4} .$$



**Remark 8.2.1** We stress that, independent of the detection rate  $A$ , the optimal energy dependence of  $\Delta\tau$  is limited to  $E^{-3/4}$  already by the dependence of  $\Delta\tau$  on the width of the reset state in position space,  $\Delta\tau_{\text{reset},x} \sim \Delta x_{\text{reset}}$  [see Equation (8.3)], and on its width in momentum space,  $\Delta\tau_{\text{reset},p} \sim \Delta p_{\text{reset}} \sim 1/\Delta x_{\text{reset}}$  [see Equation (8.4)]. This will be discussed further in Section 8.2.3.

For the example of a cesium atom with  $v_0 = 0.717$  cm/s and a distance of  $d = 100$   $\mu\text{m}$  between the detectors (with rectangular sensitivity function) of the preceding section, optimal values would be according to Equations (8.7) and (8.9)

$$\Delta x_{\text{opt}} = 1.83 \text{ } \mu\text{m}, \text{ and } A_{\text{opt}} = 1.959 \times 10^3 \text{ s}^{-1}.$$

Considering the wave packet with  $\Delta x = 1$   $\mu\text{m}$  actually investigated in the examples, the optimal decay rate according to Equation (8.9) would be  $A_{\text{opt}}(\Delta x = 1 \text{ } \mu\text{m}) = 3.585 \times 10^3 \text{ } \mu\text{s}^{-1}$ . This is consistent with the observation that the example with  $A$  closest to  $A_{\text{opt}}(\Delta x = 1 \text{ } \mu\text{m})$  yields the narrowest density.

### 8.2.3 A detector-independent lower bound for the width

In view of Remark 8.2.1 one may ask whether or not the  $E^{-3/4}$  limitation is valid solely for the spin-boson detector model or for *any* measurement scheme based on two spatially separated detectors, independent of the particular detector model involved. The latter is indeed the case as can be seen from the fact that up to Equation (8.8) only the influence of the reset state on the width of the passage-time density was discussed, and only the shape of the reset state was optimized. For greater clarity, however, we give a reasoning very much in parallel to that of Equation (8.6) through Equation (8.8) of the previous section, but without assuming a particular detector model.

Assume that a particle is detected by the first detector ('entry'). Then it travels a distance  $d_0$ , and then it is detected by the second detector ('exit'). If the particle has a velocity  $v_0$ , the time elapsed between the two detections will be

$$\tau = d_0/v_0.$$

This is the measured passage time.

Independent of the particular detector model, there are two 'intrinsic' sources of uncertainty: Both  $d_0$  and  $v_0$  are not known exactly. We take  $d_0$  and  $p_0 = mv_0$  as average values of probability densities of the distance to be traversed and of the momentum of the particle. The width of the passage-time density,  $\Delta\tau$ , depends on the width of the distance density,  $\Delta d$ , and of the momentum density,  $\Delta p$ , according to

$$\Delta\tau_{\text{intrinsic}} = \frac{m}{p_0} \Delta d + \frac{md_0}{p_0^2} \Delta p. \quad (8.10)$$

We are not interested in classical contributions to the widths  $\Delta d$  and  $\Delta p$ , which could (in principle) be reduced by choosing a more accurate scheme for measuring the distance to be traversed and for preparing the particle.

According to quantum mechanics, however, the particle is described by a wave function. This wave function has a width in momentum space,  $\Delta p$ , and



in position space,  $\Delta x$ . These widths are related by the Heisenberg uncertainty relation

$$\Delta x \Delta p \geq \frac{\hbar}{2}. \quad (8.11)$$

If we drop the restriction to two identical detectors, we may assume that the second detector ('exit') is responding very quickly to the presence of the particle. Thus, the width of the wave function in position space immediately after the detection by this detector is very narrow. In other words, we know quite exactly *where* the particle has been detected by the 'exit' detector. The distance  $d$  which the particle has traversed then since it has been detected by the first detector ('entry'), however, cannot be known more exactly than the position of the particle immediately after this first detection. Thus, one has

$$\Delta d \approx \Delta x_{\text{reset}},$$

where  $\Delta x_{\text{reset}}$  is the width, in position space, of the reset state immediately after the first detection. The width of the reset state in momentum space,  $\Delta p_{\text{reset}}$ , is related to  $\Delta x_{\text{reset}}$  by the Heisenberg uncertainty relation Equation (8.11). Equation (8.10) then yields

$$\begin{aligned} \Delta \tau_{\text{intrinsic}} &= \frac{m}{p_0} \Delta x_{\text{reset}} + \frac{m d_0}{p_0^2} \Delta p_{\text{reset}} \\ &\geq \frac{m}{p_0} \Delta x_{\text{reset}} + \frac{m d_0}{p_0^2} \frac{\hbar}{2 \Delta x_{\text{reset}}}. \end{aligned}$$

The right hand side is minimal for

$$\Delta x_{\text{reset}}^{\text{opt}} = \sqrt{\frac{\hbar d_0}{m v_0}},$$

leading to

$$\Delta \tau_{\text{intrinsic}}^{\text{opt}} = \sqrt{\hbar d_0 \sqrt{m/2}} E^{-3/4}$$

with  $E = m v_0^2/2$ . Thus, the  $E^{-3/4}$  limitation is obtained solely from the Heisenberg uncertainty relation Equation (8.11), and without any assumption about the detector model used for the particle detection.



## **Part III**

# **Summary and Conclusion**







## Chapter 9

# Time observables from a spin-boson detector model

### 9.1 Summary

In Part [I](#) of the present thesis a fully quantum mechanical spin-boson detector model for the detection of a moving, spread-out quantum particle has been investigated, and in Part [II](#) its application to passage times has been discussed. Such an operational approach to time observables in quantum mechanics is interesting since nowadays experiments with ultra-cold atoms are possible in which the quantum nature of the center-of-mass motion yields noticeable effects. In contrast to this, the description of time observables in the framework of quantum mechanics is not yet clear.

As concerns the application of the spin-boson detector to arrival times in Part [I](#), it has been shown in Chapter [4](#) that in the limit of continuous boson modes it is effectively described by means of a complex potential model. A similar result had been obtained earlier for the fluorescence model for particle detection, but only under additional assumptions which yield a one-channel limit for that model. This close relation, though, is seen only as a result of the careful analysis of both the models. It is by no means obvious from the start since the two models for particle detection are physically different. The derivation of complex potentials from two different physical models for the detection process helps to illuminate the physical background of otherwise heuristically introduced complex potentials. In particular, it suggests that complex potentials provide an effective description for arrival-time measurements which to some extent is independent of the particular detector model under consideration. Only the interpretation of the height of the complex potential depends on the particular model. When applied to an arrival-time measurement, complex potentials show typical and generally unwanted features: There is a detection delay and there is also necessarily the possibility of reflection without detection. However, these features are as general for operational approaches to arrival times as the effective description by complex potentials is. We stress in particular that as in any complex potential model also in the spin-boson model there



is the possibility of reflection without detection, showing a back-reaction of the measurement on the particle. This is in contrast to what one might expect since there is no direct interaction of the particle, neither with the detector nor with the bath modes. The particle is regarded merely as a catalyst for a change in the detector-bath state. Further, no measurement is performed on the particle or on the detector; only the bath is checked for bosons. The possibility of reflection without detection even in such a minimally invasive detector model suggests that this reflection may indeed be a very general feature of operational approaches to arrival times. Possible optimization schemes for the detection of wave packets of a given energy range, though, have been discussed in Section 5.2.

The measurement scheme for passage times investigated in Part II mimicks typical time-of-flight experiments: The particle is detected upon entry and exit, and the correlation between these detections yields the passage time. In Chapter 7 analytical expressions have been derived for the reset state, i.e., the state immediately after the detection of a boson, and for the ‘measured’ passage-time density. Further, numerical examples have been presented in Section 8.1.1. The application of the present spin-boson detector model to the above measurement scheme has shown that the spin-boson detector model has a special feature which makes it particularly useful for this kind of *Gedanken* experiment: The evaluation of the reset state in Section 7.3 has yielded no explicit recoil of the created boson on the particle of interest. Physically, this is due to the fact that the boson is emitted by the spin lattice and not by the particle, hence the recoil is experienced by this lattice similarly to the Mössbauer effect. This is in contrast to, e.g., the fluorescence model. There, the fluorescence photon is emitted by the particle of interest, and hence the reset state explicitly contains a recoil. But in spite of the absence of an explicit recoil in the spin-boson model there still is an effect of the reset operation on the wave function: The reset operation is essentially a projection of the wave packet in position space onto the detector region, and this projection changes the wave function in position space and in momentum space. The more accurate the individual detection is, i.e., the faster the detector responds to the presence of the particle, the stronger is the distortion of the wave function by the reset operation. In particular, very fast detectors yield typical reset states which are very narrow in position space and hence, by the Heisenberg uncertainty relation, very broad in momentum space. This has been illustrated by the numerical examples in Section 8.1.1. Such reset states which are broad in momentum space then lead to broad passage-time densities. This broadening mechanism is essentially based on the Heisenberg uncertainty relation and hence is a quantum effect. Very slow detectors, on the contrary, also yield broad passage-time densities. This is simply due to the poor quality of the individual detections. Intermediate detectors, however, yield narrower passage-time densities. It has been argued in Section 8.2 that for optimal parameters the precision of the measurement behaves like  $E^{-3/4}$ , where  $E$  is the kinetic energy of the incident particle. For slow particles this is better than, and in contrast to, the  $E^{-1}$  behavior obtained from a quantum clock model. We thus conclude that this  $E^{-1}$  behavior cannot be due to a



fundamental quantum limit. It has further been argued that for the present measurement scheme the  $E^{-3/4}$  behavior is already the optimum that can be obtained, independent of the particular detector model under consideration.

In the present thesis the examination of the spin-boson model has mainly been based on the quantum jump approach, treating the limit of continuous boson modes under the assumption that the Markov property holds. In Section 3.2, however, a simplified, single-spin model has also been treated in the case of discrete boson modes, by means of standard unitary quantum mechanics. For a number of examples we have compared the results obtained from the two approaches, i.e., from unitary quantum mechanics in the discrete case and from the quantum jump approach in the limit of continuous bath modes. It has turned out that the results are in good agreement, up to revivals in the discrete case. This agreement illustrates the validity of the quantum jump approach for the model under consideration. This is interesting since the quantum jump approach has originally been developed in the framework of quantum optics, and the successful application to the spin-boson model shows that the approach is valid also beyond quantum optics. We further stress that in the examples only modest numbers of boson modes,  $N \approx 15 \dots 40$ , were necessary to obtain the agreement with the quantum jump approach. This suggests that the quantum jump approach may provide a convenient and accurate approximation to situations where one actually has to deal with a discrete model, as, e.g., in cavity quantum optics. All examples presented in the present thesis have in common that the correlation time is much smaller than the inverse decay rate,  $\tau_c \ll 1/A$ . This is a necessary condition for the applicability of the quantum jump approach, as outlined in Section 4.1.

## 9.2 Outlook

The results presented in the present thesis provide a basis for further research. A rather obvious extension, e.g., would be the application of the spin-boson detector model to arrival or passage times in the presence of interaction. In other words, one would consider model Hamiltonians as in Section 3.1.2 but with an additional real potential  $U(\mathbf{x})$ . The application of such a model to arrival times should proceed along similar lines as the investigation presented in Part I of the present thesis, and we expect that the detection again is effectively described by a complex potential. Besides the complex potential describing the detector, the conditional Hamiltonian should contain the real potential just as it would occur in the original model Hamiltonian. The measurement of arrival times by complex potentials in the presence of interaction, i.e., real potential, was investigated in Reference [HSMN04]. The results were compared to phase-time approaches, and the Hartman effect [Har62] was explicitly seen in numerical examples. As soon as it is verified that the spin-boson model in the presence of interaction is indeed described by a complex potential model, these results immediately carry over to the spin-boson model. In order to model a measurement of tunneling times, one may further extend the measurement



scheme of Part II and put a real potential  $U(\mathbf{x})$  between the detectors at entry and exit.

Another interesting line of further research would be to precisely determine the conditions under which the continuum limit of the quantum jump approach agrees with the unitary investigation of models with discrete bath modes. Since there are no recurrences in the quantum jump approach, i.e., no transitions of the kind  $|\downarrow 1_{\ell}\rangle \rightarrow |\uparrow 0\rangle$ , it is clear that the agreement can only hold up to the time of recurrences in the discrete model. Further, in the derivation of the quantum jump approach it is assumed that the Markov property holds, and that the correlation time of the system under consideration is much shorter than the inverse decay rate of the excited state(s) of the multi-level which is supposed to emit a boson. This is necessary to ensure that the separation in time,  $\Delta t$ , between the instantaneous measurements on the bath may fulfill  $\tau_c \ll \Delta t \ll 1/A$ . In the framework of photon statistics it has been shown, however, that one obtains the correct statistics even if in the evaluation of the reset states one formally considers a limit  $\Delta t \rightarrow 0$  which physically is not justified [HS96]. This suggests that the validity of the quantum jump approach may exceed the assumptions under which it was derived. Indeed, while investigating the examples presented in the present thesis, we noted that an excellent agreement between the quantum jump approach and the discrete model is sometimes seen even for parameters  $\tau_c \approx 1/A$ . Since it is generally more convenient to work with the quantum jump approach than with a number of discrete bath modes, a detailed clarification of the validity of the quantum jump approach as an approximation to a discrete model would be useful.



## Part IV

# Appendix







## Appendix A

# Pauli's 'No-Go footnote'

The existence of a self-adjoint time operator conjugate to the Hamiltonian is widely regarded as precluded for most of the systems of physical interest by an argument Pauli put forward in a famous footnote [Pau33]. We briefly sketch his argument.

Assume that there is an operator  $\hat{T}$  such that

$$[H, \hat{T}] = -i\hbar \quad (\text{A.1})$$

holds, mirroring the well known commutation relation for momentum and position, and let  $|E\rangle$  be an energy eigenstate with eigenvalue  $E \in \mathbb{R}$ ,

$$H |E\rangle = E |E\rangle ; \quad (\text{A.2})$$

consider then the state  $e^{-iE_1\hat{T}/\hbar} |E\rangle$ ,  $E_1 \in \mathbb{R}$ . By means of the series expansion

$$e^{-iE_1\hat{T}/\hbar} = \sum_n \frac{(-iE_1\hat{T}/\hbar)^n}{n!} \quad (\text{A.3})$$

one finds from Equation (A.1) the commutation relation

$$[H, e^{-iE_1\hat{T}/\hbar}] = -E_1 e^{-iE_1\hat{T}/\hbar}.$$

Then it follows from Equation (A.2) that

$$H \left( e^{-iE_1\hat{T}/\hbar} |E\rangle \right) = (E - E_1) \left( e^{-iE_1\hat{T}/\hbar} |E\rangle \right), \quad E_1 \in \mathbb{R},$$

and consequently the spectrum of  $H$ , i.e., the energy spectrum, would extend continuously over the whole range  $(-\infty, \infty)$ . This contradicts the assumption of a lower bound for the energy spectrum, which is crucial for the stability of matter, and also precludes the possibility of discrete energy eigenvalues typical for bound states. Pauli thus concluded that there cannot be such a thing as a time operator conjugate to  $H$ .

Although often regarded as a No-Go theorem, we note that Pauli presented this statement as a casual remark in a footnote, based on the mere formal argument above, and by no means as a theorem proved with mathematical rigor.



In particular, he did not pay attention to the question of domains of the respective operators. Galapon emphasized this point and investigated the question under which conditions and for which  $E_1 \in \mathbb{R}$  the expansion (A.3) makes sense. He showed that one can consistently assume a self-adjoint *bounded* operator conjugate to a Hamiltonian with unbounded, semi-bounded, or countable point spectrum [Gal02].



# Bibliography

- [AB61] Y. Aharonov and D. Bohm, *Time in the quantum theory and the uncertainty relation for time and energy*, Phys. Rev. **122**, 1649 (1961).
- [AK85] A. Auerbach and S. Kivelson, *The path decomposition expansion and multidimensional tunneling*, Nucl. Phys. B **257**, 799 (1985).
- [AKN84] A. Auerbach, S. Kivelson, and D. Nicole, *Path decomposition for multidimensional tunneling*, Phys. Rev. Lett. **53**, 411 (1984).
- [All69a] G. R. Allcock, *The time of arrival in quantum mechanics I. Formal considerations*, Ann. Phys. (NY) **53**, 253 (1969).
- [All69b] G. R. Allcock, *The time of arrival in quantum mechanics II. The individual measurement*, Ann. Phys. (NY) **53**, 286 (1969).
- [All69c] G. R. Allcock, *The time of arrival in quantum mechanics III. The measurement ensemble*, Ann. Phys. (NY) **53**, 311 (1969).
- [AS68] M. Abramowitz and I. A. Stegun (eds.), *Handbook for mathematical functions*, Dover Publications, New York, 1968.
- [ASM03] D. Alonso, R. Sala Mayato, and J. G. Muga, *Quantum time-of-flight measurements: Kicked clock versus continuous clock*, Phys. Rev. A **67**, 032105 (2003).
- [Baz67] A. Baz', Sov. J. Nucl. Phys. **5**, 182 (1967).
- [BD97] P. Balcou and L. Dutriaux, *Dual optical tunneling times in frustrated total internal reflection*, Phys. Rev. Lett. **78**, 851 (1997).
- [BF02] R. Brunetti and K. Fredenhagen, *Time of occurrence observable in quantum mechanics*, Phys. Rev. A **66**, 044101 (2002).
- [BGL95] P. Busch, M. Grabowski, and P. J. Lathi, *Operational quantum mechanics*, Springer Verlag, Berlin, 1995.
- [BH96] A. Beige and G. C. Hegerfeldt, *Projection postulate and atomic quantum Zeno effect*, Phys. Rev. A **53**, 53 (1996).



- [BHJ26] M. Born, W. Heisenberg, and P. Jordan, *Zur Quantenmechanik II*, Z. Phys. **35**, 557 (1926).
- [BJ26] M. Born and P. Jordan, *Zur Quantenmechanik*, Z. Phys. **34**, 858 (1926).
- [BJ93] P. Blanchard and A. Jadczyk, *On the interaction between classical and quantum systems*, Phys. Lett. A **175**, 157 (1993).
- [BN67] A. Beskow and J. Nilsson, *The concept of wave function and the irreducible representations of the Poincaré group*, Arkiv för Fysik **34**, 561 (1967).
- [Büt83] M. Büttiker, *Lamor precession and the traversal time for tunneling*, Phys. Rev. B **27**, 6178 (1983).
- [Car93] H. Carmichael, *An open system approach to quantum optics*, LNP, vol. m 18, Springer Verlag, Berlin, 1993.
- [CGH<sup>+</sup>96] R. M. Corless, G. H. Gonnet, D. E. G. Hare, D. J. Jeffrey, and D. E. Knuth, *On the Lambert W function*, Adv. Comp. Math. **5**, 329 (1996).
- [DCM92] J. Dalibard, Y. Castin, and K. Mølmer, *Wave-function approach to dissipative processes in quantum optics*, Phys. Rev. Lett. **68**, 580 (1992).
- [DEHM02] J. A. Damborenea, I. L. Egusquiza, G. C. Hegerfeldt, and J. G. Muga, *Measurement based approach to quantum arrival times*, Phys. Rev. A **66**, 052104 (2002).
- [DEHM03] J. A. Damborenea, I. L. Egusquiza, G. C. Hegerfeldt, and J. G. Muga, *On atomic time-of-arrival measurements with a laser of finite beam width*, J. Phys. B: At. Mol. Opt. Phys. **36**, 2657 (2003).
- [DEMN04] J. A. Damborenea, I. L. Egusquiza, J. G. Muga, and B. Navarro, *Quantum dwell times*, quant-ph/0403081, 2004.
- [Dir26] P. A. M. Dirac, *On quantum algebra*, Proc. Cam. Philos. Soc. **23**, 412 (1926).
- [EM00a] I. L. Egusquiza and J. G. Muga, *Erratum: Free-motion time-of-arrival operator and probability distribution*, Phys. Rev. A **61**, 059901 (2000).
- [EM00b] I. L. Egusquiza and J. G. Muga, *Free-motion time-of-arrival operator and probability distribution*, Phys. Rev. A **61**, 012104 (2000), see also Reference [EM00a].
- [EMNRh03] I. L. Egusquiza, J. G. Muga, B. Navarro, and A. Ruschhaupt, *Comment on: "On the "standard" quantum mechanical approach to times of arrival"*, Phys. Lett. A **313**, 498 (2003).



- [ES71] H. Ekstein and A. J. F. Siegert, *On a reinterpretation of decay experiments*, Ann. Phys. (NY) **68**, 509 (1971).
- [Fey48] R. P. Feynman, *Space-time approach to non-relativistic quantum mechanics*, Rev. Mod. Phys. **20**, 367 (1948).
- [Gal02] E. A. Galapon, *Pauli's theorem and quantum canonical pairs: the consistency of a bounded, self-adjoint time operator canonically conjugate to a Hamiltonian with a non-empty point spectrum*, Proc. R. Soc. Lond. A **458**, 451 (2002).
- [GS90] B. Gaveau and L. S. Schulman, *Model apparatus for quantum measurements*, J. Stat. Phys. **58**, 1209 (1990).
- [GS95] B. Gaveau and L. S. Schulman, *Limited quantum decay*, J. Phys. A **28**, 7359 (1995).
- [Hal99] J. J. Halliwell, *Arrival times in quantum theory from an irreversible detector model*, Progr. Theor. Phys. **102**, 707 (1999).
- [Har62] T. E. Hartmann, *Tunneling of a wave packet*, J. Appl. Phys. **33**, 3427 (1962).
- [Heg93] G. C. Hegerfeldt, *How to reset an atom after a photon detection: Applications to photon-counting processes*, Phys. Rev. A **47**, 449 (1993).
- [Heg03] G. C. Hegerfeldt, *The quantum jump approach and quantum trajectories*, Irreversible Quantum Dynamics (F. Benatti and R. Floreanini, eds.), LNP, vol. 622, Springer, 2003, pp. 233 – 242.
- [Hei25] W. Heisenberg, *Über quantentheoretische Umdeutung kinematischer und mechanischer Beziehungen*, Z. Phys. **33**, 879 (1925).
- [HHM05] V. Hannstein, G. C. Hegerfeldt, and J. G. Muga, *Quantum optical time-of-arrival model in three dimensions*, J. Phys. B **38**, 409 (2005).
- [HNS06] G. C. Hegerfeldt, J. T. Neumann, and L. S. Schulman, *Investigation of a quantum mechanical detector model for moving, spread-out particles*, J. Phys. A **39**, 14447 (2006).
- [HNS07] G. C. Hegerfeldt, J. T. Neumann, and L. S. Schulman, *Passage-time distributions from a spin-boson detector model*, Phys. Rev. A **75**, 012108 (2007).
- [HS89] E. H. Hauge and J. A. Støvneng, *Tunneling times: a critical review*, Rev. Mod. Phys. **61**, 917 (1989).
- [HS96] G. C. Hegerfeldt and D. G. Sondermann, *Conditional Hamiltonian and reset operator in the quantum jump approach*, Quantum Semiclass. Opt. **8**, 121 (1996).



- [HSM03] G. C. Hegerfeldt, D. Seidel, and J. G. Muga, *Quantum arrival times and operator normalization*, Phys. Rev. A **68**, 022111 (2003).
- [HSMN04] G. C. Hegerfeldt, D. Seidel, J. G. Muga, and B. Navarro, *Operator normalized quantum arrival times in the presence of interactions*, Phys. Rev. A **70**, 012110 (2004).
- [HW92] G. C. Hegerfeldt and T. S. Wilser, *Ensemble or individual system, collapse or no collapse: A description of a single radiating atom*, Classical and Quantum Systems (H. D. Doebner, W. Scherer, and F. Schroeck, eds.), Proceedings of the Second International Wigner Symposium, July 1991, World Scientific, Singapore, 1992, pp. 104 – 115.
- [Jad95] A. Jadczyk, *Particle tracks, events and quantum theory*, Progr. Theor. Phys. **93**, 631 (1995).
- [Jam74] M. Jammer, *The philosophy of quantum mechanics*, John Wiley & Sons, New York, 1974.
- [JC63] E. T. Jaynes and F. W. Cummings, *Comparison of quantum and semiclassical radiation theories with application to the beam maser*, Proc. IEEE **51**, 89 (1963).
- [JW88] W. Jaworski and D. M. Wardlaw, *Time delay in tunneling: Transmission and reflection time delays*, Phys. Rev. A **37**, 2843 (1988).
- [Kha68] L. A. Khalfin, *Phenomenological theory of  $K^0$  mesons and the non-exponential character of decay*, JETP Lett. **8**, 65 (1968), english translation of: L. A. Khalfin, Zh. Eksp. Teor. Fiz. Pis. Red. **8**, 106 (1968).
- [Kij74] J. Kijowski, *On the time operator in quantum mechanics and the heisenberg uncertainty relation for energy and time*, Rep. Math. Phys. **6**, 361 (1974).
- [KKW87] M. S. Kim, P. L. Knight, and K. Wodkiewicz, *Correlations between successively emitted photons in resonance fluorescence*, Opt. Commun. **62**, 385 (1987).
- [Lea02] C. R. Leavens, *On the “standard” quantum mechanical approach to times of arrival*, Phys. Lett. A **303**, 154 (2002).
- [Lea05] C. R. Leavens, *Reply to comment on: “On the “standard” quantum mechanical approach to times of arrival”*, Phys. Lett. A **345**, 251 (2005).
- [LM94] R. Landauer and T. Martin, *Barrier interaction time in tunneling*, Rev. Mod. Phys. **66**, 217 (1994).



- [Lüd51] G. Lüders, *Über die Zustandsänderung durch den Meßprozeß*, Ann. d. Physik **443**, 322 (1951).
- [MBM95] J. G. Muga, S. Brouard, and D. Macías, *Time of arrival in quantum mechanics*, Ann. Phys. (NY) **240**, 351 (1995).
- [MBS92] J. G. Muga, S. Brouard, and R. Sala, *Transmission and reflection tunneling times*, Phys. Lett. A **167**, 24 (1992).
- [ML00] J. G. Muga and C. R. Leavens, *Arrival time in quantum mechanics*, Phys. Rep. **338**, 353 (2000).
- [MLP98] J. G. Muga, C. R. Leavens, and J. P. Palao, *Space-time properties of free-motion time-of-arrival eigenfunctions*, Phys. Rev. A **58**, 4336 (1998).
- [MS77] B. Misra and E. C. G. Sudarshan, *The Zeno's paradox in quantum theory*, J. Math. Phys. **18**, 756 (1977), for further references see [BH96].
- [MSE02] J. G. Muga, R. Sala Mayato, and I. L. Egusquiza (eds.), *Time in quantum mechanics*, LNP, vol. m 72, Springer Verlag, Berlin Heidelberg, 2002.
- [MSP98] J. G. Muga, R. Sala, and J. P. Palao, *The time of arrival concept in quantum mechanics*, Superlattices Microstruct. **23**, 833 (1998).
- [NEMH03a] B. Navarro, I. L. Egusquiza, J. G. Muga, and G. C. Hegerfeldt, *Optimal atomic detection by control of detuning and spatial dependence of laser intensity*, J. Phys. B **36**, 3899 (2003).
- [NEMH03b] B. Navarro, I. L. Egusquiza, J. G. Muga, and G. C. Hegerfeldt, *Suppression of Rabi oscillations for moving atoms*, Phys. Rev. A **67**, 063819 (2003).
- [ORU99] J. Oppenheimer, B. Reznik, and W. G. Unruh, *Time-of-arrival states*, Phys. Rev. A **59**, 1804 (1999).
- [Pau33] W. Pauli, *Die allgemeinen Prinzipien der Wellenmechanik*, Handbuch der Physik (H. Geiger and K. Scheel, eds.), vol. XXIV/1, Springer Verlag, Berlin, 2<sup>nd</sup> ed., 1933, (english translation see [Pau58]), pp. 83 – 272.
- [Pau58] W. Pauli, Encyclopedia of Physics (S. Flugge, ed.), vol. 5/1, Springer Verlag, Berlin, 1958, p. 60.
- [Per80] A. Peres, *Measurement of time by quantum clocks*, Am. J. Phys. **48**, 552 (1980).
- [PK98] M. B. Plenio and P. L. Knight, *The quantum-jump approach to dissipative dynamics in quantum optics*, Rev. Mod. Phys. **70**, 101 (1998).



- [PMS98] J. P. Palao, J. G. Muga, and R. Sala, *Composite absorbing potentials*, Phys. Rev. Lett. **80**, 5469 (1998).
- [RDN<sup>+</sup>04] A. Ruschhaupt, J. A. Damborenea, B. Navarro, J. G. Muga, and G. C. Hegerfeldt, *Exact and approximate potentials for modelling time observables*, Europhys. Lett. **67**, 1 (2004).
- [Ryb67] V. Rybachenko, Sov. J. Nucl. Phys. **5**, 635 (1967).
- [SB87] D. Sokolovski and L. M. Baskin, *Traversal time in quantum scattering*, Phys. Rev. A **36**, 4604 (1987).
- [SC92] D. Sokolovski and J. N. L. Connor, *Negative probability and the distributions of dwell, transmission, and reflection times for quantum tunneling*, Phys. Rev. A **44**, 1500 (1992).
- [Sch26] E. Schrödinger, *Quantisierung als Eigenwertproblem*, Ann. d. Phys. **79**, 361 (1926).
- [Sch91] L. S. Schulman, *Definite quantum measurements*, Ann. Phys. (NY) **212**, 315 (1991).
- [Sch97] L. S. Schulman, *Time's arrows and quantum measurement*, Cambridge monographs on mathematical physics, Cambridge University Press, Cambridge, 1997.
- [SGOAD96] P. Szriftgiser, D. Guéry-Odelin, M. Arndt, and J. Dalibard, *Atomic wave diffraction and interference using temporal slits*, Phys. Rev. Lett. **77**, 4 (1996).
- [SK93] B. W. Shore and P. L. Knight, *The Jaynes-Cummings model*, J. Mod. Opt. **40**, 1195 (1993).
- [Smi60] F. T. Smith, *Lifetime matrix in collision theory*, Phys. Rev. **118**, 349 (1960).
- [SW58] H. Salecker and E. P. Wigner, *Quantum limitations of the measurement of space-time distances*, Phys. Rev. **109**, 571 (1958).
- [vN32] J. v. Neumann, *Mathematische Grundlagen der Quantenmechanik*, Springer-Verlag, Berlin, Heidelberg, 1932, english translation: [vN55].
- [vN55] J. v. Neumann, *Mathematical foundations of quantum mechanics*, Investigations in Physics, vol. 2, Princeton Univ. Press, Princeton, 1955.



## Danksagungen

Zum Gelingen dieser Arbeit haben etliche Menschen beigetragen, und dafür bin ich dankbar. Einige von ihnen möchte ich namentlich erwähnen.

Herrn Prof. Dr. Gerhard C. Hegerfeldt danke ich für die interessante Themenstellung und die gute Betreuung der Arbeit. Außerdem bin ich ihm dankbar für die Möglichkeit, neben der Arbeit an der Dissertation an einem weiteren interessanten Projekt forschen zu können.

Herrn Prof. Dr. Kurt Schönhammer danke ich für die Übernahme des Korreferats.

Volker Hannstein und Dirk Seidel danke ich für viele interessante und hilfreiche Diskussionen. Emmanuel O. Yewande, Martin Stoll und Sebastian Fuchs danke ich für ein gutes Arbeitsklima im Büro.

Volker Hannstein, Anneke Neumann, Emmanuel O. Yewande und Sandra Moser-Neumann danke ich, dass sie die undankbare Arbeit des Korrekturlesens übernommen haben.

Und vor allem danke ich meiner lieben Ehefrau Sandra Moser-Neumann für viel Geduld vor allem während der letzten Wochen der Fertigstellung des Manuskripts.

## Acknowledgments

I thank Prof. J. Gonzalo Muga and his group in Bilbao for their repeated hospitality. I am also thankful for the opportunity to present my results in several talks at the workshops in Bilbao and on Teneriffe.

I thank Prof. Lawrence S. Schulman for helpful discussions and a number of interesting ideas which have been elaborated in the present thesis.







## Lebenslauf

**Name:** Jens Timo Neumann  
**Geburtstag:** 2. April 1977  
**Geburtsort:** Hildesheim  
**Staatsangehörigkeit:** deutsch

## Wissenschaftlicher Werdegang

**1983 – 1987:** Grundschule Moritzberg in Hildesheim  
**1987 – 1996:** Gymnasium Andreanum in Hildesheim  
staatl. anerkannte Privatschule in freier Trägerschaft  
der ev.-luth. Landeskirche Hannovers  
**21. Mai 1996:** Abitur am Gymnasium Andreanum in Hildesheim  
**Aug. 1996 – Aug. 1997:** Zivildienst  
Altenwohn- und Pflegestift Christophorus  
in Hildesheim  
**WiSe 97/98 – SoSe 99:** Studium der Physik  
Eberhard-Karls-Universität zu Tübingen  
**27. Sep. 1999:** Diplomvorprüfung im Fach Physik  
Eberhard-Karls-Universität zu Tübingen  
**WiSe 99/00 – WiSe 02/03:** Studium der Physik  
Georg-August-Universität zu Göttingen  
Diplomarbeit in der  
Arbeitsgruppe Prof. Dr. K.-H. Rehren  
Institut für Theoretische Physik  
**7. Feb. 2003:** Diplomprüfung im Fach Physik  
Georg-August-Universität zu Göttingen  
**seit April 2003:** Promotion  
Arbeitsgruppe Prof. Dr. Gerhard C. Hegerfeldt  
Institut für Theoretische Physik  
Georg-August-Universität zu Göttingen